(2)

TECHNICAL REPORT BRL-TR-3149

BRL

SMALL SCALE SHOCK TUBE EXPERIMENTS USING A COMPUTER CONTROLLED ACTIVE RAREFACTION WAVE ELIMINATOR

STEPHEN J. SCHRAML
RICHARD J. PEARSON

SEPTEMBER 1990

U.S. ARMY LABORATORY COMMAND

BALLISTIC RESEARCH LABORATORY
ABERDEEN PROVING GROUND, MARYLAND

NOTICES

Destroy this report when it is no longer needed. DO NOT return it to the originator.

Additional copies of this report may be obtained from the National Technical Information Service, U.S. Department of Commerce, 5285 Port Royal Road, Springfield, VA 22161.

The findings of this report are not to be construed as an official Department of the Army position, unless so designated by other authorized documents.

The use of trade names or manufacturers' names in this report does not constitute indorsement of any commercial product.

REPORT DOCUMENT PAGE

Form Approved OMB No. 0704-0188

1. AGENCY USE ONLY *(Leave blank)*	2. REPORT DATE	3. REPORT TYPE AND DATES COVERED
	September 1990	Final, Aug 89 - Aug 90

4. TITLE AND SUBTITLE
Small Scale Shock Tube Experiments Using a Computer Controlled Active Rarefaction Wave Eliminator

5. FUNDING NUMBERS
1L162120AH25

6. AUTHOR(S)
Stephen J. Schraml and Richard J. Pearson

7. PERFORMING ORGANIZATION NAME(S) AND ADDRESS(ES)
Director
U.S. Army Ballistic Research Laboratory
ATTN: SLCBR-TB-BD
Aberdeen Proving Ground, MD 21005-5066

8. PERFORMING ORGANIZATION REPORT NUMBER

9. SPONSORING/MONITORING AGENCY NAMES(S) AND ADDRESS(ES)
U.S. Army Ballistic Research Laboratory
ATTN: SLCBR-DD-T
Aberdeen Proving Ground, MD 21005-5066

10. SPONSORING/MONITORING AGENCY REPORT NUMBER
BRL-TR-3149

11. SUPPLEMENTARY NOTES

12a. DISTRIBUTION/AVAILABILITY STATEMENT
Approved for public release; distribution is unlimited.

12b. DISTRIBUTION CODE

13. ABSTRACT ***(Maximum 200 words)***

The technology needed to construct a facility for testing full scale military equipment, termed the Large Blast/Thermal Simulator (LB/TS), is under development. One of the major components of the proposed facility will be a large valve controlling the flow exiting the downstream end, called a rarefaction wave eliminator (RWE). An active RWE, one which adapts its open area to changing flow conditions, will be used in the LB/TS. Using an active RWE allows a relatively short facility to produce the same range of blast simulations that would otherwise require a very long expansion section.

A small scale active rarefaction wave eliminator was constructed and tested through a series of blast conditions. Shock overpressures ranged from 40 - 100 kPa, while positive phase durations were in the range of 14 - 54 ms. Pressure histories and impulse values obtained from tests using the RWE compared well with long expansion section baseline data. The results of this program show that an active rarefaction wave eliminator can be used in place of a long expansion section to achieve successful nuclear blast simulation. Knowledge gained from the use of this RWE will be employed during construction and testing of the 1:6 scale and full scale active RWE's.

14. SUBJECT TERMS	15. NUMBER OF PAGES
Shock Tubes, Shock Waves, Blast Loads, Rarefaction	80
	16. PRICE CODE

17. SECURITY CLASSIFICATION OF REPORT	18. SECURITY CLASSIFICATION OF THIS PAGE	19. SECURITY CLASSIFICATION OF ABSTRACT	20. LIMITATION OF ABSTRACT
UNCLASSIFIED	UNCLASSIFIED	UNCLASSIFIED	UNLIMITED

INTENTIONALLY LEFT BLANK.

Acknowledgement

The authors wish to acknowledge the efforts of J. Chosta of Dynamic Science, Inc., who was responsible for the configuration and proper functioning of the entire 1:57 scale LB/TS model. Mr. Chosta also reduced and plotted a great deal of the experimental data collected during the course of this project.

INTENTIONALLY LEFT BLANK.

Table of Contents

Table of Contents (Continued)

List of Figures

List of Figures (Continued)

List of Figures (Continued)

INTENTIONALLY LEFT BLANK.

List of Tables

INTENTIONALLY LEFT BLANK.

I. Introduction

The Defense Nuclear Agency, through the Army Corps of Engineers, is in the process of designing a facility called the Large Blast/Thermal Simulator (LB/TS). The US Army Ballistic Research Laboratory (BRL) has been assigned the task of developing the blast and thermal simulation technology necessary for the design of this facility. The facility is intended to subject military vehicles such as tanks and helicopters to the blast and thermal loading associated with a nuclear burst. An illustration of the proposed facility can be seen in Figure 1.

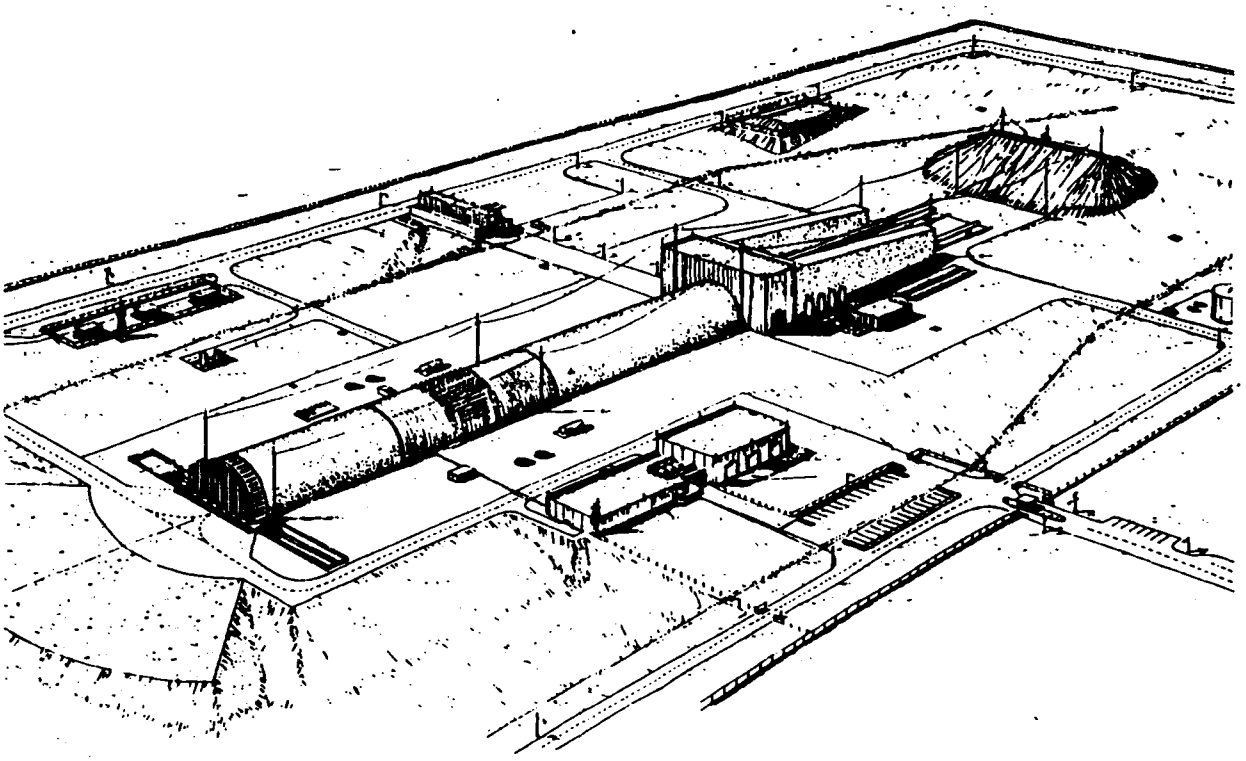

Figure 1. The Proposed Large Blast/Thermal Simulator

The LB/TS is essentially a large shock tube in which compressed gas is quickly released from a reservoir called the driver to form a shock wave which travels down the expansion section of the shock tube. By adjusting the volume of the driver and the initial driver pressure, a desired combination of shock overpressure and simulated weapon yield can be obtained. Thermal radiation is simulated through combustion of an aluminum/oxygen mixture near the target.

In shock tube operation, when a shock wave meets the open end of the expansion section a rarefaction wave is generated. This rarefaction wave travels back into the expansion section in the opposite direction of the initial shock wave and degrades the flow characteristics of the shock wave, thus ruining the nuclear blast simulation.

In a small shock tube the obvious solution to this problem is to make the expansion

section long enough that the rarefaction wave does not arrive at the test section until after the period of interest has past. This, however, is not a feasible alternative for a facility as large as the LB/TS. As currently conceived, the expansion section of the LB/TS has a cross sectional area of 163 m^2 and a length of 160 m. Computational studies have shown that a design without an RWE would require a much longer expansion section. For a 13.4 kPa, 600 kT simulation an expansion section length greater than 1500 m would be required. Obviously the cost of building such a facility would be prohibitive.

The alternative solution to this problem is to use a device called an active Rarefaction Wave Eliminator (RWE) which would be attached to the end of the expansion section. An RWE is essentially a converging nozzle whose exit plane cross-sectional area can be changed with time. As the flow passes through the RWE it is accelerated by the area reduction so that the static pressure of the flow is equal to that of the atmosphere or the Mach number at the RWE exit is equal to 1. If one of these two conditions exists then no rarefaction wave is generated. The RWE exit plane area is continuously changing to satisfy these conditions for the varying flow.

II. The 1:57 Scale Shock Tube

To verify the theory of RWE operation developed at the University of Toronto and BRL[1, 2, 3], a small scale active RWE was installed on a shock tube at BRL. This shock tube, shown in Figure 2, has an expansion section diameter of 25.40 cm, a single cylindrical driver whose diameter is 10.16 cm and a throat diameter of 6.40 cm. When compared to the proposed full scale LB/TS this shock tube scales linearly to 1:57 of its size. All diameters noted here and hereinafter are internal diameters unless stated otherwise.

The shock is initiated by the natural burst of a diaphragm located in the throat. The desired driver pressure determines the appropriate thickness of diaphragm. During the testing, three different lengths of driver section were used. These lengths were 30.48 cm, 55.88 cm and 106.68 cm resulting in driver volumes of 2840 cm^3, 4988 cm^3 and 9018 cm^3 respectively.

Figure 2 shows that the expansion section length was set at either 856.61 cm or 1719.58 cm during the tests. The longer expansion section was used to generate baseline data which had no rarefaction wave during the positive phase of the flow. This baseline data served two purposes. Primarily, the data from the long expansion section tests was used to generate the driving functions for the RWE. Also, the pressure histories obtained from the long expansion section tests were the standard by which the RWE tests were judged. The shorter expansion section was used during tests with and without the RWE. The short expansion section tests with no RWE were performed to show what effect the rarefaction wave had on the pressure histories. This same expansion section length was used in the tests of the RWE.

A total of nine channels of data is recorded for each test of this shock tube. A static pressure transducer is used to measure the pressure in the driver. A stagnation probe is

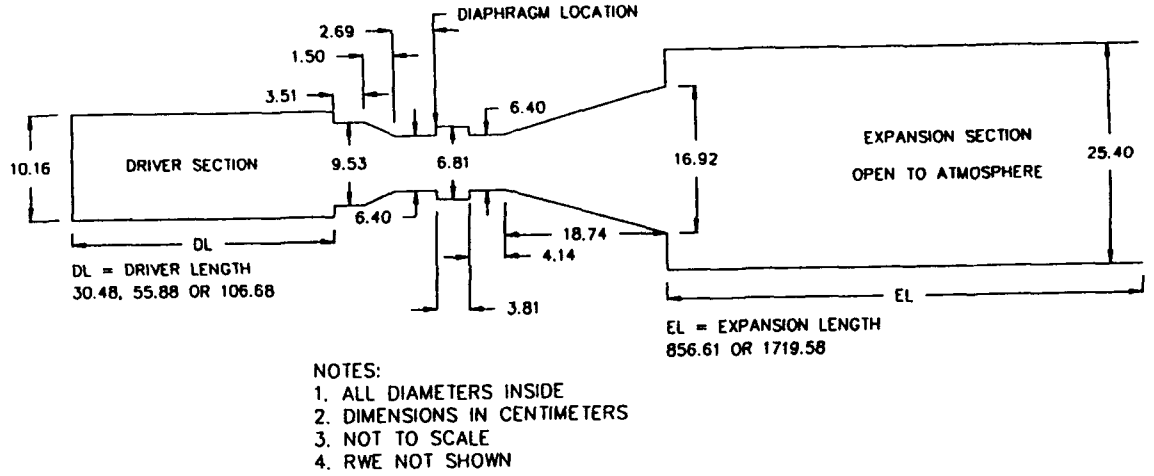

Figure 2. The 25.40 *cm* Diameter Shock Tube

located in the expansion section 52.1 *cm* downstream from the diaphragm. This gage is used to trigger the recording sequence and the RWE. A pair of static and stagnation probes is mounted in the expansion section at three locations, resulting in six additional gages. The first pair of gages is located 7.519 *m* from the diaphragm. The second and third pairs are at 7.900 *m* and 8.281 *m*, respectively. Finally, a rotary potentiometer was used to measure the angle of attack of the RWE louvers. The RWE resembles a shutter valve and the angle of its louvers determines the amount of area available for the gas to flow through the device. Thus the rotary potentiometer makes it possible to record the exit plane area time histories.

The location of the three static and stagnation pairs is significant. The test station located 8.281 *m* from the diaphragm is the station closest to the eventual placement of the RWE. Therefore the data collected at this station is used to generate the driving functions for the RWE. The station at 7.519 *m* is important because the distance from this station to the RWE, when scaled, is equivalent to the distance from the downstream end of the test section to the RWE in the full scale LB/TS. The data collected at this station ultimately determines whether or not the RWE functioned successfully. The remaining station is to be used as a backup in the event that gages at one of the other stations fails during a test.

III. The 1:57 Scale Active Rarefaction Wave Eliminator

The active rarefaction wave eliminator which was tested is illustrated in Figures 3 and 4. In section I the RWE was described as a simple converging nozzle placed at the open end of a shock tube. Inspection of these drawings shows that in reality the RWE is much more complex. While it is possible to computationally model a conical nozzle whose shape changes with time, designing a machine to do the same is quite difficult. The end result is the device shown in the figures. This RWE uses rotating louvers to block a controlled portion of the exit area thus creating the same effect as a converging nozzle.

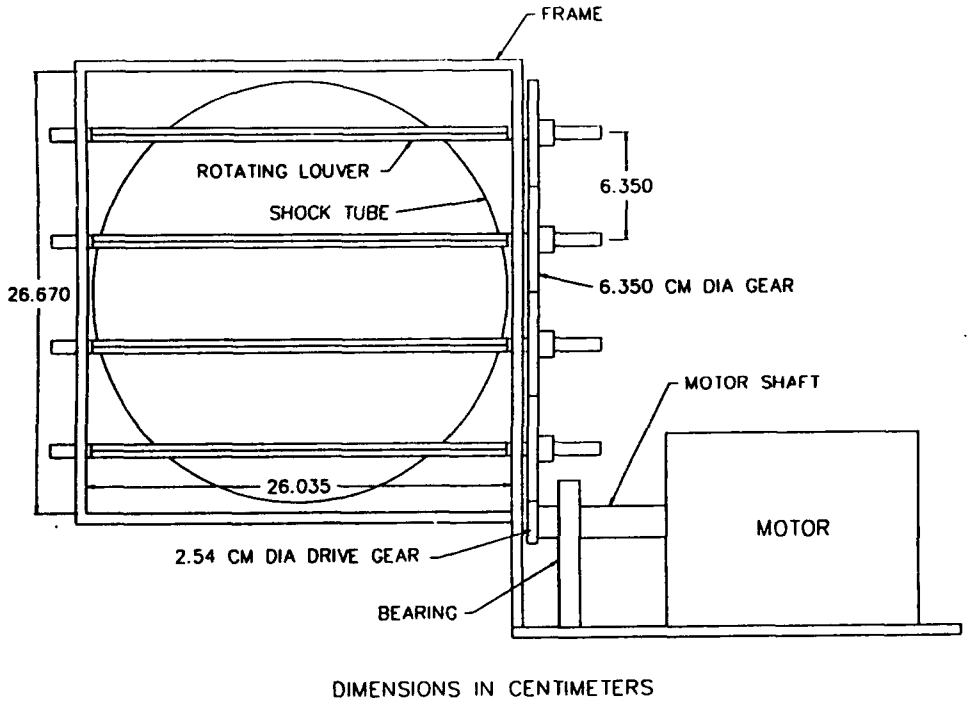

Figure 3. The 1:57 Scale RWE (front view)

1. Louver Overlap

By examining the illustrations, one can see that as a louver rotates, the amount of its area which is presented to the shock tube is proportional to the *sine* of the angle between the louver and the axis of the shock tube. Consider for a moment a single, thin, flat plate in space. When the plate is nearly horizontal, a modest angular displacement will result in a sizable change in area presented to a flow field traveling horizontally. However, when the plate is nearly vertical a great change in angle is required to achieve the same change in presented area. From this it can be seen that as the attack angle of the plate increases,

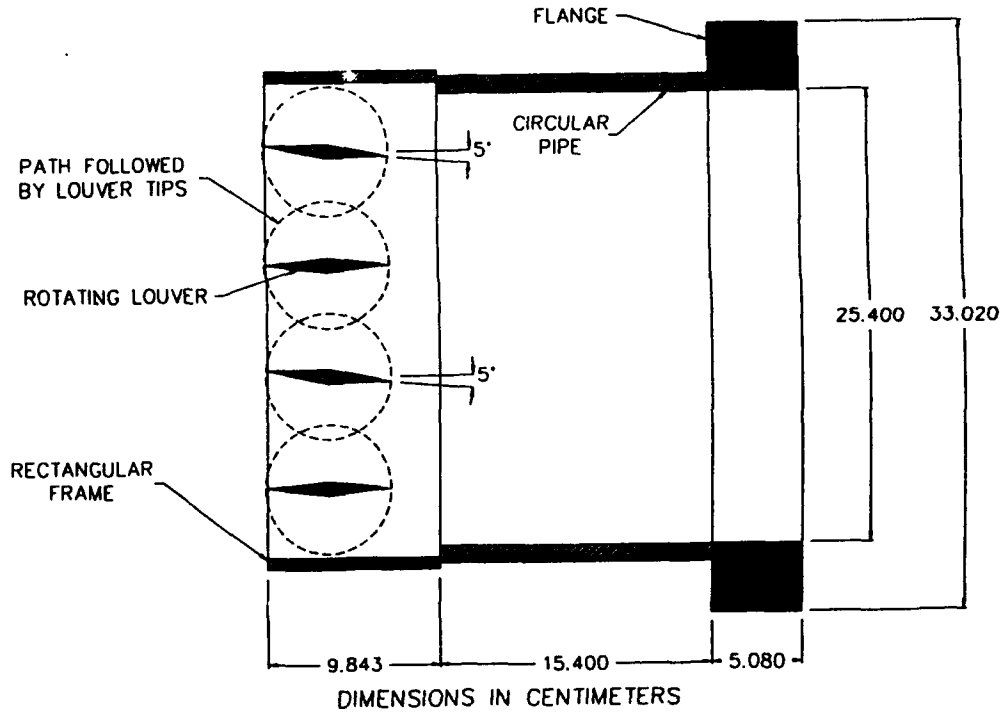

Figure 4. The 1:57 Scale RWE (side section)

its angular velocity must increase rapidly for a constant rate of area change. This high acceleration rate places a large torque requirement on the motor and the rotating louvers.

To overcome this problem the louvers were designed in such a way that they overlap. Adjacent louvers are offset by an angle of 5 degrees so that they will not interfere with one another. As a result, the overlap first occurs at a louver angle of about 61degrees. When the overlap condition occurs, the area of the shock tube is completely blocked by the projected area of the louvers. This design greatly reduces the torque and speed requirements of the motor.

2. Relationship Between Louver Angle and Open Area

The RWE open area is determined by the amount of louver area seen by the expansion section. Imagine looking down the expansion section into the RWE. One cannot see the portions of the louver which lie outside the circular area of the expansion section. Thus, these portions of the louvers are not considered when calculating the RWE open area. Only that area projected onto the louvers by the shock tube is considered.

The area of the exit plane of the RWE is always given relative to the area of the expansion section of the shock tube. Therefore, if the exit plane area of the RWE is equal to the area of the expansion section then the RWE open area is said to be 100 percent. In reality the open area cannot reach 100 percent because the louvers have some finite thickness

which is presented to the expansion section even when the louvers are horizontal. This can be seen in Figure 5, which is a chart defining the RWE open area as a function of louver angle.

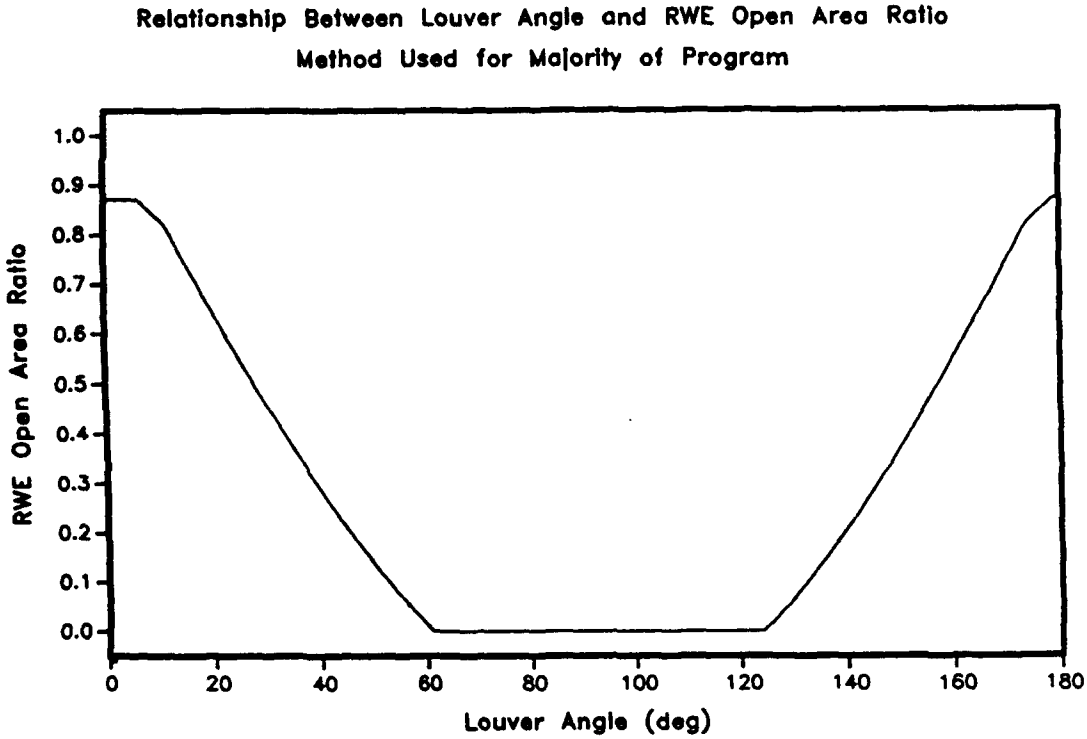

Figure 5. Relationship Between Louver Angle and Open Area

The maximum open area of the RWE is 87 percent. The open area is constant from zero to about 6 degrees due to the diamond shaped cross section of the louvers. A louver must rotate approximately 6 degrees before its tips will exit the area blocked by the thicker mid-section of the louver. The flat portion of the graph represents 0 percent open area, where the presented area of the louvers equals the area of the expansion section of the shock tube. When the louvers begin to overlap (at about 61 degrees), the open area goes to 0 percent and stays there until the louvers exit the overlap condition at about 124 degrees.

3. The Electric Servomotor

The four louvers are connected to a gear train and driven by an electric servomotor. The gears attached to the louvers are each 6.35 *cm* in diameter and the gear attached to the motor shaft is 2.54 *cm* in diameter. Included in the documentation that came with the motor was the manufacturers technical data about the motor [4]. From this the peak torque, rated speed, rotor inertia and acceleration at peak torque were obtained. From the drawings of the RWE, the inertia of the louvers and gears was determined. With all of this information it was possible to calculate the louver's maximum angular acceleration and the maximum angular velocity. These calculations can be found in Appendix A.

4. Triggering and Computer Control

As previously stated, a stagnation probe mounted in the expansion section near the diaphragm was used to trigger the recording device and the RWE.

Control of the motor was accomplished through a circuit board supplied with the motor and placed into a Zenith 248 personal computer system. Communication with the circuit board was made possible via a computer program (written in BASIC) which the end user could write to suit his own needs. Prior to a shot, the louvers would be set to a predetermined angle and this program would be run. The program reads in a series of execution commands from an ASCII file and loads them into the motor's memory. At this point the RWE is armed and awaiting the trigger signal. The driver is then supplied with nitrogen gas until the diaphragm is ruptured. The rupturing of the diaphragm releases the driver gas and initiates a shock in the expansion section. When the shock impinges on the probe at 52.1 *cm* it triggers the recording sequence and the RWE motor.

IV. The Experimental Program

The purpose of an RWE is to eliminate the rarefaction wave formed at the exit plane of a shock tube. If the RWE is functioning properly, the experimental records should appear as if the expansion section length were infinite. Therefore a series of baseline tests were performed using a very long expansion section (1719.6 *cm*). Using this long expansion section, a rarefaction wave is still formed but it does not affect the recorded pressure histories until well after the period of interest. The data collected from these long expansion section tests is also used to generate the driving functions for the RWE.

Another series of tests was performed employing a short expansion section (856.6 *cm*). These tests were conducted to show the effect of the rarefaction wave on the pressure histories when no RWE is used.

For the final test series the RWE was attached to the end of this short expansion section. The functions generated from the long expansion section tests were fed into the RWE for each shot. In theory, the long expansion section test and the RWE test should be nearly identical for a given driver condition while the short expansion test with no RWE will be quite different due to the effect of the rarefaction wave.

In order for the experimental program to be successful, the set of driver conditions had to be nearly identical for each test series. However, due to varying diaphragm characteristics the driver conditions at diaphragm rupture could not be repeated exactly from test to test. Each set of driver conditions was comprised of four driver pressure levels and three different driver volumes, resulting in twelve tests per series. The three driver volumes were obtained by adjusting the length of the cylindrical driver and were 2839.9 cm^3, 4899.2 cm^3 and 9017.7 cm^3. The four driver pressure levels resulted from varying the thickness of the diaphragm which was ruptured naturally. From these, four different shock overpressures

were obtained and were approximately 40 *kPa*, 68 *kPa*, 88 *kPa* and 100 *kPa*.

V. Development of the RWE Driving Functions

The RWE driving functions were generated by a FORTRAN computer program which used the data collected from the long expansion section tests as input. The objective of the program is to control the motion of the RWE louvers in such a way that the blast wave resulting from a test using the RWE is nearly identical to the long expansion section test that generated that particular RWE function.

It should be noted that this program can also generate functions from computational results. Currently the program can employ results of the BRL-Q1D code and can be easily modified to accept results of other hydrodynamic computer codes (hydrocodes). Thus far, the computational models which have been used have not proven accurate enough to provide reliable input to the RWE function generating program. For this reason, experimental data was used to generate the functions outlined in this report.

1. Theory of RWE Operation

The object of using an RWE is the elimination or suppression of the waves that are generated when a shock exits the downstream end of a shock tube. It will not be used to deliberately emit a shock or rarefaction wave in order to tailor the flow in the test section. All tailoring of the flow in the test section will be accomplished by changes in the driver end of the shock tube.

Using an RWE to help modify a blast wave in a shock tube involves some difficulties. First, the waves generated by the RWE are not the type of waves found in free field blast. The shocks or rarefactions generated by the RWE run upstream into the flow. In the free field case the pressure histories are controlled by rarefactions and secondary shocks running downstream and overtaking the primary shock which cause the pressure to decay with time. The influence of the waves on the flow depends on their direction. A rarefaction overtaking the shock causes a decrease in static pressure, flow velocity and dynamic pressure. An upstream moving rarefaction causes a decease in static pressure but also causes an increase in flow velocity and can cause an increase in dynamic pressure.

The second difficulty is that an RWE can influence only part of the flow history. Changes at the driver end, on the other hand, influence the entire history. The magnitude of the shock or rarefaction returned by the RWE depends on the RWE open area and the strength of the incident shock. The time at which waves generated at the RWE arrive at the test station depends on the decay rate of the shock wave as well as the incident shock overpressure and RWE open area. Controlling the strength and arrival time of the RWE generated wave to produce a desired change in the test section flow is a fairly complicated task. Because of these difficulties it was decided to limit the goal of RWE operation to simply eliminating

waves generated at the downstream end rather than using them to control flow at the test station.

In order to eliminate the rarefaction waves generated at the downstream end, one of two conditions must exist. Either the flow exiting the shock tube has to have the same static pressure as the atmosphere or the flow exiting must be sonic with an exiting static pressure equal to or greater than the atmospheric pressure. None of the shocks in the design envelope of the LB/TS are sufficiently strong to produce sonic or supersonic flow behind them. Therefore, the following analysis is intended only for shock waves which generate subsonic flow.

The initial interaction of the shock and RWE will not be analyzed. This initial interaction produces a pressure spike that moves upstream and can affect the flow in the test section. This effect, however, is small and the addition it makes to the positive phase impulse is negligible.

The following assumptions have been made to simplify the analysis:

1. The RWE will be assumed to act as a simple converging nozzle.
2. The flow will be considered one dimensional.
3. The interaction between the flow behind the shock and the RWE is assumed to be isentropic. Entropy is generated when gas is processed by the leading shock but the flow behind the shock can be reasonably modeled as isentropic.
4. The flow is assumed to be inviscid.
5. The gas involved is assumed to have an ideal gas, polytropic, equation of state.
6. The period of interest is only that period in which the flow is exiting the shock tube. The analysis does not consider flow from the atmosphere back into the expansion tunnel.

For isentropic flow through a converging nozzle to reach sonic velocity in expanding from a stagnation pressure of P_{0i} to a static atmospheric pressure of p_∞, the ratio p_∞/P_{0i} must be larger than the critical ratio given by Equation 1 [5].

$$\frac{p_\infty}{P_{0i}} = \left(\frac{2}{\gamma+1}\right)^{\frac{\gamma}{\gamma-1}} \tag{1}$$

If the ratio of specific heats, γ, is equal to 1.400, this critical ratio is 0.528282. If the result of Equation 1 is greater than 0.528282 the flow will remain subsonic at the exit of the RWE converging nozzle. If the ratio is less than that, then with the proper RWE setting the flow will choke and become sonic at the exit of the RWE converging nozzle. These are the two cases to be considered in determining the open area at the end of the RWE converging nozzle. In one case the flow remains subsonic and in the other the flow becomes sonic at the RWE exit.

The flow behind a 72.2 *kPa* overpressure shock has a p_∞/P_{0i} ratio greater than 0.528282 and will therefore have subsonic flow exiting the RWE. For shock overpressures exceeding 72.2 *kPa* the ratio is less than 0.528282 and the flow exiting the RWE through the appropriate area reduction initially will be sonic.

The case in which the flow remains subsonic will be considered first. The Mach number at the inlet to the RWE is assumed to be the undisturbed local Mach number behind the shock. Using the definition of stagnation pressure, P_{0i} and solving for the flow Mach number at the RWE inlet, M_i yields Equation 2 [6].

$$M_i = \left[\left(\frac{2}{\gamma-1}\right)\left[\left(\frac{P_{0i}}{p_i}\right)^{\frac{\gamma-1}{\gamma}} - 1\right]\right]^{0.5} \tag{2}$$

If p_i and P_{0i} are the static and stagnation pressures respectively at the RWE inlet then the Mach number at the inlet, M_i, can be calculated using Equation 2.

For isentropic flow the stagnation pressure remains constant through the converging nozzle. Therefore the stagnation pressure at the RWE exit, P_{0e}, equals P_{0i} (the known inlet stagnation pressure). For the rarefaction wave to be eliminated the static pressure at the RWE exit must match the atmospheric pressure, p_∞, which is also known. Therefore Equation 2 can be modified and used to determine the Mach number at the RWE exit, M_e as a function of P_{0i} and p_∞ as shown in Equation 3.

$$M_e = \left[\left(\frac{2}{\gamma-1}\right)\left[\left(\frac{P_{0i}}{p_\infty}\right)^{\frac{\gamma-1}{\gamma}} - 1\right]\right]^{0.5} \tag{3}$$

The relationship between Mach number and area ratio for an isentropic flow is given by Equation 4.

$$\frac{A_e}{A_i} = \left(\frac{M_i}{M_e}\right)\left[\frac{2+(\gamma-1)M_e^2}{2+(\gamma-1)M_i^2}\right]^{\frac{\gamma+1}{2(\gamma-1)}} \tag{4}$$

In Equation 4, A_i is the known inlet area to the RWE. A_e is the RWE exit area which will produce a match between the static pressure of the exiting flow and the atmosphere.

For a decaying blast wave simulation, the static and stagnation pressures at the inlet of the RWE change with time. As long as these pressure histories are known, an RWE open area history can be found by repeated calculations using Equations 2, 3 and 4.

For the second case, in which the ratio p_∞/P_{0i} is less than 0.528282, the flow at the exit plane of the RWE is sonic, thus $M_e = 1.0$. Equation 2 is still used to calculate M_i but since M_e is known Equation 3 is not used. In this case Equation 4 simplifies to Equation 5.

$$\frac{A_e}{A_i} = M_i\left[\frac{\gamma+1}{2+(\gamma-1)M_i^2}\right]^{\frac{\gamma+1}{2(\gamma-1)}} \tag{5}$$

For a decaying blast wave simulation with an initial p_∞ / P_{0i} ratio less than 0.528282, Equation 5 is used from the start of the calculation until the value of this ratio reaches 0.528282. When this point is reached, Equation 4 is used for all subsequent area ratio calculations in the history.

2. Adaptation of the RWE Theory

The original intent of the experimental program was to use the FORTRAN code "ELIM" [2] developed by Dr. J. Gottlieb of the University of Toronto Space Institute to develop the RWE functions. The ELIM code extends the theory given in the preceding section to take into account edge effects and also handles inflow as well as outflow. The BRL-Q1D [7] code was used to calculate the static pressure, sound speed and flow velocity as a function of time for the 1:57 scale blast simulator equipped with a very long expansion tunnel but no RWE. Attempts were then made to use the BRL-Q1D code results to produce RWE functions which would control the active RWE in experiments on the 1:57 scale blast simulator. These attempts proved unsuccessful. Comparison with actual experiments showed that while the BRL-Q1D code provides a reasonable approximation of the flow conditions, it is not accurate enough in its details for proper RWE control. Attempts using the Random Choice Method (RCM) code to model the flow in the 1:57 scale blast simulator also failed to produce acceptable functions.

An attempt was then made to generate the RWE functions from experimental flow measurements recorded during long expansion tunnel tests. This was recognized as an expedient alternative in order to carry out the small scale active RWE testing. In a large scale blast simulator it will be impossible to obtain long expansion tunnel pressure histories experimentally due to the impracticality of changing tunnel lengths. Work continues in finding a hydrocode with sufficient accuracy to produce flow histories on which RWE control functions can be based.

The ELIM code was not used to generate RWE functions from the experimental data. The sound speed and velocity required by ELIM could not be derived from the experimental instrumentation available for this work. A new FORTRAN subroutine, "AREARP", was developed based on the theory outlined in the previous section and requires only atmospheric conditions and the RWE inlet static and stagnation histories as input. The subroutine AREARP can use either experimental or calculated stagnation and static pressure histories as input. The histories must be for a flow in which there are no waves generated at the RWE, (i.e., the histories that would exist if the expansion tunnel continued to infinity beyond the RWE location). Such histories can be approximated by using long expansion tubes in experiments or calculations which keep waves from returning during the period of interest. The stagnation and static pressure histories were used to determine the RWE area ratio histories for subsequent experiments which employed a short expansion tunnel and an active RWE. Due to the nature of the pressure histories and the shock overpressures obtainable in the 1:57 scale blast simulator these attempts also proved unsuccessful.

In the experimental setup shock overpressures were limited to a maximum of 140 *kPa*. Also, in order to test the theory for subsonic flow through the RWE, part of the testing had to be conducted with shock overpressures less than 72.2 *kPa*. Unfortunately, at low overpressures the ratio of p_i to P_{0i} is very close to unity. Under these conditions the random noise which exists in the experimental pressure histories tends dominate the calculation of inlet Mach number, M_i. The resulting random variations in M_i in turn produce an RWE area ratio history with large random variation, which is unacceptable.

R. Guice [8] of Applied Research Associates, Inc., suggested that the following equation could be substituted in place of Equation 2.

$$M_i = \frac{p_i/p_\infty - 1}{\gamma\sqrt{((\gamma-1)/2\gamma)\,(p_i/p_\infty)\,((\gamma-1)/(\gamma+1) + (p_i/p_\infty))}} \tag{6}$$

Equation 6 is normally used to calculate the Mach number of the flow directly behind a moving shock. For the moving shock case p_∞ would be the pressure ahead of the shock and p_i would be the pressure behind the shock. Here we are using the equation to calculate Mach number not only directly behind the shock but also upstream where the pressure has decayed from its initial value behind the shock front.

The pressure decay behind the shock in the blast simulator is caused by rarefaction waves generated in the driver which overtake the shock. The Mach number directly behind the incident shock, M_s, is calculated using Equation 7.

$$M_s = \frac{p_s/p_\infty - 1}{\gamma\sqrt{((\gamma-1)/2\gamma)\,(p_s/p_\infty)\,((\gamma-1)/(\gamma+1) + p_s/p_\infty)}} \tag{7}$$

In Equation 7, p_s is the static pressure directly behind the shock. M_i, the local Mach number of the flow after its pressure has decayed from p_s to p_i, is given by Equation 8.

$$M_i = \left(\frac{1}{\gamma-1}\right)\left[((\gamma-1)M_s - 2)\left(\frac{p_s}{p_i}\right)^{\frac{\gamma-1}{2\gamma}} + 2\right] \tag{8}$$

It has been found that using Equation 6 to calculate M_i (after the pressure has decayed behind the shock) provides a very good estimate. This Mach number falls within 1 % of the value that is calculated more formally by first calculating M_s using Equation 7, then using Equation 8 to calculate M_i. Equation 6 provides a good estimate only if the flow behind the shock is subsonic and the contact surface between the driver gas and the original expansion section gas does not pass through the measurement location. A relatively long distance was used between the diaphragm and the measurement stations in the test series reported here. The driver gas behind the contact surface therefore did not reach the measurement stations during the time of interest. A review of the stagnation histories showed that the contact surface passed though very late in the experiments.

A new FORTRAN subroutine, "RWE5", was written based on the use of Equation 6 to calculate the RWE inlet Mach number, M_i. Equation 3 uses the inlet stagnation pressure,

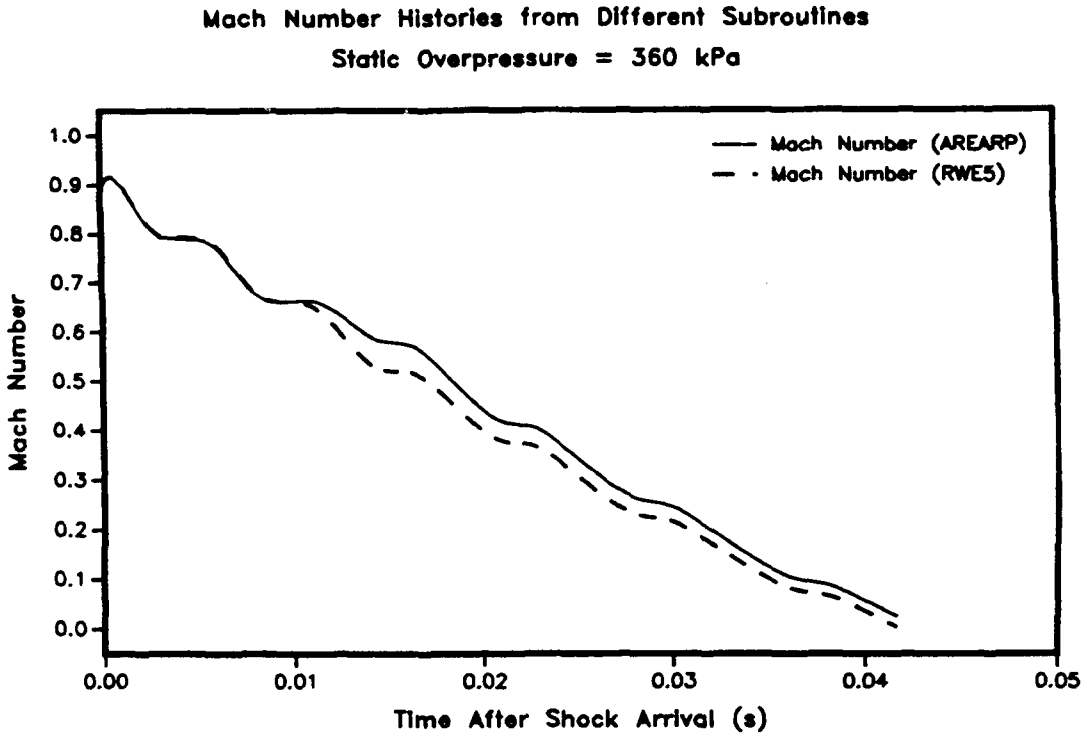

Figure 6. Comparison of Mach Number Histories

P_{0i} in order to calculate RWE exit Mach number, M_e. Equation 2, when solved for P_{0i} in terms of M_i, yields Equation 9.

$$P_{0i} = p_i \left[\frac{2 + (\gamma - 1) M_i^2}{2} \right]^{\frac{\gamma}{\gamma - 1}} \tag{9}$$

Once P_{0i} has been calculated using Equation 9, "RWE5" proceeds like "AREARP". Depending on the ratio p_∞ / P_{0i}, the RWE area ratio A_e/A_i is calculated using either Equation 4 or Equation 5.

Figure 6 shows a comparison of the Mach numbers calculated in "AREARP" and "RWE5". One can see the results are very close. Similar comparisons for other flow conditions of interest showed that the Mach numbers calculated by the two algorithms were also very close.

3. The Overall RWE Function

Several characteristics of the RWE motion profile were decided upon early in the program. The most obvious of these is the idea that the final RWE function should not attempt to exceed the motor's torque and speed limitations. Secondly, the direction of rotation of the louvers should not change during a test. As a result of these limitations, the final motion profile fed to the motor will not exactly match that of the exact function which was

generated from the pressure data alone. The final RWE function will adhere as closely as possible to the exact function, smoothing through reversals in direction and quick changes in velocity which exceed the peak torque of the motor. The differences between the exact and final functions are illustrated in Figure 7.

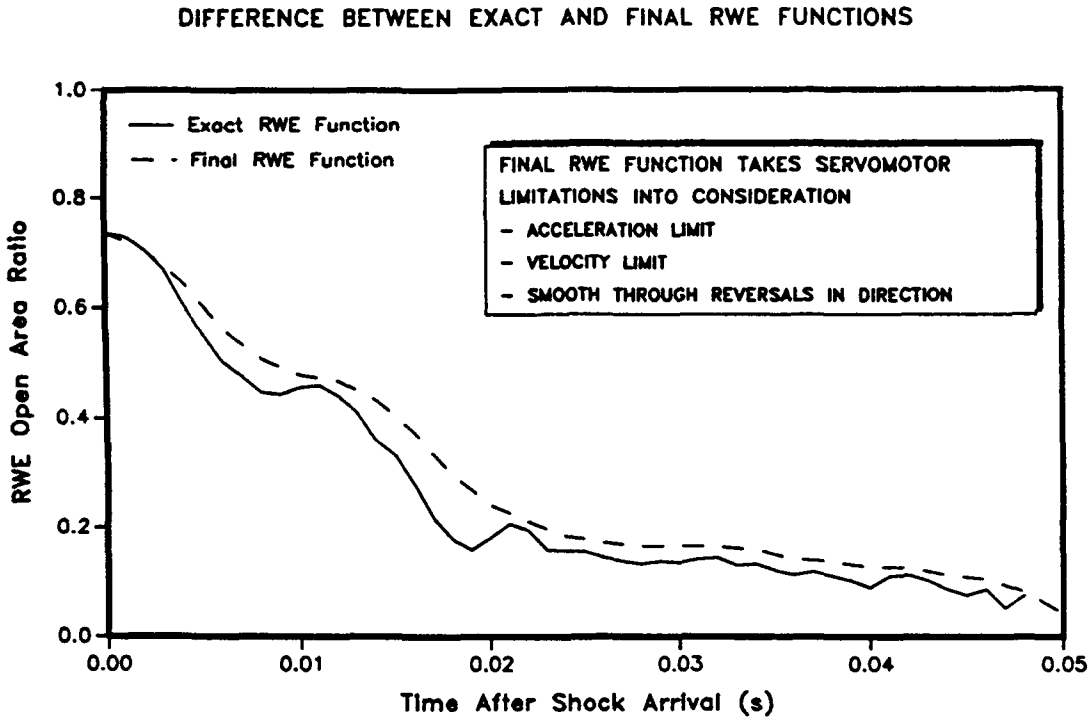

Figure 7. Exact and Final Open Area versus Time

It should be noted that the equations used to calculate the RWE open area are only valid during the positive phase of the blast. Computational studies were performed to determine the nature of the open area history after the positive phase. The computer program ELIM developed by Dr. J. Gottlieb was used in this study. This study determined that after the positive phase the RWE open area would oscillate about zero in a manner similar to that of the static pressure. A few tests were performed using this approach. These tests resulted in damaged louvers. At this point it was decided that the function should reopen the RWE as quickly as possible following the positive phase. Therefore, when the louvers begin to overlap, the louvers are accelerated at the maximum rate until the peak velocity is reached. This velocity is maintained until the RWE is once again fully open. Then the louvers are brought to rest in the maximum open position.

Since the RWE is a machine with torque limitations, some time interval is required for the motor to start from rest and achieve the initial velocity defined in the function. Therefore, the louvers are set in motion as soon as the trigger signal senses the flow, and the motor is able to overcome the resistance to initial acceleration prior to the arrival of the shock wave. The louvers are pre-positioned in such a way that when the shock arrives at the RWE, the louvers are at the appropriate angle to eliminate the rarefaction wave.

4. Servomotor Execution Commands

The motion commands which are sent to the motor are simply a series of angular displacement values to be executed during a fixed time interval. This angular displacement value represents the angular distance to be moved in that time interval, i.e., a displacement relative to the position at the start of that time interval. The commands are not absolute commands to go to some specific angular position relative to a fixed origin. The fixed time interval can be defined within the RWE controller program discussed earlier. For the electric motor used, this time interval must be in the range of $2 - 50$ ms. Since the blast waves in question are short duration events (less than 50 ms), the minimum time interval of 2 ms was chosen so that the control of the motor could be as fine as possible.

The angular displacement value for a particular time interval is represented by the amount of motor angular units (MAU) the rotor should move in that time period. It takes 25000 MAU for one complete rotation (360 degrees) of a louver. Therefore, 69.4 MAU are required to move the louvers 1 degree in one time interval.

The series of motor commands is generated by first breaking up the ideal function into even time steps of 2 ms, interpolating for RWE open area where necessary. For each area ratio in the function there is a correct louver angle which is calculated from the RWE geometry. The change in louver angle from one time period to the next is multiplied by 69.4 to yield the number of MAU to be executed for that time interval. The calculated MAU value is then rounded to the nearest integer.

Calculations in Appendix A indicate that the motor should be able to achieve an angular velocity of 46.08 rad/s and an angular acceleration of 5687.6 rad/s^2. This angular velocity limitation means that the maximum angular displacement that the motor can achieve in a two millisecond time interval is 0.09216 rad or 366.7 MAU. To be conservative, the computer code which generates the motor commands limited the maximum angular displacement in any 2 ms time interval to 342 MAU. If the desired displacement exceeded 342 MAU that displacement value was set to 342 MAU. The limit on angular acceleration means the maximum change in angular velocity during a 2 ms time step is 11.38 rad/s. The computer code which generates the commands was constructed in such a way that if the desired acceleration exceeded the maximum, the acceleration was set equal to the maximum.

5. The Effect of Driver Volume on the RWE Function

The initial open area of the RWE is defined by the shock pressure. The positive phase duration (PPD) of the blast wave defines the time required for the RWE to change from the initial setting to the overlap (fully closed) position. As the driver volume is reduced, the PPD decreases. From this one can see that smaller driver volumes require the greatest angular velocities and accelerations of the RWE.

Another problem posed by the small driver volume is the size of the time increment. For a blast wave whose PPD is 50 ms, 25 motor commands will be executed during the positive

phase. When the PPD is reduced to 14 *ms*, only 7 commands will be executed during the positive phase. Therefore, as the driver volume is reduced the resolution of control becomes more coarse, possibly resulting in greater error between the ideal and real functions.

VI. Preliminary Tests

Before the test series used to validate the theory of RWE operation was performed, a number of preliminary tests were conducted. Several tests were performed to confirm that the RWE hardware and software had been properly integrated with the 1:57 scale blast simulator. In these early tests a simple linear change in RWE area ratio was used. The linear closing function started with the RWE set for the flow condition immediately behind the shock and then closed to 0 percent open area linearly in a time equal to the positive phase duration for the blast wave in the simulator. The linear change in RWE open area produced acceptable results in the few preliminary tests in which it was used. The object of this study, however, was to validate a general theory of RWE operation, not to obtain empirically derived RWE closing functions. For this reason linear closing functions were not pursued further.

The next set of tests attempted to use flow field data generated by the BRL-Q1D code as input to the program which generates the RWE closing functions. The BRL-Q1D code was used to simulate the flow in the 1:57 scale blast simulator equipped with a very long expansion section. The purpose of this exercise was to eliminate the necessity of actually performing tests in the 1:57 scale blast simulator with an additional expansion tunnel length downstream of the normal RWE location. The flow field data generated by the BRL-Q1D code, however, was not accurate enough to produce acceptable functions. After several unsuccessful attempts, this method was abandoned. In all subsequent tests, the RWE functions were generated from data gathered in experiments performed with an additional expansion tunnel length added downstream of the normal RWE location.

Many tests were performed to determine the best way of modeling the geometry of the flow passing through the RWE. At one extreme the flow can be thought of as filling the entire cross-section of the RWE which has a rectangular cross-sectional area larger than that of the circular expansion section. In the other case, the flow is considered to form a jet which retains the shape of the original expansion tunnel. The real case actually lies somewhere between the two extremes and changes with time during a test. In the preliminary tests, it was assumed that the flow filled the entire cross-section of the RWE. The area of the frame and the entire lengths of the louvers were considered when calculating the open area of the RWE. The relationship between louver angle and open area for this method is shown in Figure 8. Since the area of the RWE frame is greater than that of the expansion section, the maximum open area for this method is greater than 100 percent. Also, the tolerance between the louvers and the frame causes the minimum open area to be greater than 0 percent.

Several tests were performed using RWE closing functions derived on the assumption that the flow filled the entire cross-section of the RWE. A pressure history from one such

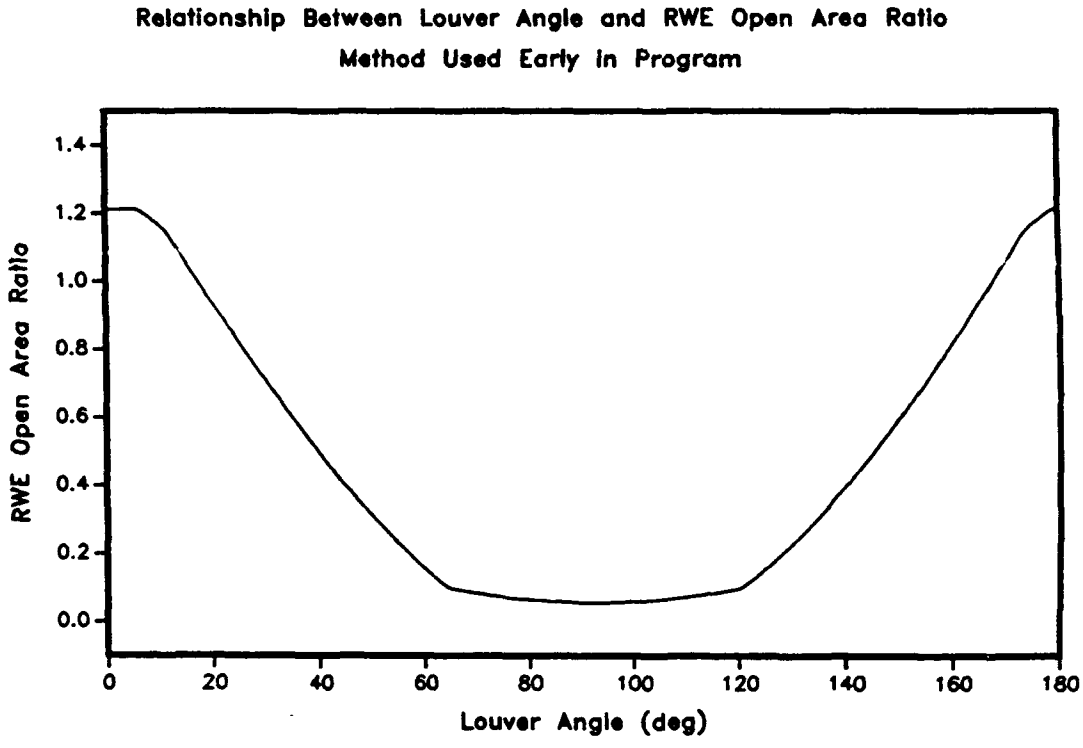

Figure 8. The Relationship between Louver Angle and Open Area (Old)

test is compared to a long expansion section test in Figure 9. The pressure histories in this figure were recorded at the station located 7.519 m from the diaphragm. In this figure, one can see that the greater louver angle associated with this method generated an upstream travelling compression wave which caused the flow to back up in the shock tube. Also, the louvers in the RWE were damaged by the flow during some of these tests. From these results it is obvious that this was not the correct method of calculating the open area of the RWE. The better method is that which assumes the flow retains the shape of the expansion section. This alternative method, discussed earlier, was used in all subsequent tests.

In the preliminary testing it was found that the RWE was incapable of following the ideal function through the negative pressure phase of the flow. In light of this it was decided to decelerate the louvers after they had overlapped and bring them to rest to the closed position. This procedure was intended to reduce "organ piping" (repeated passage of secondary waves up and down the simulator). Holding the RWE closed, however, resulted in damaged louvers. In all tests to follow the louvers were rotated rapidly through the overlap condition and brought to rest in the maximum open position.

Finally, a series of tests was conducted in which the RWE functions used were derived by applying a curve fit to the data gathered from long expansion section tests. This was an attempt to reduce the torque requirements placed on the motor by candidate functions. Unfortunately, the RWE closing functions based on this method were not satisfactory.

In all, the preliminary tests far outnumbered the tests performed in the main test

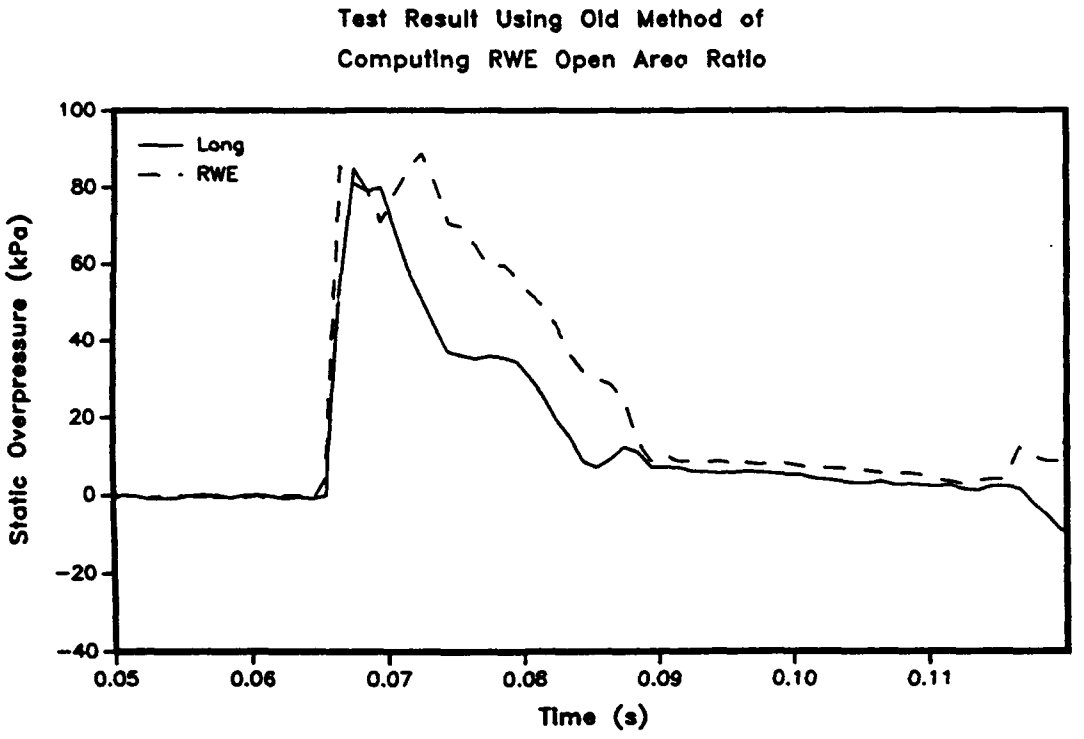

Figure 9. Pressure History from Old Louver Angle/Open Area Relation

series. The preliminary tests played a valuable role in developing a workable, if not optimal, methodology for operating the 1:57 scale RWE. The objective of this study was to validate a general theory of RWE operation for use in designing other blast simulators, particularly the proposed LB/TS facility. The following results section will concentrate on the main test series which grew out of the knowledge gained in the preliminary tests and is the vehicle by which the general theory was validated.

VII. Discussion of the Results

Pressure-time histories are the primary output collected from the tests. The effectiveness of the RWE can be determined by overlaying the pressure-time histories from a long expansion section test, a short expansion section test and an RWE test for a given set of driver conditions. Positive phase duration and impulse can also be determined from these pressure-time histories. Comparison of these values is another way of determining the effectiveness of the RWE.

The main test series consisted of 12 different driver conditions and 3 expansion section configurations resulting in a total of 36 shots. The shock tube configuration and initial conditions for these shots are outlined in Table 1.

As stated earlier, the measurement station located 7.519 m from the diaphragm is

important because the scaled distance from this station to the RWE is equivalent to that in the full scale LB/TS. Therefore, the data collected at this station ultimately determines the success or failure of the RWE in eliminating the rarefaction waves. For this reason, the emphasis of this discussion will be placed on data collected at this station. A complete set of pressure-time histories from all of the stations is presented in Appendix B.

The ability of the RWE to eliminate the rarefaction wave is diminished as driver volume is reduced. For this reason the experimental results are discussed in order of decreasing driver volume.

1. Results for the 9018 cm^3 Driver

The results of tests using driver a volume of 9018 cm^3 are shown in Tables 2, 3 and 4. The positive phase duration for long expansion section shots using this driver averaged about 50 ms. As a result, there are about 25 data points in the RWE function during the positive phase. Also, the long positive phase duration means the average angular velocity will not be as great as that of a smaller driver. As a result, the RWE should be able to follow the input function more closely.

Figures 10 through 17 are graphs showing the results of shots using the 9018 cm^3 driver. Each pair of graphs corresponds to one of the four pressure levels. Each pressure level corresponds to a set of tests performed using a particular thickness of diaphragm. Pressure level 1 corresponds to the thinnest diaphragm while pressure level 4 represents the thickest. The first graph in each set compares the input RWE function to the measured RWE motion for that pressure level. The second graph in a set overlays pressure histories from long expansion, short expansion and active RWE tests. In all the graphs, the time scale is given relative to the time of shock arrival at the station located 8.281 m from the diaphragm.

Overall, the RWE was able to follow the input function for the four cases. However, for the tests at pressure levels 2, 3 and 4 the RWE seems to overshoot the input function late in the positive phase. For each of these cases the area ratio history appears to be correct during the early part of the positive phase. The greatest deviation in the area ratio occurs late in the positive phase. In spite of this difference, the resulting pressure-time histories show excellent agreement between the long expansion section shots and the active RWE shots.

The effect of the rarefaction wave can be seen in the short expansion section traces. While this trace initially follows that of the long expansion section, the rarefaction wave eventually passes through the test station causing the two traces to deviate. When this happens the overpressure quickly goes negative, then slowly returns to zero. As a result, the PPD and the impulse for a short expansion section test are both much less than those associated with a long expansion section test.

Residing in the active RWE pressure-time histories are several short duration, positive

pressure spikes. These transient spikes are caused by reflections from the louvers of the RWE. This phenomenon is inherent to any rarefaction wave eliminator and can never be completely eliminated. Thus, the resulting impulse of the RWE test is slightly greater than the impulse of the baseline test.

Figures 18 and 19 compare the impulse and PPD respectively for all the tests using the 9018 cm^3 driver. In the first of these two charts, the long expansion section impulse and the active RWE impulse are similar with the latter slightly higher than the former, as one would expect. The positive phase durations for these cases compare just as well in the bottom chart. In fact they are exactly the same for the highest pressure. As expected, the impulse and the PPD data for the short expansion section tests fall well below the results of the other cases.

Table 1. Test Matrix

Test Name	Driver Volume (cm^3)	Expansion Length (cm)	RWE Used ($-$)	Ambient Pressure (kPa)	Ambient Temperature (C)	Driver Overpressure (kPa)
RWE92	2839.9	1719.6	No	103.1	13.9	1276
RWE93	2839.9	1719.6	No	103.1	13.9	2344
RWE94	2839.9	1719.6	No	103.1	13.9	3241
RWE95	2839.9	1719.6	No	103.1	13.9	3930
RWE100	2839.9	856.6	No	102.9	17.8	1207
RWE101	2839.9	856.6	No	102.9	17.8	2241
RWE102	2839.9	856.6	No	102.9	17.8	3172
RWE103	2839.9	856.6	No	102.9	17.8	3792
RWE96	2839.9	856.6	Yes	102.9	17.8	1276
RWE97	2839.9	856.6	Yes	102.9	17.8	2517
RWE98	2839.9	856.6	Yes	102.9	17.8	3172
RWE99	2839.9	856.6	Yes	102.9	17.8	4068
RWE61	4988.2	1719.6	No	104.1	18.3	1069
RWE63	4988.2	1719.6	No	104.1	18.3	2310
RWE65	4988.2	1719.6	No	104.1	18.3	3034
RWE67	4988.2	1719.6	No	104.1	18.3	4137
RWE68	4988.2	856.6	No	104.1	18.3	1138
RWE71	4988.2	856.6	No	104.1	18.3	2344
RWE72	4988.2	856.6	No	104.1	18.3	3068
RWE74	4988.2	856.6	No	104.1	18.3	3965
RWE77	4988.2	856.6	Yes	104.7	15.0	1172
RWE79	4988.2	856.6	Yes	104.7	15.0	2310
RWE80	4988.2	856.6	Yes	104.7	15.0	3137
RWE82	4988.2	856.6	Yes	104.7	15.0	3758
RWEBL2	9017.7	1719.6	No	103.5	22.2	1482
RWEBL3	9017.7	1719.6	No	103.5	22.2	2310
RWEBL5	9017.7	1719.6	No	103.5	22.2	3172
RWEBL7	9017.7	1719.6	No	103.5	22.2	4275
RWES2	9017.7	856.6	No	103.5	23.9	1586
RWES3	9017.7	856.6	No	103.5	23.9	2413
RWES5	9017.7	856.6	No	103.5	23.9	3275
RWES7	9017.7	856.6	No	103.5	23.9	4206
RWE85	9017.7	856.6	Yes	102.5	21.7	1379
RWE87	9017.7	856.6	Yes	102.5	21.7	2551
RWE88	9017.7	856.6	Yes	102.5	21.7	3241
RWE90	9017.7	856.6	Yes	102.5	21.7	3965

Table 2. Static Overpressure for Driver Volume = 9018 cm^3

Diaphragm Thickness (in)	Static Overpressure (kPa) Station Location = 7.519 m from Diaphragm			
	Long Expansion	Short Expansion	RWE	Average
0.010	44.349	47.751	45.278	45.793
0.020	71.431	70.609	69.380	70.473
0.030	89.676	87.607	88.984	88.756
0.040	107.724	107.157	105.895	106.925

Table 3. Static Overpressure Impulse for Driver Volume = 9018 cm^3

Average Static Overpressure (kPa)	Static Overpressure Impulse ($kPa - s$) Station Location = 7.519 m from Diaphragm		
	Long Expansion	Short Expansion	RWE
45.793	0.515	0.262	0.585
70.473	0.778	0.456	0.894
88.756	1.099	0.628	1.255
106.925	1.348	0.810	1.422

Table 4. Positive Phase Duration for Driver Volume = 9018 cm^3

Average Static Overpressure (kPa)	Positive Phase Duration (ms) Station Location = 7.519 m from Diaphragm		
	Long Expansion	Short Expansion	RWE
45.793	42.0	9.0	48.0
70.473	50.0	9.0	41.0
88.756	54.0	12.0	47.0
106.925	46.0	12.0	46.0

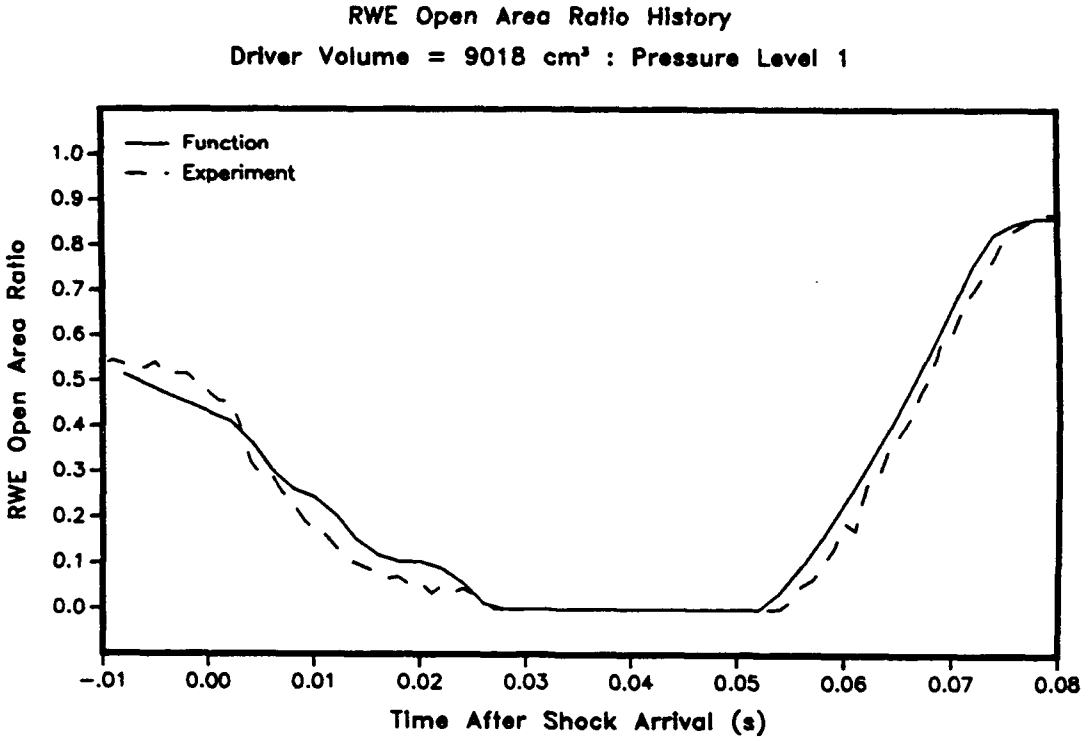

Figure 10. RWE Area History for 9018 cm^3 Driver; Pressure Level 1

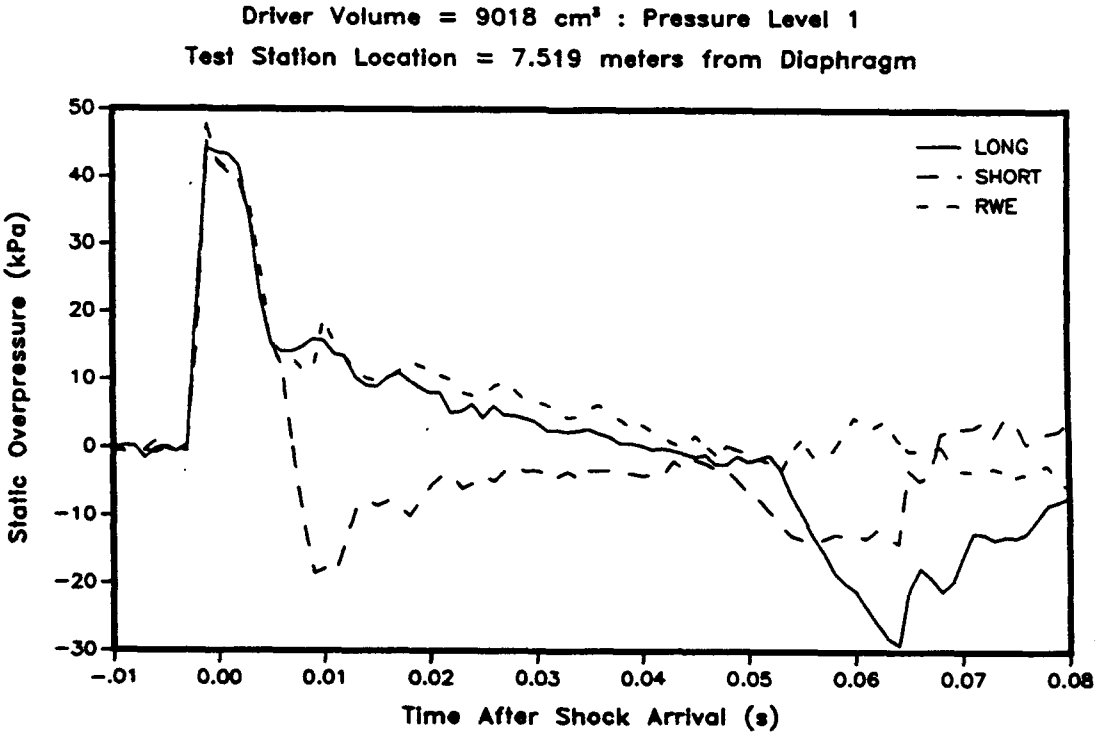

Figure 11. Pressure Histories for 9018 cm^3 Driver; Pressure Level 1

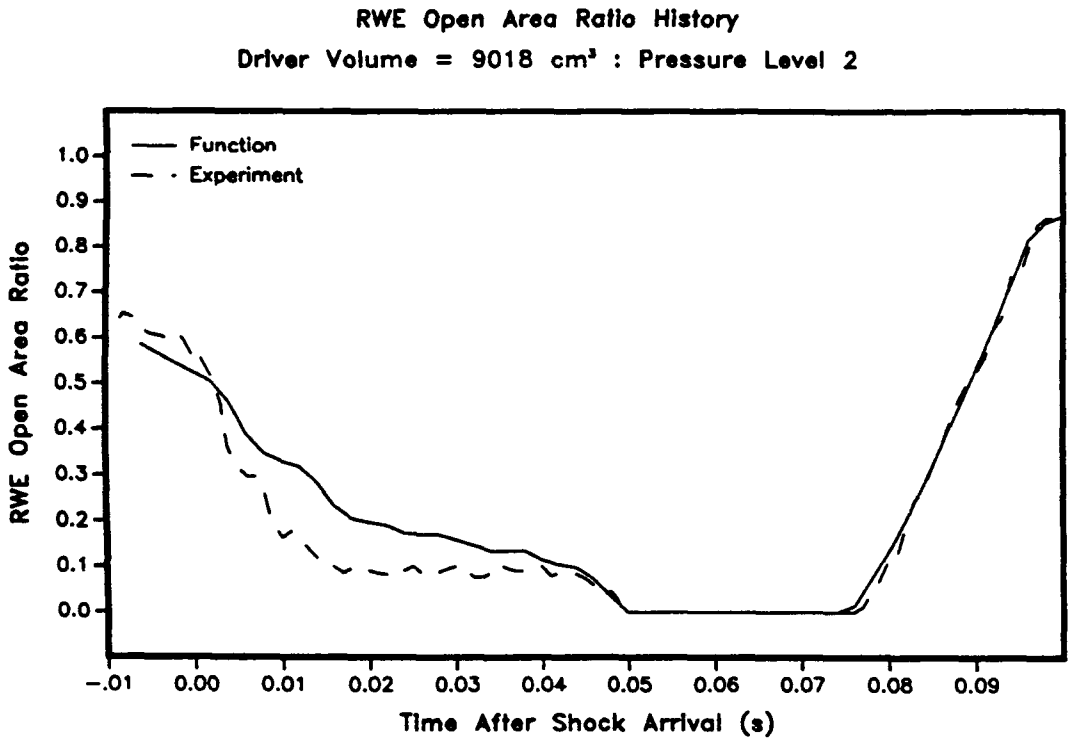

Figure 12. RWE Area History for 9018 cm^3 Driver; Pressure Level 2

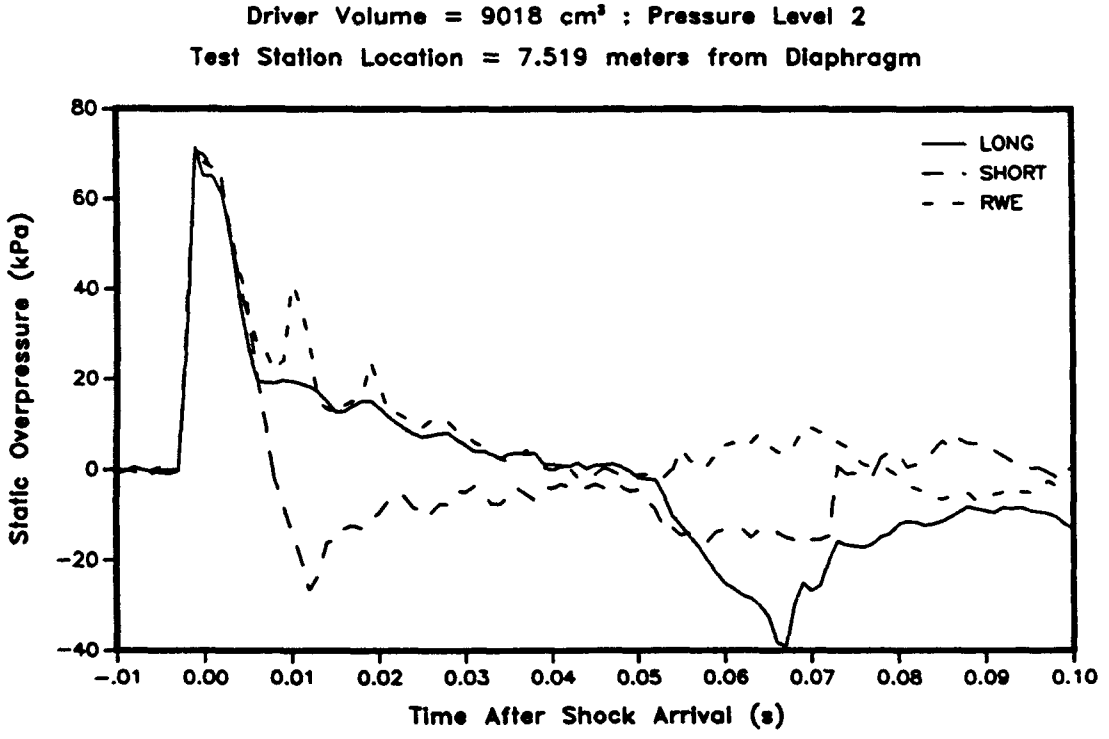

Figure 13. Pressure Histories for 9018 cm^3 Driver; Pressure Level 2

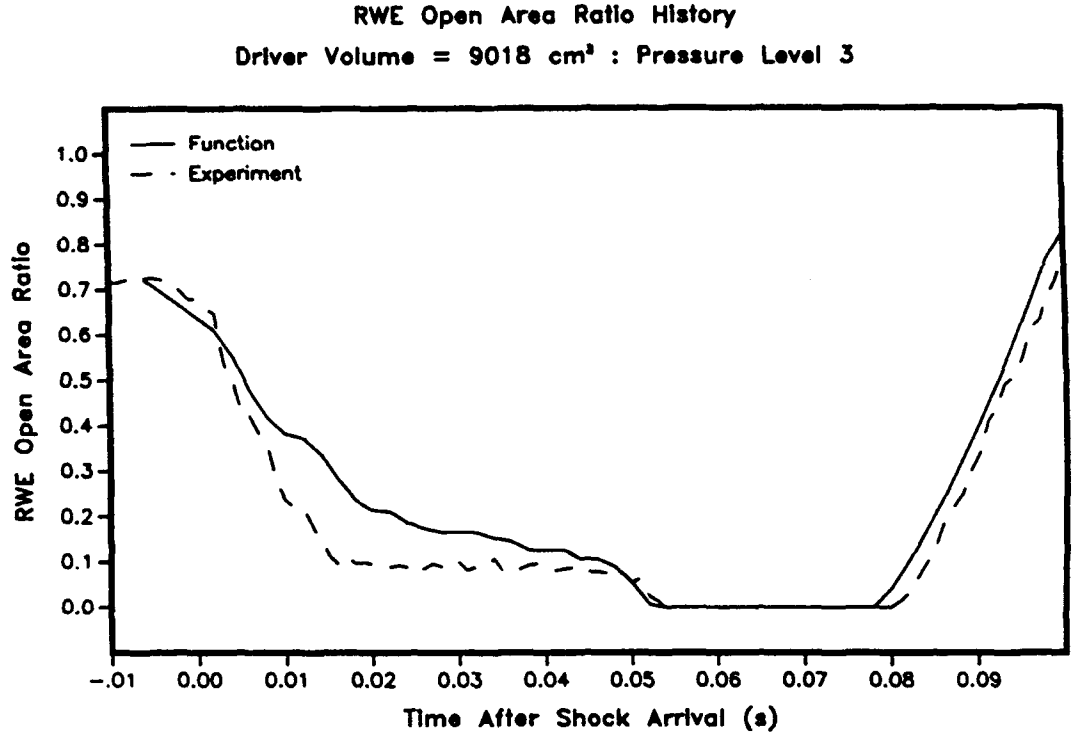

Figure 14. RWE Area History for 9018 cm^3 Driver; Pressure Level 3

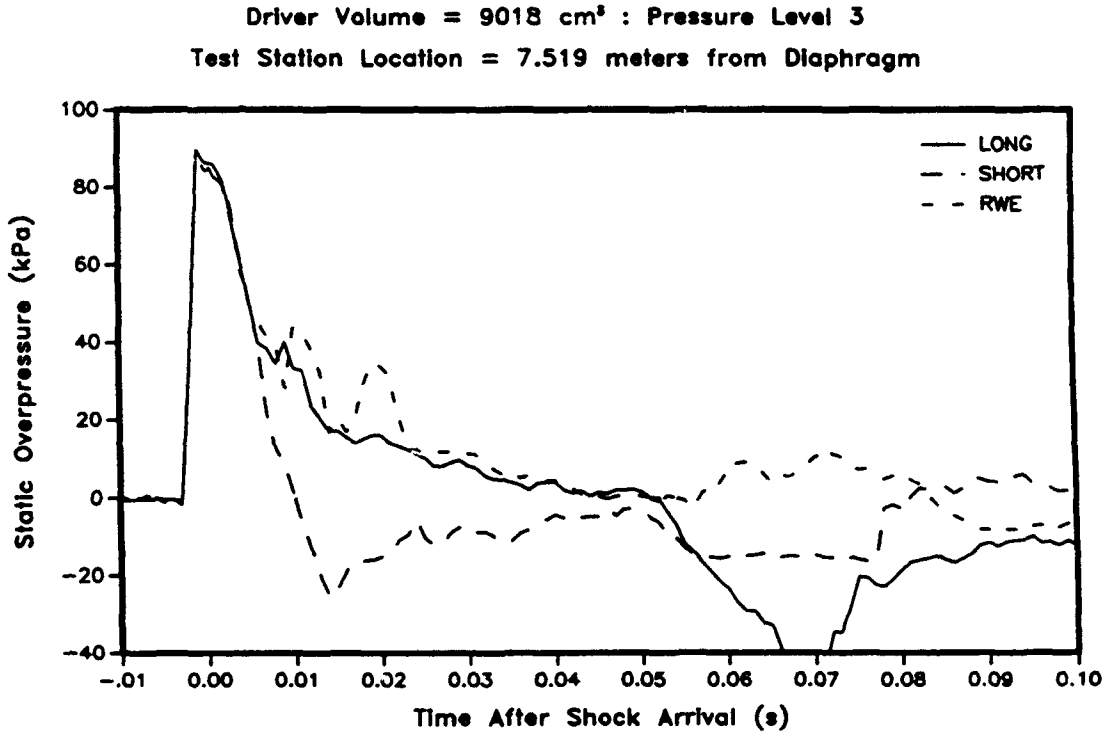

Figure 15. Pressure Histories for 9018 cm^3 Driver; Pressure Level 3

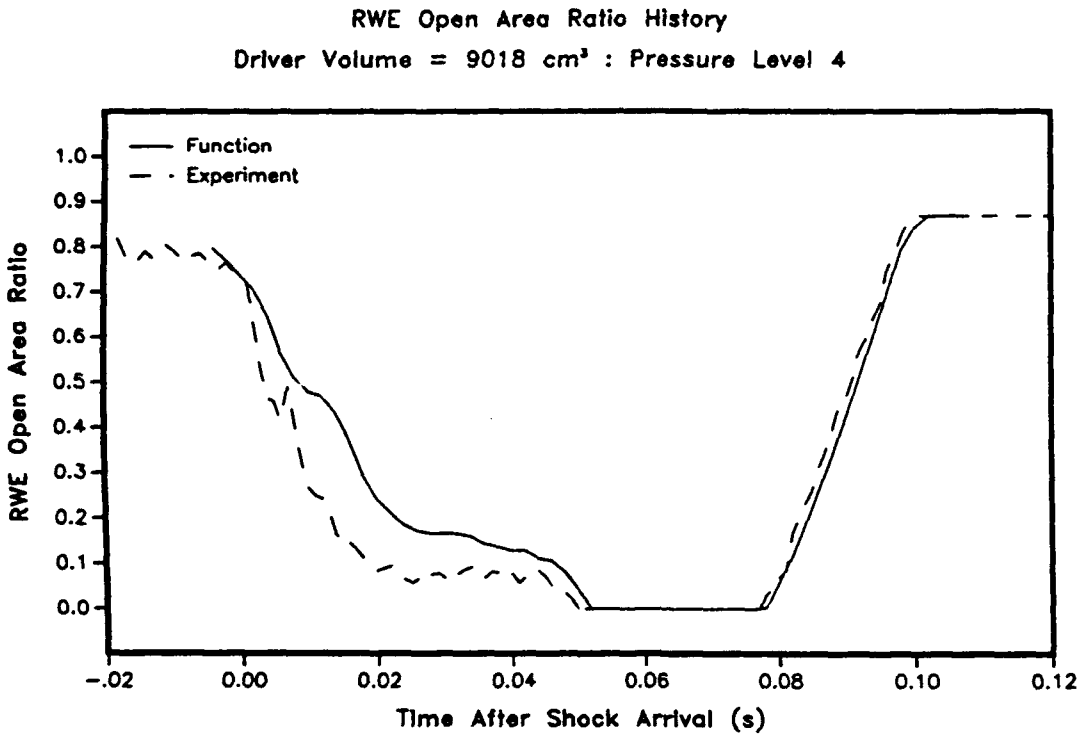

Figure 16. RWE Area History for 9018 cm^3 Driver; Pressure Level 4

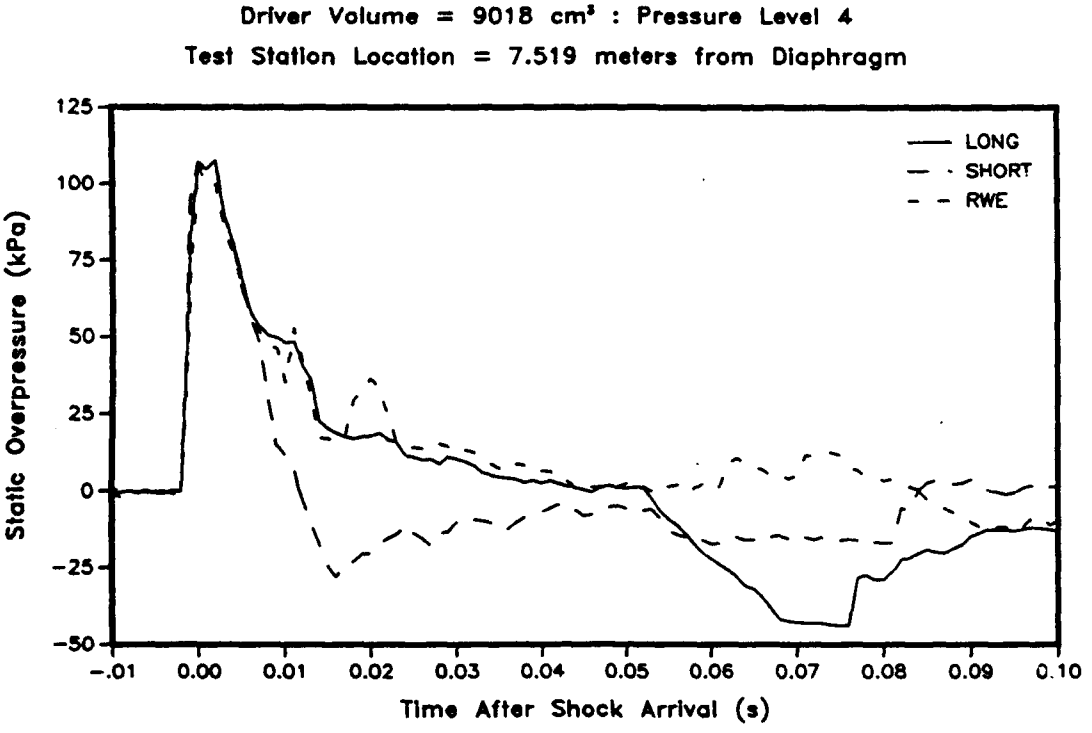

Figure 17. Pressure Histories for 9018 cm^3 Driver; Pressure Level 4

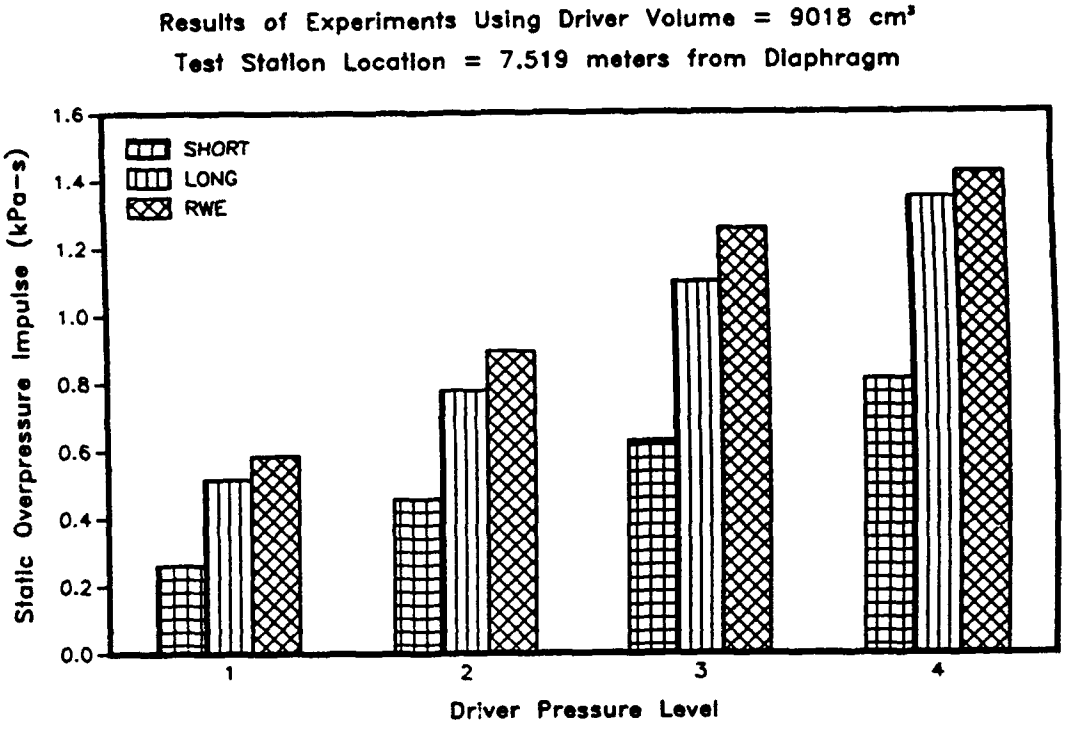

Figure 18. Comparison of Impulse for 9018 cm^3 Driver

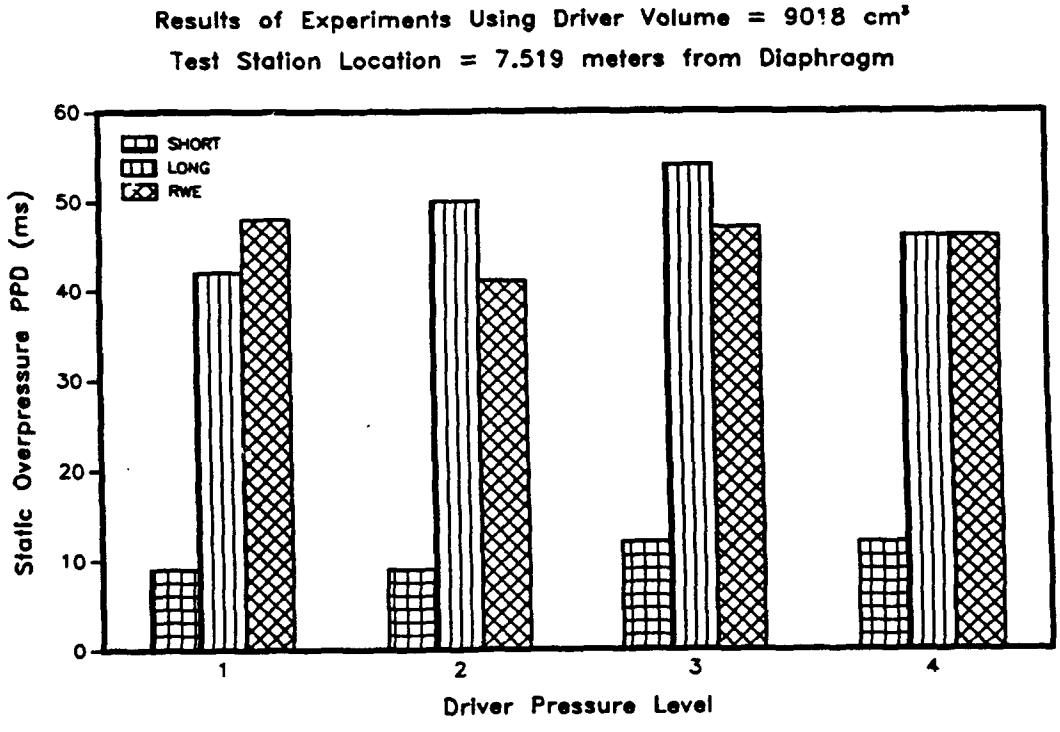

Figure 19. Comparison of Positive Phase Duration for 9018 cm^3 Driver

2. Results for the 4988 cm^3 Driver

The results of experiments using the 4988 cm^3 driver are presented in the same format as those of the previous driver. The experimental results for this driver are shown in Tables 5, 6 and 7. Figures 20 through 27 show the time histories obtained from some of the tests. The average long expansion section positive phase duration was about 30 ms. Therefore, the demand placed on the RWE by the functions should be greater for this driver than the larger one.

For this driver configuration the RWE followed the function well with the greatest error occurring late in the positive phase. The pressure-time histories also compare well for the long expansion and the RWE tests. Figures 28 and 29 illustrate the comparisons of impulse and positive phase duration. As expected, the impulse values for the long expansion and RWE tests were similar but not as close as those of the 9018 cm^3 driver, and the PPD for the short expansion tests were well below the others.

It is interesting to note that as the driver volume decreases, the difference between the short expansion and long expansion impulse values also decreases. This occurs because the flow in the test section has a shorter duration due to the decreased driver volume, leaving less time for the wave returning from the RWE to influence it.

Table 5. Static Overpressure for Driver Volume = 4988 cm^3

Diaphragm Thickness (in)	Static Overpressure (kPa) Station Location = 7.519 m from Diaphragm			
	Long Expansion	Short Expansion	RWE	Average
0.010	31.905	33.785	31.821	32.504
0.020	68.293	68.157	68.180	68.210
0.030	83.917	88.269	85.159	85.782
0.040	92.712	95.898	96.091	94.900

Table 6. Static Overpressure Impulse for Driver Volume = 4988 cm^3

Average Static Overpressure (kPa)	Static Overpressure Impulse ($kPa - s$) Station Location = 7.519 m from Diaphragm		
	Long Expansion	Short Expansion	RWE
32.504	0.219	0.143	0.273
68.210	0.466	0.345	0.571
85.782	0.598	0.469	0.763
94.900	0.731	0.547	0.811

Table 7. Positive Phase Duration for Driver Volume = 4988 cm^3

Average Static Overpressure (kPa)	Positive Phase Duration (ms) Station Location = 7.519 m from Diaphragm		
	Long Expansion	Short Expansion	RWE
32.504	26.0	7.0	30.0
68.210	29.0	8.0	30.0
85.782	33.0	9.0	36.0
94.900	29.0	9.0	37.0

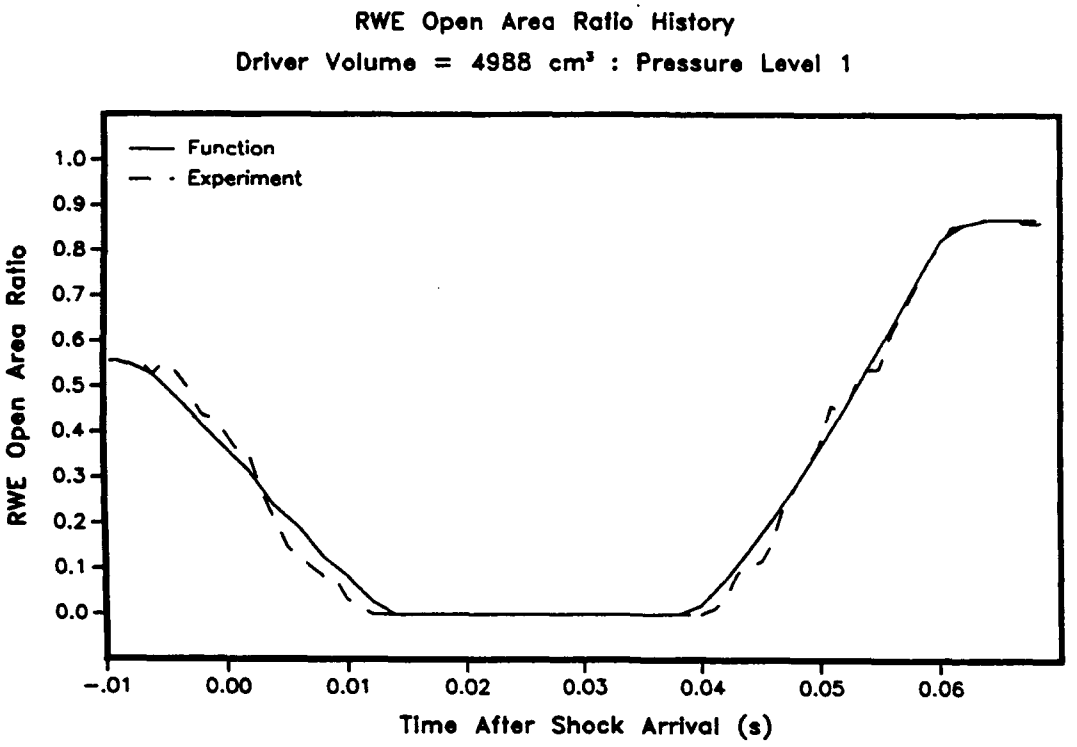

Figure 20. RWE Area History for 4988 cm^3 Driver; Pressure Level 1

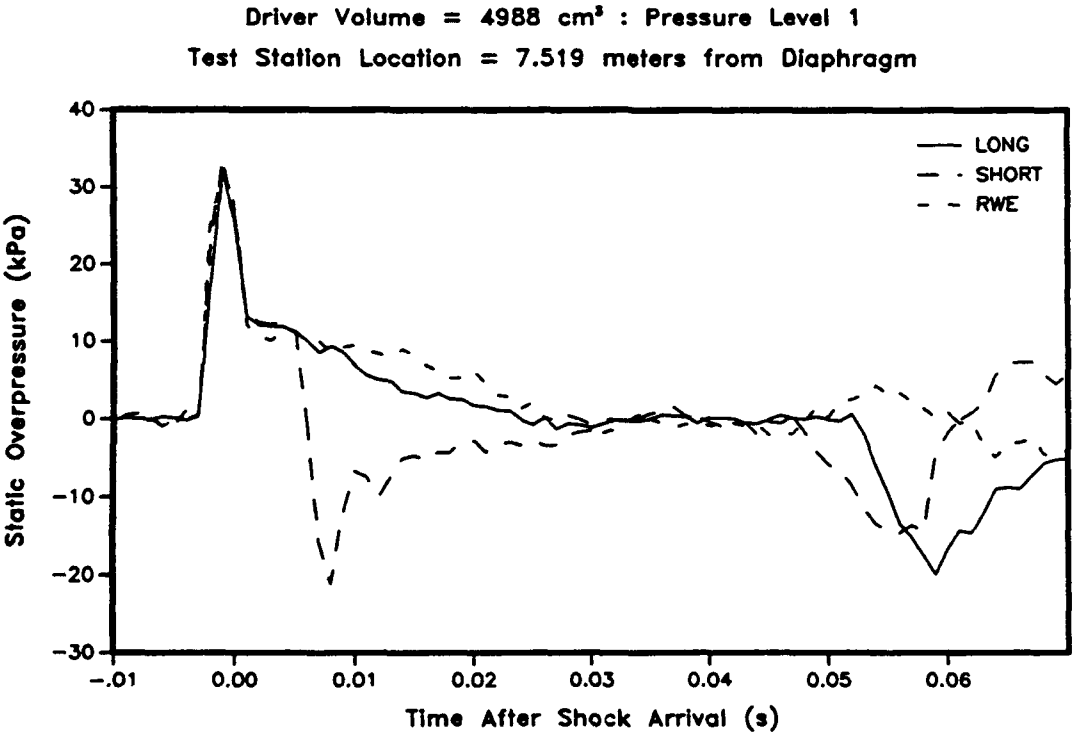

Figure 21. Pressure Histories for 4988 cm^3 Driver; Pressure Level 1

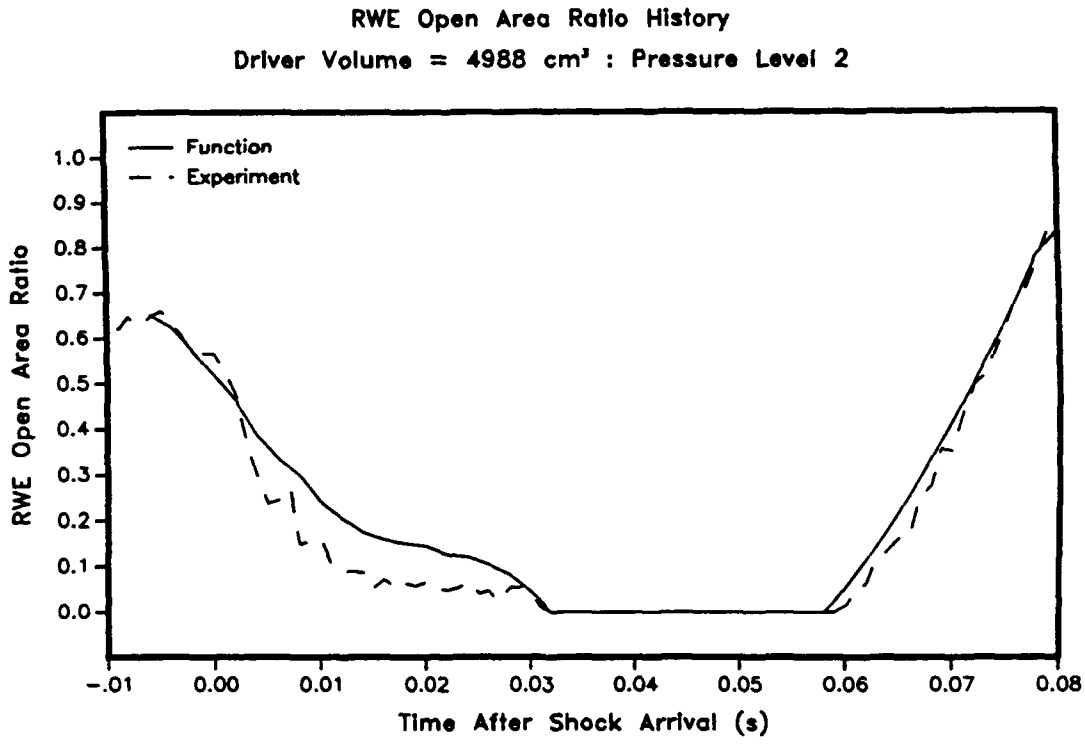

Figure 22. RWE Area History for 4988 cm^3 Driver; Pressure Level 2

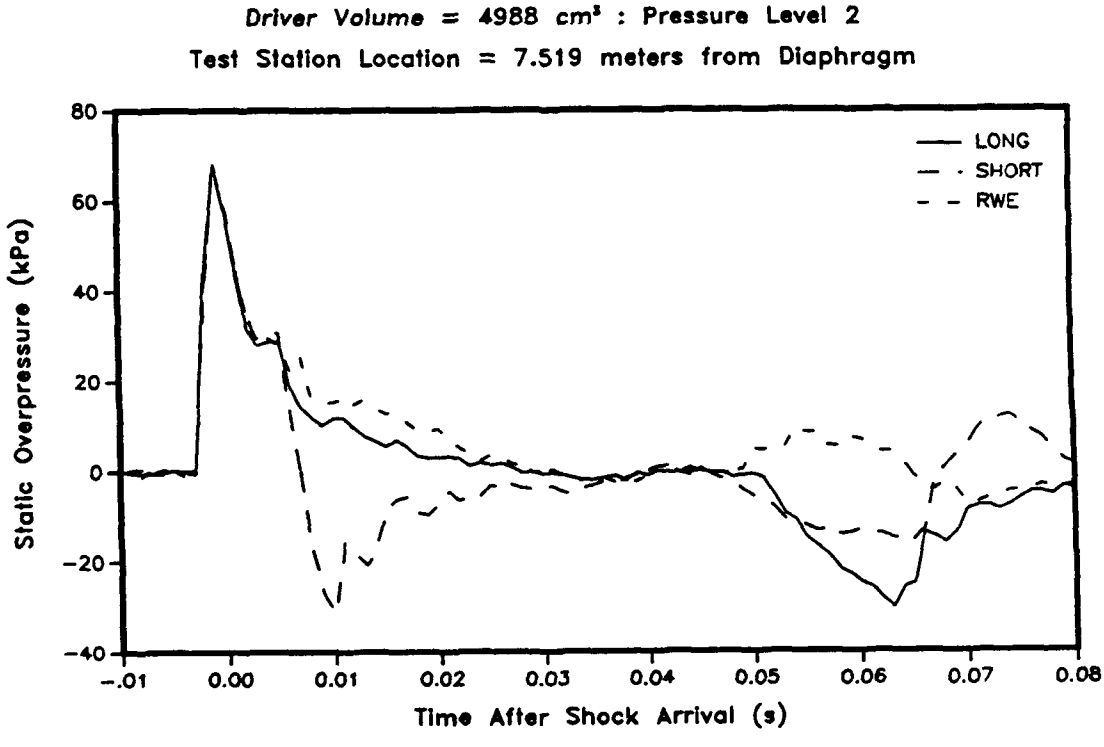

Figure 23. Pressure Histories for 4988 cm^3 Driver; Pressure Level 2

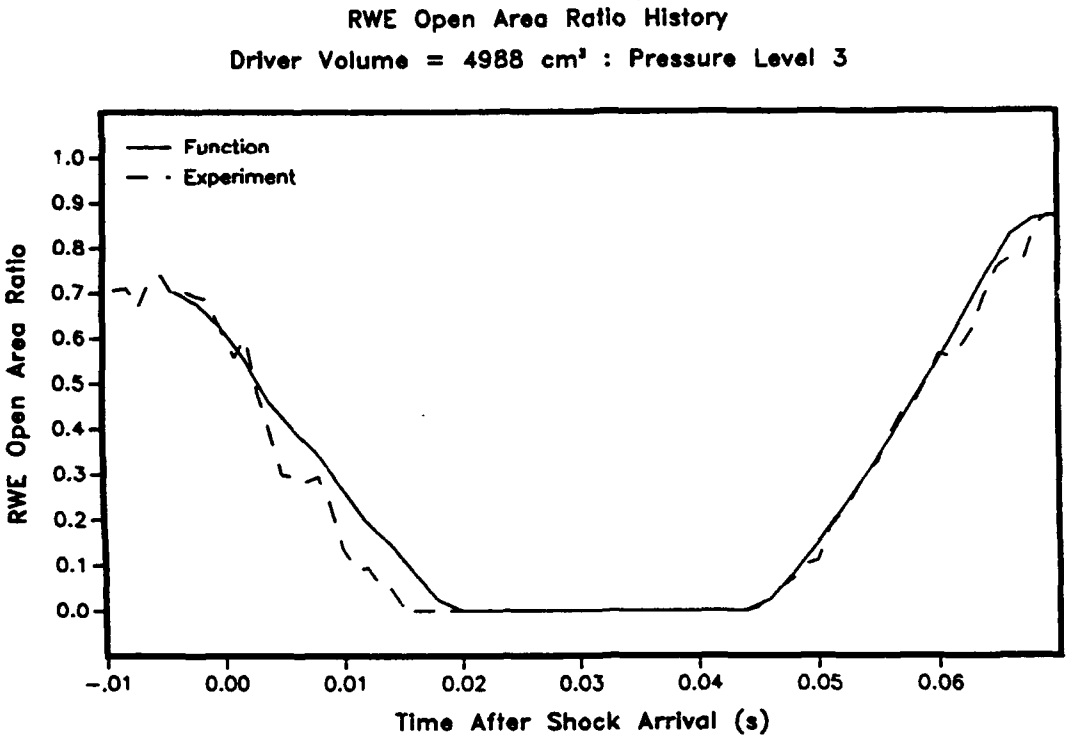

Figure 24. RWE Area History for 4988 cm^3 Driver; Pressure Level 3

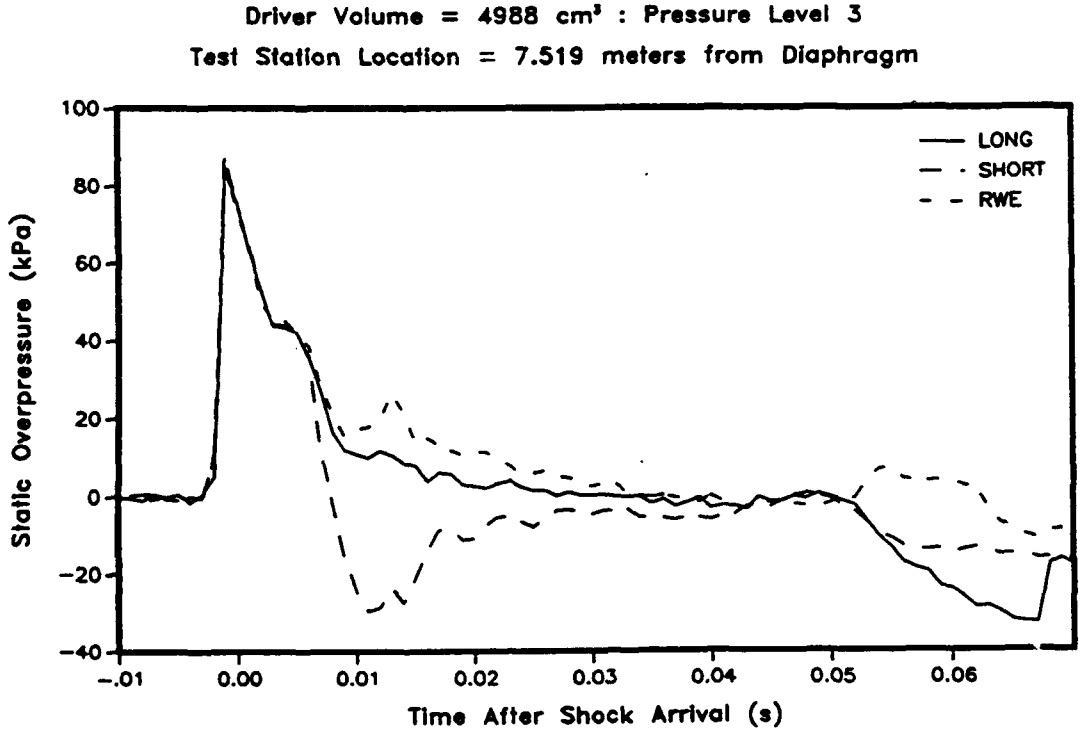

Figure 25. Pressure Histories for 4988 cm^3 Driver; Pressure Level 3

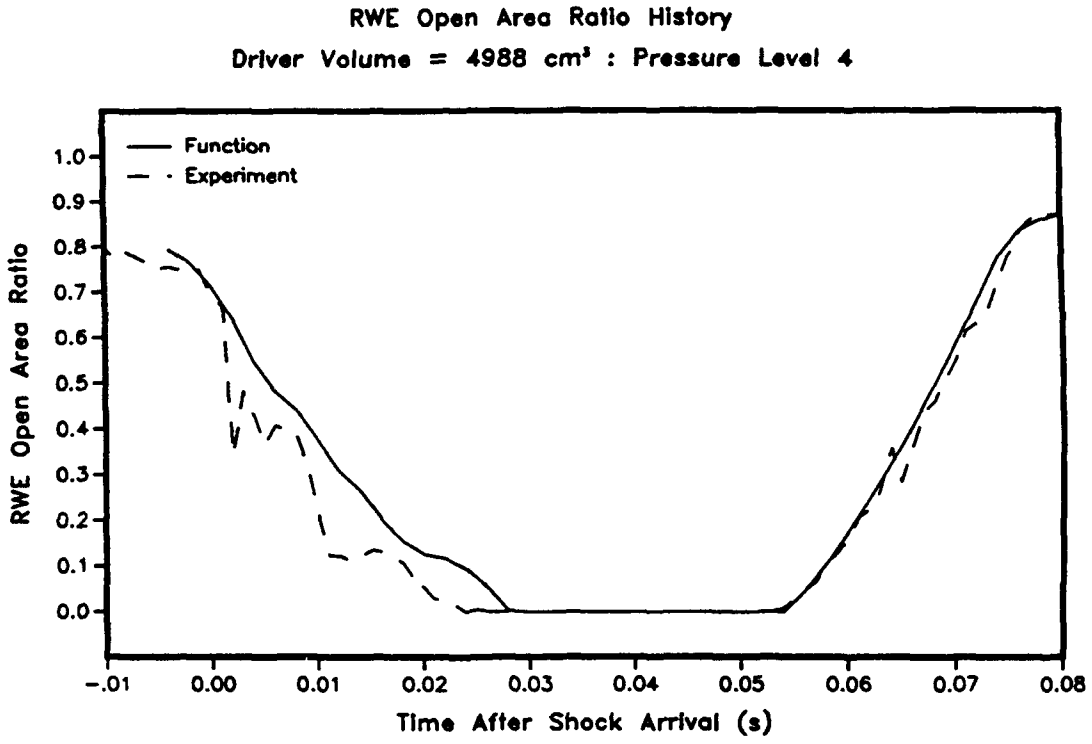

Figure 26. RWE Area History for 4988 cm^3 Driver; Pressure Level 4

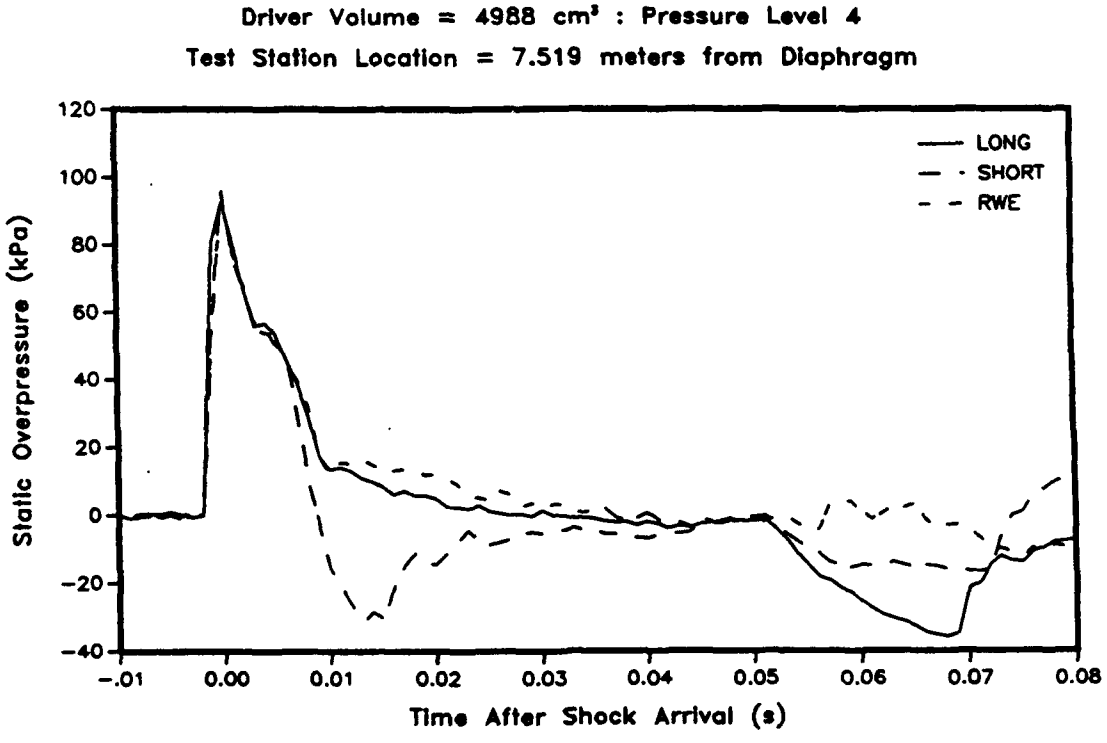

Figure 27. Pressure Histories for 4988 cm^3 Driver; Pressure Level 4

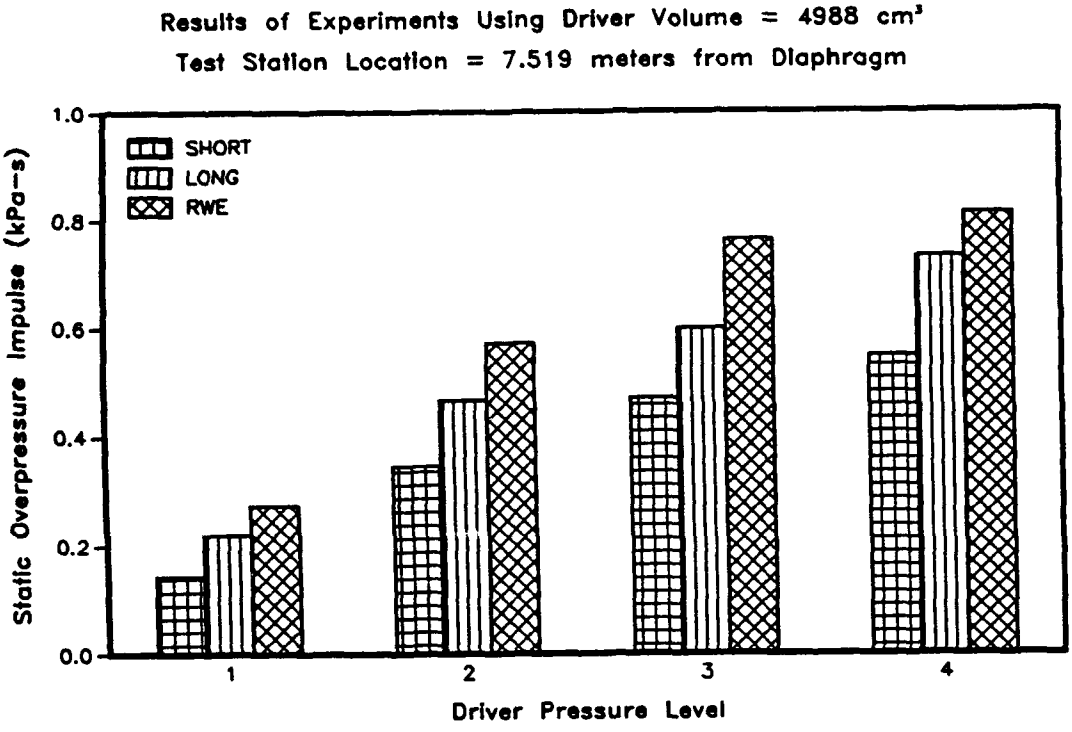

Figure 28. Comparison of Impulse for 4988 cm^3 Driver

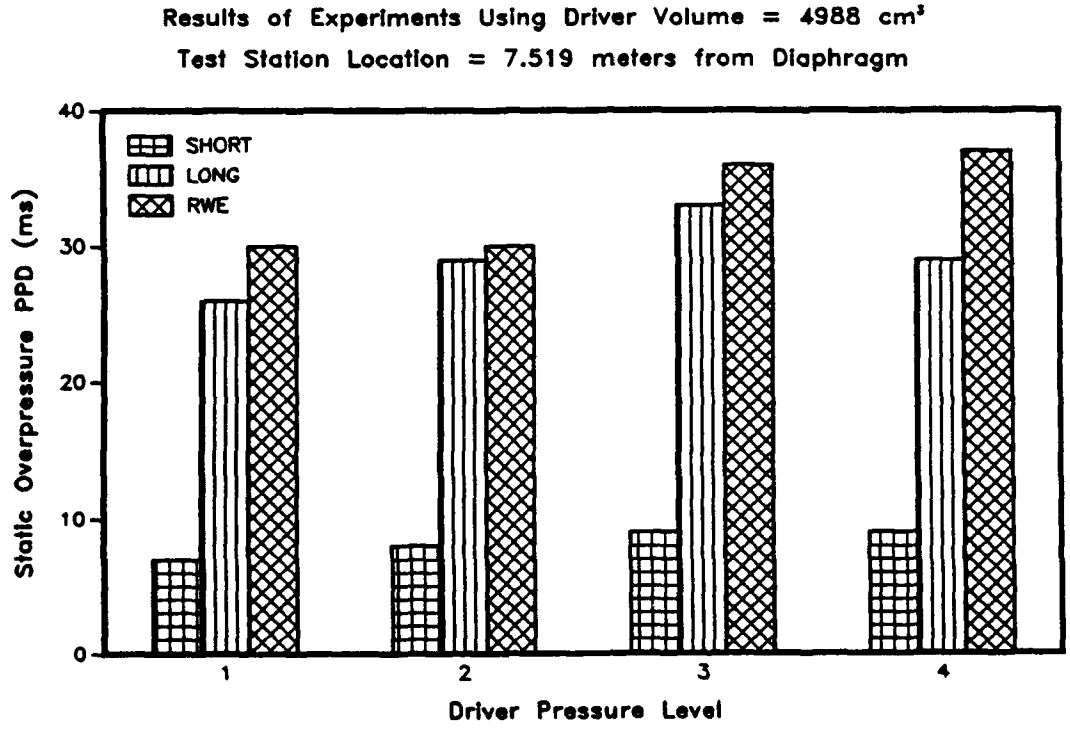

Figure 29. Comparison of Positive Phase Duration for 4988 cm^3 Driver

3. Results for the 2840 cm^3 Driver

Finally, the results of the tests using the 2840 cm^3 driver are presented in Tables 8, 9 and 10 and in Figures 30 through 37. Again, the format is the same as the previous sets. The PPD for the long expansion section tests using this driver averaged 15 ms. This short PPD indicated that the RWE would function only marginally as intended. This supposition was proved correct in the experiments using the active RWE.

The charts in Figures 38 and 39 show the marginal success of the RWE in these tests. The impulse values of the RWE tests compare well with those of the long expansion section tests. However, the positive phase duration results are quite different. This means the RWE could not close rapidly enough to eliminate the rarefaction wave for two of the four pressure levels.

The pressure-time histories in Figures 33 and 37 show a slight rarefaction formed in the RWE trace of each figure. It is also interesting to note that for these shots, the greatest error in the RWE history occurs in the early part of the positive phase as illustrated in Figure 32. In most of the other active RWE tests, the RWE history was accurate early in the positive phase but deviated from the input function late in the positive phase. Comparison of these figures indicates that in order to eliminate a rarefaction wave the accuracy of the RWE area is most critical early in the positive phase. Louver position errors which occur late in the positive phase have little effect on the resulting pressure history.

Table 8. Static Overpressure for Driver Volume = 2840 cm^3

Diaphragm Thickness (in)	Static Overpressure (kPa) Station Location = 7.519 m from Diaphragm			
	Long Expansion	Short Expansion	RWE	Average
0.010	51.013	34.865	42.074	42.651
0.020	61.044	67.271	70.515	66.277
0.030	81.868	74.481	74.264	76.871
0.040	101.025	86.395	89.187	92.202

Table 9. Static Overpressure Impulse for Driver Volume = 2840 cm^3

Average Static Overpressure (kPa)	Static Overpressure Impulse ($kPa - s$) Station Location = 7.519 m from Diaphragm		
	Long Expansion	Short Expansion	RWE
42.651	0.171	0.108	0.179
66.277	0.298	0.227	0.257
76.871	0.392	0.314	0.441
92.202	0.457	0.369	0.444

Table 10. Positive Phase Duration for Driver Volume = 2840 cm^3

Average Static Overpressure (kPa)	Positive Phase Duration (ms) Station Location = 7.519 m from Diaphragm		
	Long Expansion	Short Expansion	RWE
42.651	15.0	7.5	18.0
66.277	16.5	7.5	9.0
76.871	15.5	8.5	22.5
92.202	13.5	9.0	10.0

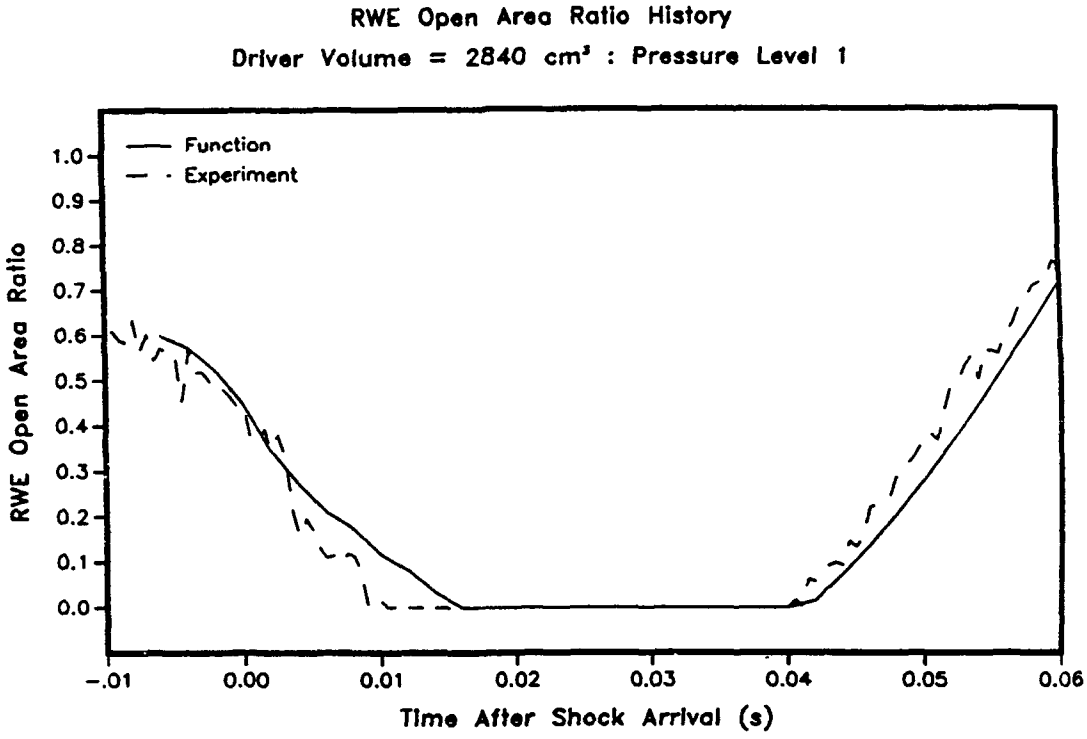

Figure 30. RWE Area History for 2840 cm^3 Driver; Pressure Level 1

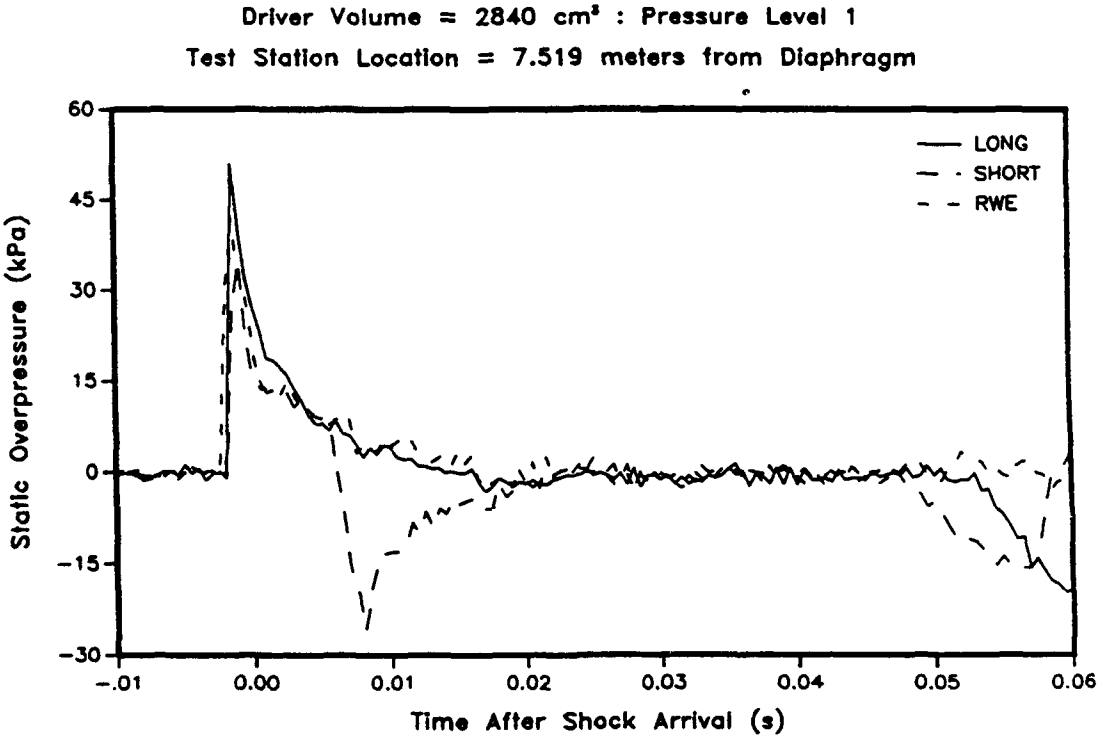

Figure 31. Pressure Histories for 2840 cm^3 Driver; Pressure Level 1

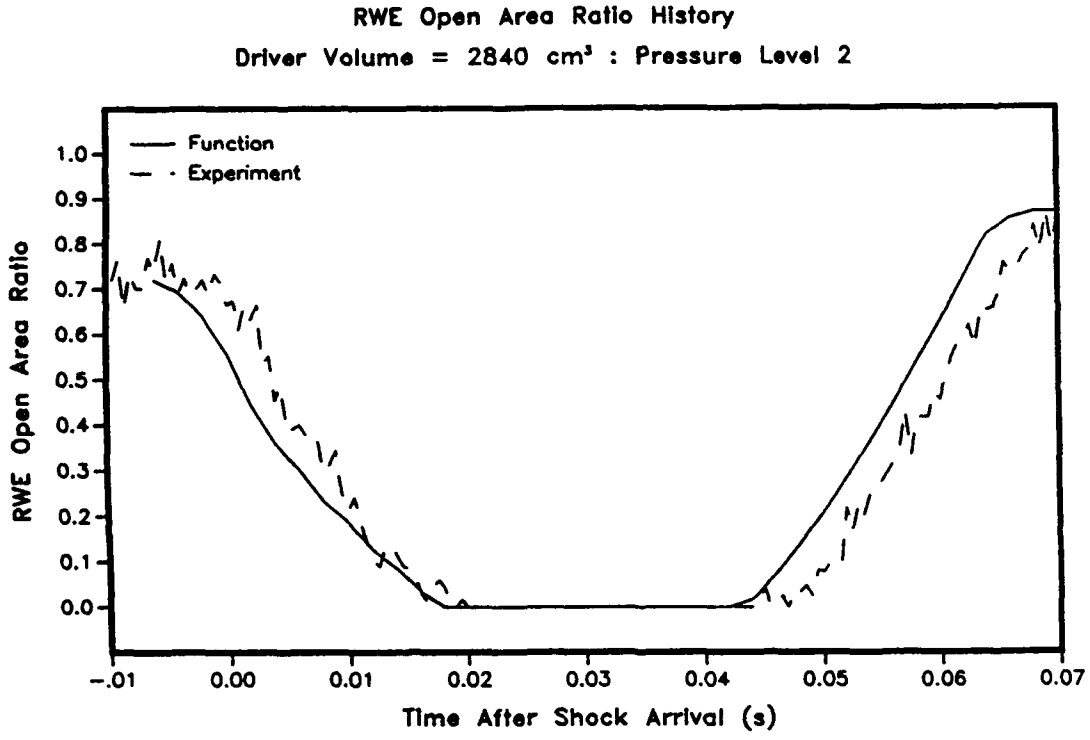

Figure 32. RWE Area History for 2840 cm^3 Driver; Pressure Level 2

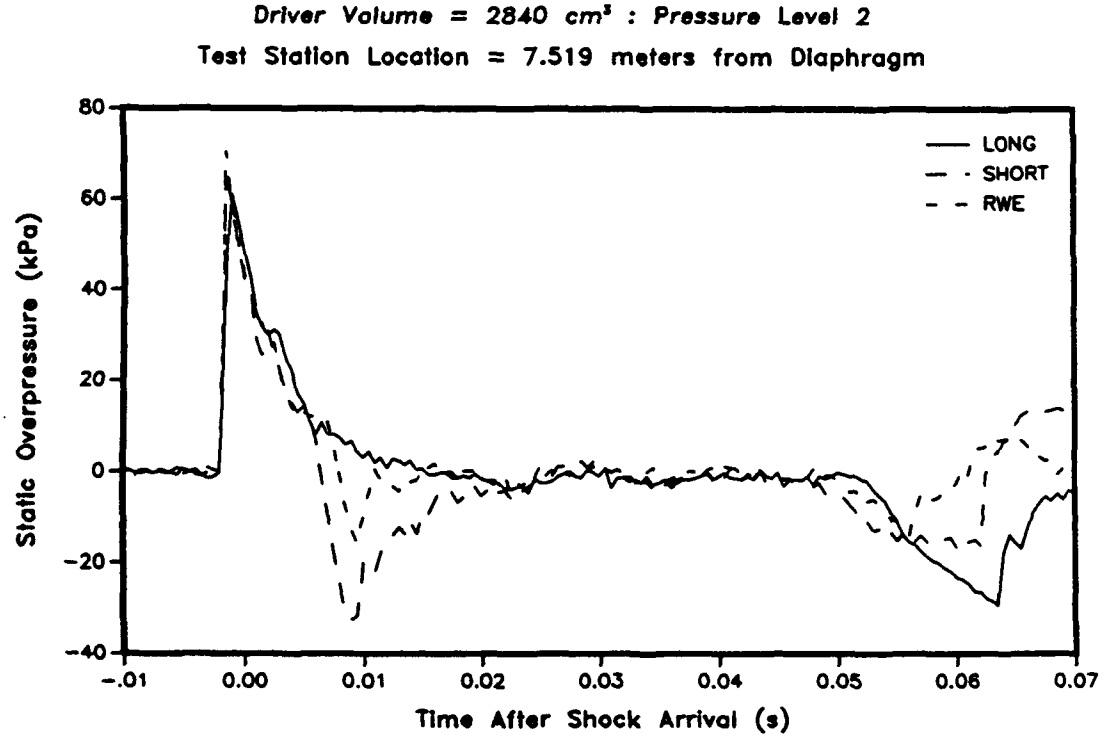

Figure 33. Pressure Histories for 2840 cm^3 Driver; Pressure Level 2

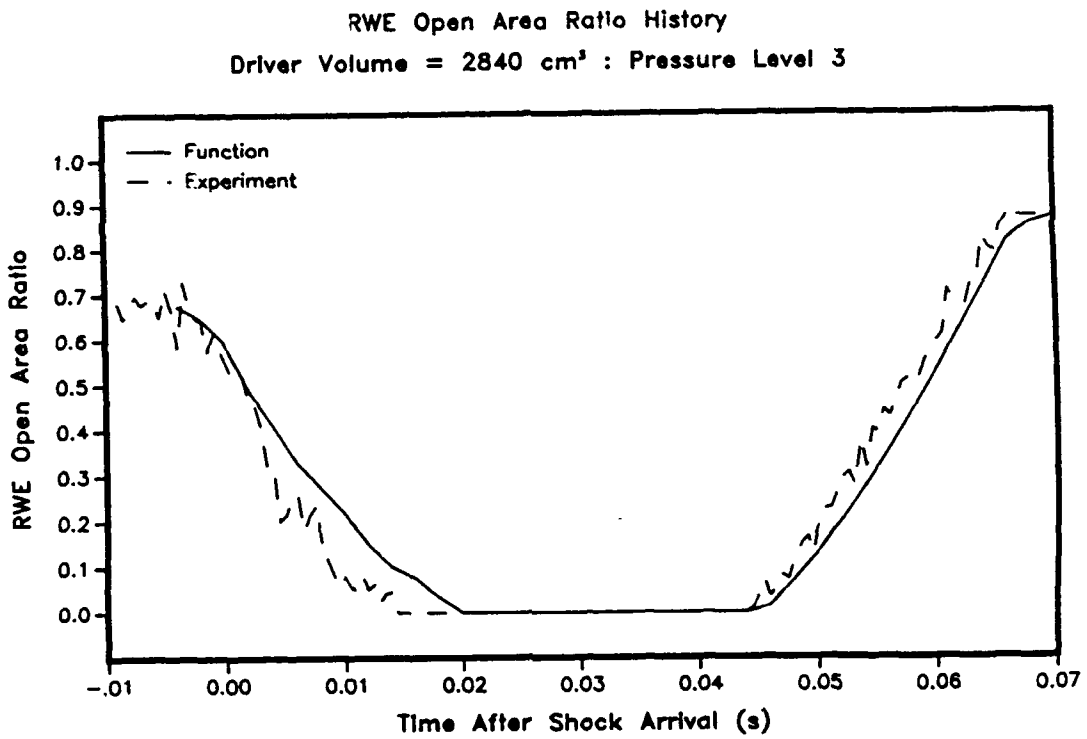

Figure 34. RWE Area History for 2840 cm^3 Driver; Pressure Level 3

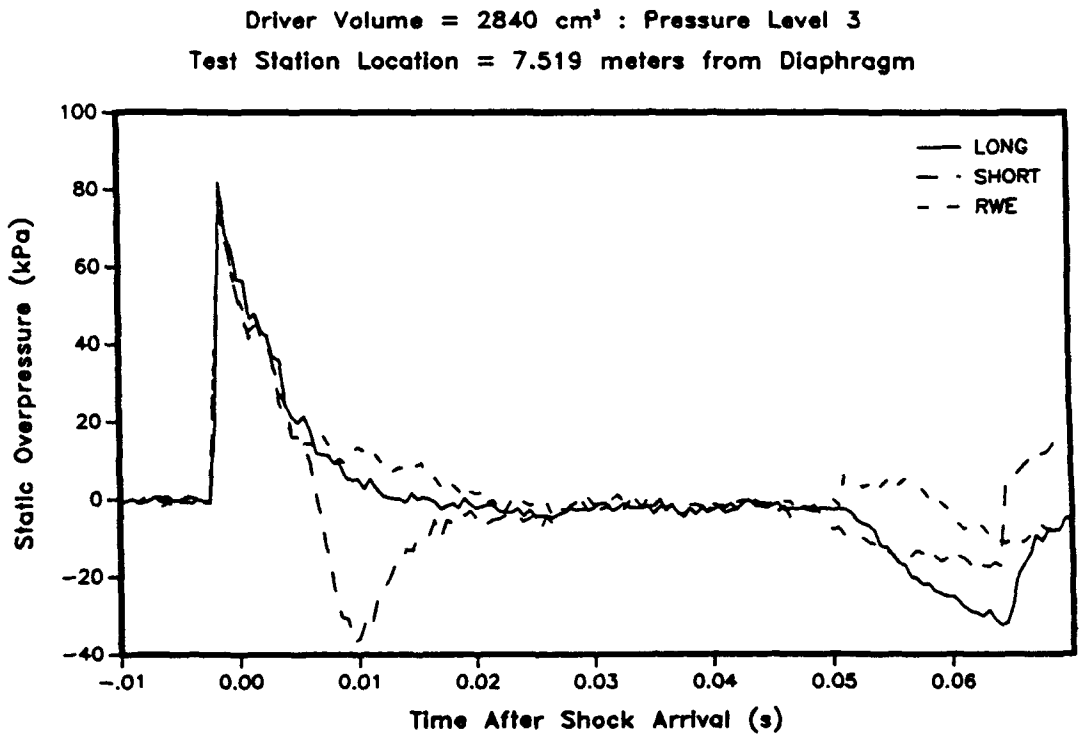

Figure 35. Pressure Histories for 2840 cm^3 Driver; Pressure Level 3

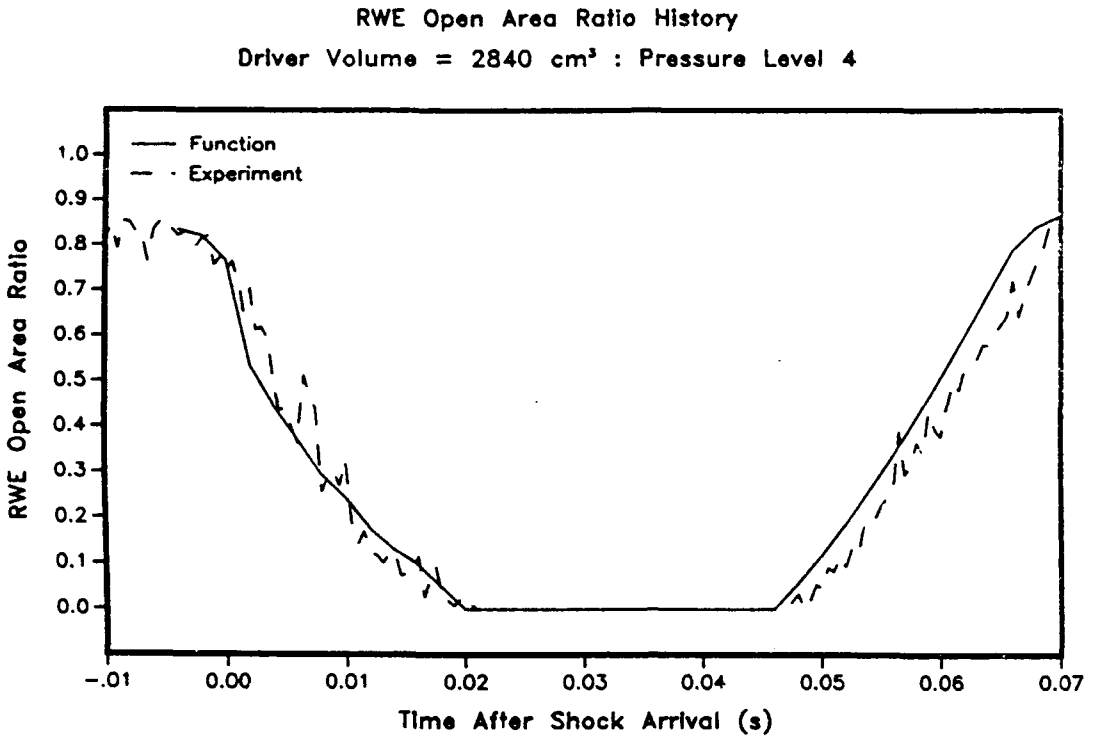

Figure 36. RWE Area History for 2840 cm^3 Driver; Pressure Level 4

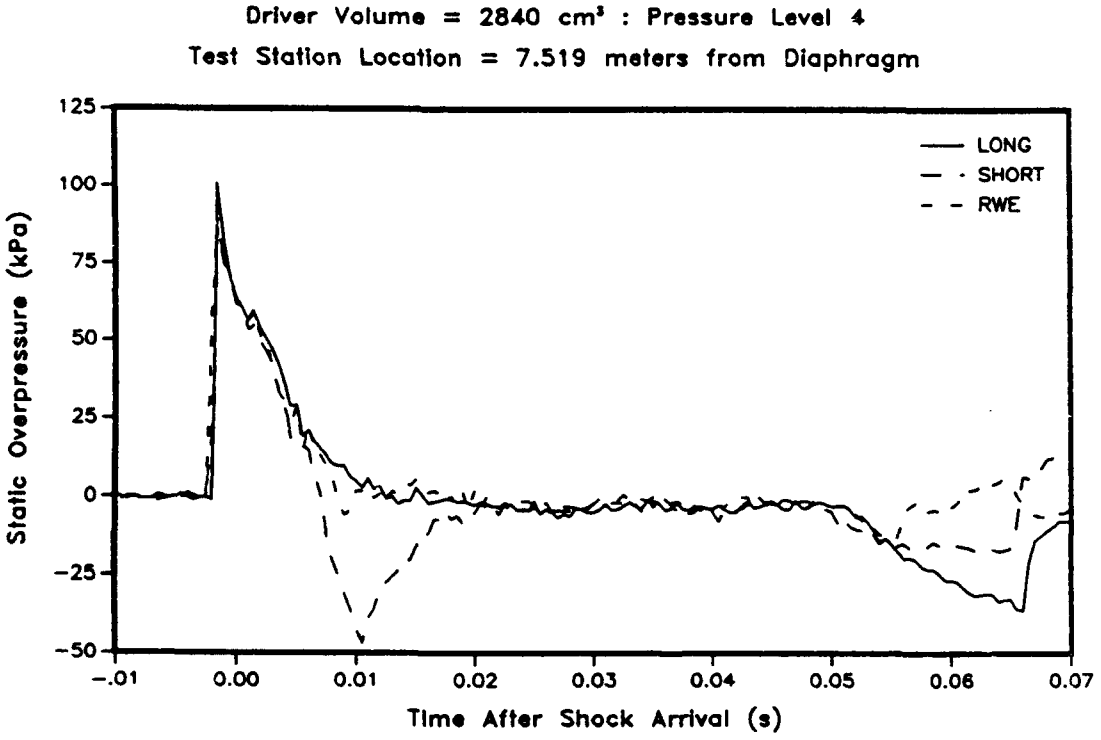

Figure 37. Pressure Histories for 2840 cm^3 Driver; Pressure Level 4

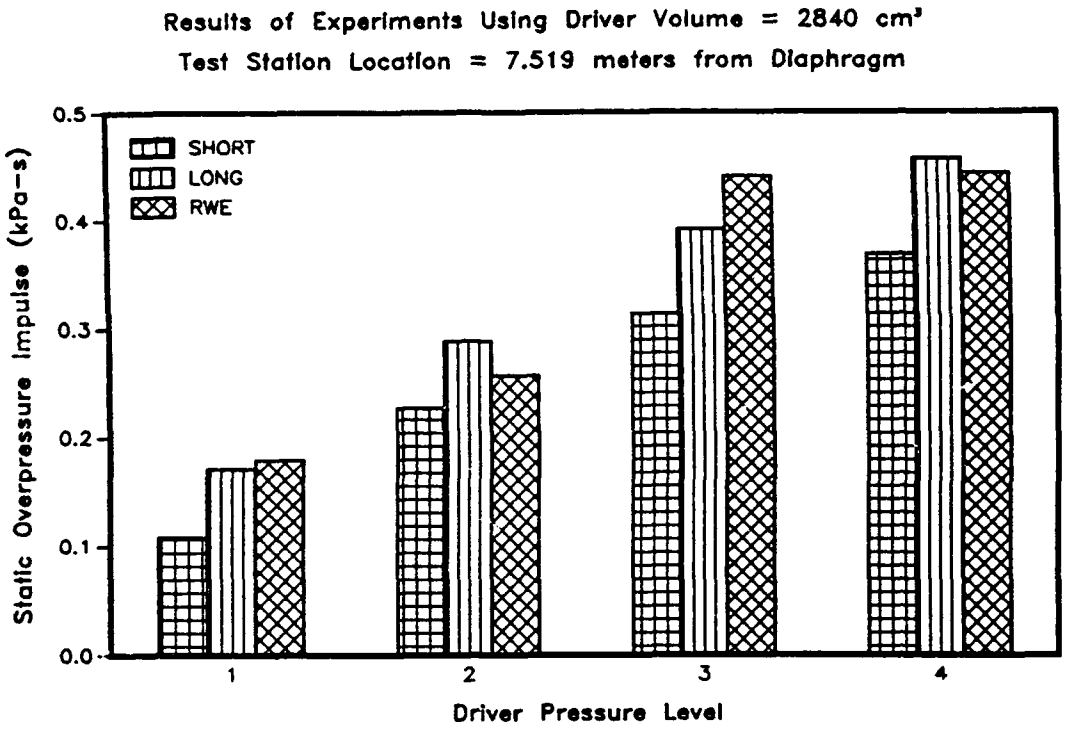

Figure 38. Comparison of Impulse for 2840 cm^3 Driver

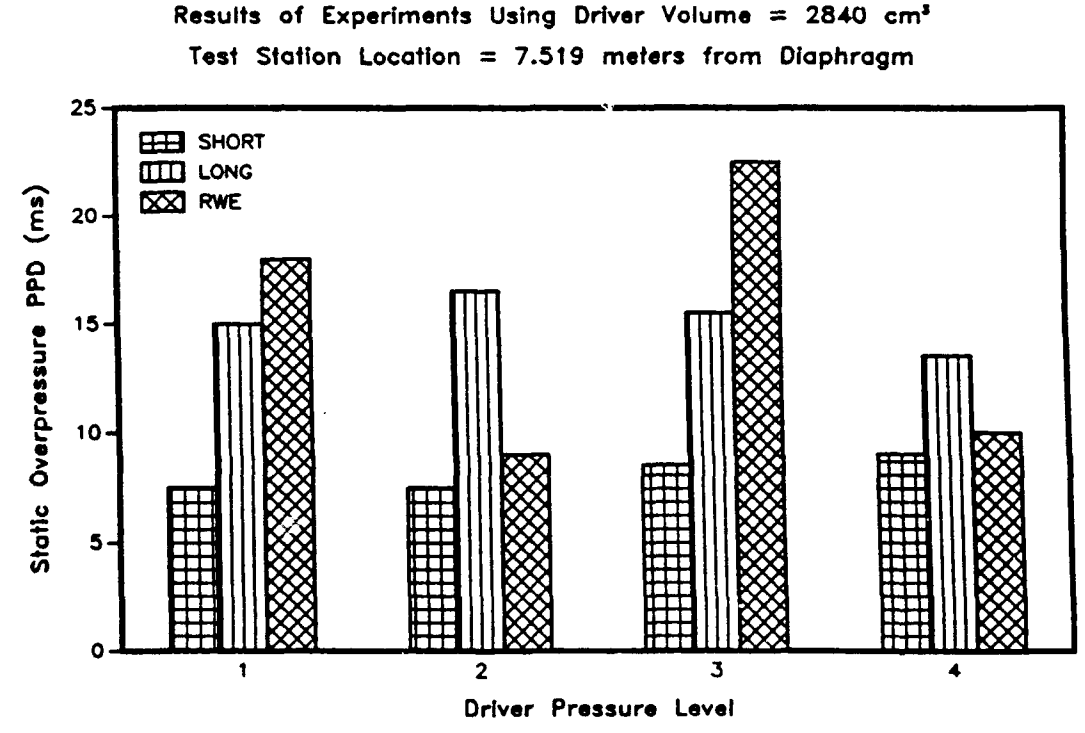

Figure 39. Comparison of Positive Phase Duration for 2840 cm^3 Driver

4. Improving on the Results

The experimental results showed that in many tests the RWE failed to follow the input function at certain times during the test. In many cases this tracking error had little effect on the resulting pressure-time histories, while in some cases it had a significant effect. These tracking errors can be attributed to three causes:

1. The motor was not able to accelerate the louvers quickly enough to follow the input function.
2. The motor accelerated the louvers properly but was unable to decelerate enough to follow the input function, resulting in the overshoot discussed with the results of the tests with the 9018 cm^3 driver.
3. The 2 ms sampling rate of the motor was too coarse to provide accurate following of the input function.

The first two of these three causes could be overcome by using a similar motor but one with greater torque and speed capabilities. The solution to the third cause is to find a motor with a better sampling rate ($0.25 - 0.50$ ms). The important point here is that all of the problems experienced with the RWE were problems that could have been solved by changing or improving the equipment. No physically insurmountable problems were discovered during the course of the testing. That was the overall goal of this project; not to build a perfect small scale RWE, but to prove that the flow theory behind the development of this RWE was sound, and also to provide a knowledge base for larger scale RWE work. In this respect the program is a success.

VIII. Conclusions

Experiments have been performed to determine the effectiveness of an active rarefaction wave eliminator (RWE) in controlling the gas flow from the exit of a shock tube. The purpose of the tests was to validate previously developed RWE flow theory. The shock tube used was the 1:57 scale blast simulator intended to study the flow phenomena that will occur in the Large Blast/Thermal Simulator being developed by the Defense Nuclear Agency. Use of a rarefaction wave eliminator is necessary in order to simulate high yield nuclear events with a relatively short shock tube.

The tests outlined in this report employed three different driver volumes, four driver pressure levels and three expansion section configurations, resulting in a total of 36 shots. Success or failure of the RWE was determined by comparing results of active RWE tests with similar long expansion section (no RWE) tests.

The test results show that the RWE did indeed eliminate the rarefaction wave formed at the exit plane of the shock tube. The results obtained using the two largest driver volumes

showed good agreement between long expansion section section shots and shots using the RWE. The results gathered from the smallest driver volume tests yielded marginal results. The short positive phase duration associated with this volume had the RWE operating at or beyond its limits of torque and velocity.

The final RWE functions outlined in this report were the result of many iterations of test, analyze and re-test. Numerous preliminary tests were conducted before the main test series results were obtained. In particular, a great deal of experimentation was performed before the correct relationship between louver angle and RWE open area ratio could be realized.

The scale on which this program was performed allowed for relatively simple changes in shock tube configuration and rapid turnaround between tests. This allowed us to learn a great deal in a very short time. This new knowledge will be a valuable asset when working on the 1:6 scale and full scale rarefaction wave eliminators.

The theory which was validated by these experiments is not influenced by the size of the system being tested. Therefore, this same theory should work for the 1:6 scale and full scale systems. However, parameters such as bearing friction, louver inertia and material stresses will not scale. It is parameters such as these that drive the design of the control system for these devices. Simply scaling up the size of the electric servomotor used in these experiments by a factor of 57 will not yield an appropriate control system for the full scale RWE.

INTENTIONALLY LEFT BLANK.

References

1. Kingery, C.N. and Coulter, G.A., "Rarefaction Wave Eliminator Concepts for Large Blast/Thermal Simulators," BRL-TR-2634, US Army Ballistic Research Laboratory, Aberdeen Proving Ground, Maryland 21005, February 1985.

2. Guice, R.L. and Gottlieb, J.J., "Passive and Active Reflection Eliminators," Proceedings of the 10^{th} International Symposium on Military Applications of Blast Simulation, 21-25 September 1987, Erprobungsstelle 52 der Bundeswehr Oberjettenberg, D-8230 Schneizlreuth, FR-Germany.

3. Guice, R.L., Gottlieb, J.J., Butz, J.R., Pearson, R.J. and Opalka, K. O., "Experimental Performance of a Small Scale Active Reflection Eliminator," Proceedings of the 11^{th} International Symposium on Military Applications of Blast Simulation, 10-15 September 1989, US Army Ballistic Research Laboratory, Aberdeen Proving Ground, Maryland 21005.

4. Parker-Compumotor Corporation, "KS-Series Operator's Manual," P/N 88-007042-01Y, 25 May 1987.

5. Zucrow, M.J., and Hoffman, J.D., 1976, "Gas Dynamics," John Wiley & Sons, Inc., page 141.

6. Zucrow, M.J., and Hoffman, J.D., 1976, "Gas Dynamics," John Wiley & Sons, Inc., page 136.

7. Opalka, K.O. and Mark, A., "The BRL-Q1D Code: A Tool for the Numberical Simulation of Flows in Shock Tubes with Variable Cross-Sectional Areas," BRL-TR-2763, US Army Ballistic Research Laboratory, Aberdeen Proving Ground, Maryland 21005, October 1986.

8. Guice, R.L., Private Communication, 7 November 1988.

INTENTIONALLY LEFT BLANK.

APPENDIX A: Velocity and Acceleration Limit Calculations

Before the closing/opening functions for the RWE could be derived, the capabilities of the machine had to be determined. Once the functional limits of the device are known, functions can be generated in such a way that these limits will not be exceeded during the course of the testing. Also, knowing what these limits are will enable users of the RWE to anticipate its effectiveness prior to a test to allow optimum utilization of its capabilities.

In order to calculate the maximum angular acceleration of the RWE, the mass moment of inertia of each rotating component must be determined. The first component examined is one of the rotating louvers which is shown in Figure A-1.

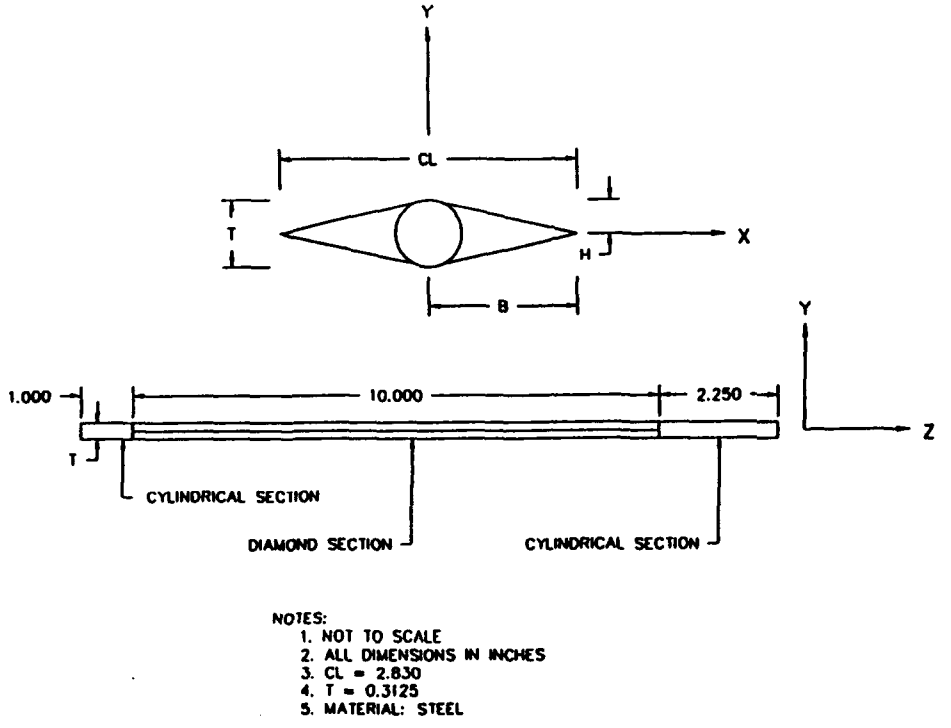

Figure A-1: Diamond Shaped Louver

The equation used to calculate the mass moment of inertia for the diamond shaped section of the louvers is shown in Equation (A-1).

$$I_d = \frac{\rho hbl}{3}(h^2 + b^2) \qquad \text{(A-1)}$$

In this equation, ρ is the density of steel and is 7849 kg/m^3. The other values can be obtained from Figure A-1. Solving this equation yields a mass moment of inertia of 1.239×10^{-4} $kg-m^2$ for the diamond shaped section of one louver.

The inertia of the remaining portions of the louver must be calculated next. These two sections are both cylindrical and can therefore be lumped together for this calculation. Equation (A-2) illustrates the means of calculating this value.

$$I_c = \frac{\rho \pi l r^4}{2} \qquad \text{(A-2)}$$

In this equation l is the total length of the cylindrical sections and r is the radius of the cylindrical section. Substitution of these values into Equation (A-2) yields $2.525 \times 10^{-7}\ kg - m^2$. When added to the value obtained from Equation (A-1) the total mass moment of inertia for one louver can be determined as seen in Equation (A-3).

$$I_{louver} = I_d + I_c = 1.242 \times 10^{-4}\ kg - m^2 \tag{A-3}$$

Connected to each louver is an aluminum gear ($\rho = 2730\ kg/m^3$). The mass moment of inertia of these gears must also be calculated. A diagram of the gear is given in Figure A-2.

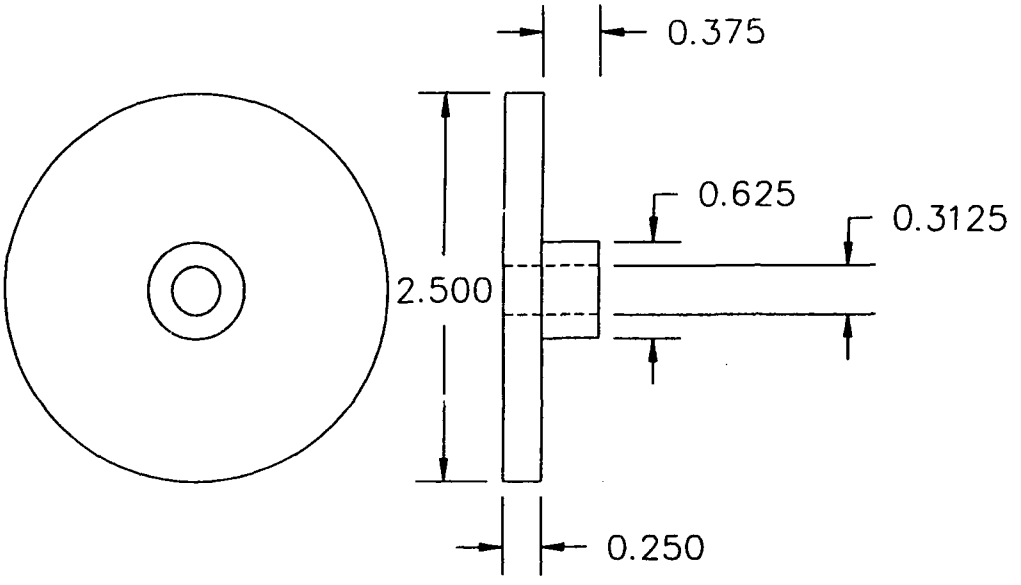

NOTES:

1. ALL DIMENSIONS IN INCHES
2. MATERIAL: ALUMINUM

Figure A-2: 2.5 Inch Louver Gear

The mass moment of inertia for this gear is calculated using Equation (A-4).

$$I = \frac{\rho \pi l (r_o^4 - r_i^4)}{2} \tag{A-4}$$

The total inertia for the gear is determined by summing the inertia values calculated for regions A and B. The result for one gear is $2.782 \times 10^{-5}\ kg - m^2$.

From this, the total mass moment of inertia for one louver/gear arrangement is calculated through use of Equation (A-5).

$$I_l = I_{gear} + I_{louver} = 1.520 \times 10^{-4}\ kg - m^2 \tag{A-5}$$

In order to calculate the maximum louver angular acceleration, other characteristics of the device are required. These are summarized below.

- Peak torque of the motor $= T_p = 6.36\ N - m$
- Rotor and drive shaft inertia $= I_d = 350.0 \times 10^{-6}\ kg - m^2$
- Radius of louver gear $= r_l = 0.03175\ m$
- Radius of drive gear $= r_d = 0.01270\ m$
- Angular acceleration of louvers $= \ddot{\theta}_l$
- Angular acceleration of drive shaft $= \ddot{\theta}_d$

The sum of torques on a body is equal to the mass moment of inertia of the body about the axis of rotation multiplied by the angular acceleration of the body. By performing this analysis on the gear train of the RWE, the maximum angular acceleration can be obtained. Equation (A-6) is the summing of torques on the drive shaft.

$$T_p - T_l = I_d \ddot{\theta}_d \tag{A-6}$$

Since the four louver/gear assemblies are all identical, the total torque that they provide to the drive shaft is simply four times that of one louver assembly. This torque is defined in Equation (A-7).

$$T_l = \frac{4 I_l \ddot{\theta}_l r_d}{r_l} \tag{A-7}$$

The relationship between the motion of the drive shaft and the motion of a louver is represented by $r_d \ddot{\theta}_d = r_l \ddot{\theta}_l$. By substituting this equation and Equation (A-7) into Equation (A-6) the maximum louver angular acceleration reduces to Equation (A-8).

$$\ddot{\theta}_d = \frac{T_p}{[(I_d r_l / r_d) + (4 I_l r_d / r_l)]} \tag{A-8}$$

When Equation (A-8) is solved, the maximum louver angular acceleration turns out to be $5687.6\ rad/s^2$.

To be sure that the capabilities of the motor would not be exceeded, the maximum angular acceleration was reduced to $5000\ rad/s^2$ from $5687.6\ rad/s^2$.

The rated speed of the motor is listed as $1100\ rev/min$ which is equivalent to $115.2\ rad/s$. By using the relation $r_d \dot{\theta}_d = r_l \dot{\theta}_l$, the maximum louver angular velocity turns out to be $46.08\ rad/s$. Again, to remain safely within the limitations of the motor, this value was reduced to $43\ rad/s$. By using Equation (A-9), the number of motor angular units (MAU) displaced at this velocity in a $2\ ms$ time interval can be found.

$$\left(\frac{43\ rad}{s}\right)\left(\frac{180^\circ}{\pi\ rad}\right)\left(\frac{25000\ MAU}{360^\circ}\right)(0.002\ s) = 342\ MAU \tag{A-9}$$

With these values known, the functions can be developed in such a way that the operational limits of the motor will not be exceeded.

APPENDIX B: Pressure Histories for all Measurement Stations

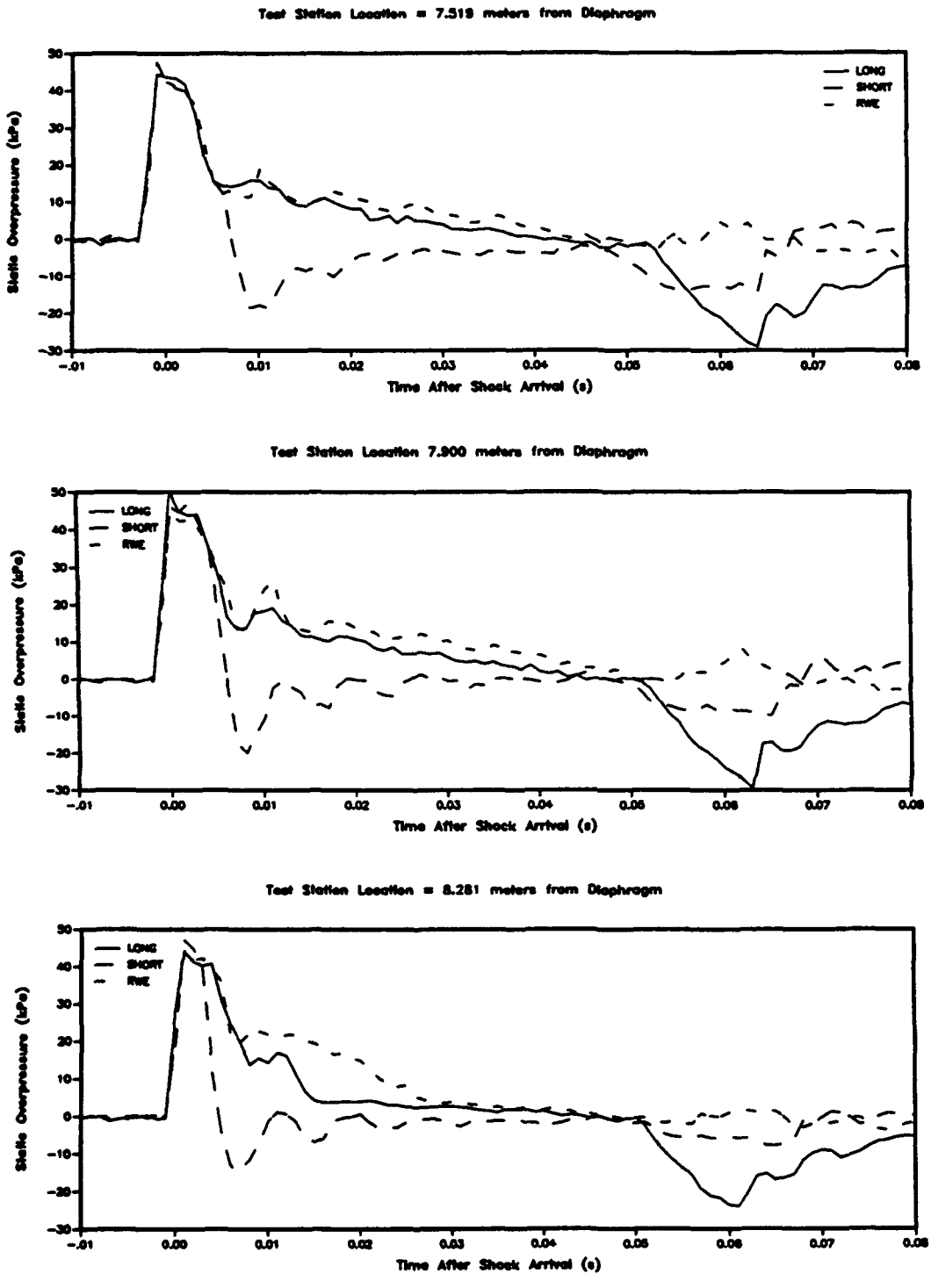

Figure B-1: Pressure Histories for 9018 cm^3 Driver; Pressure Level 1

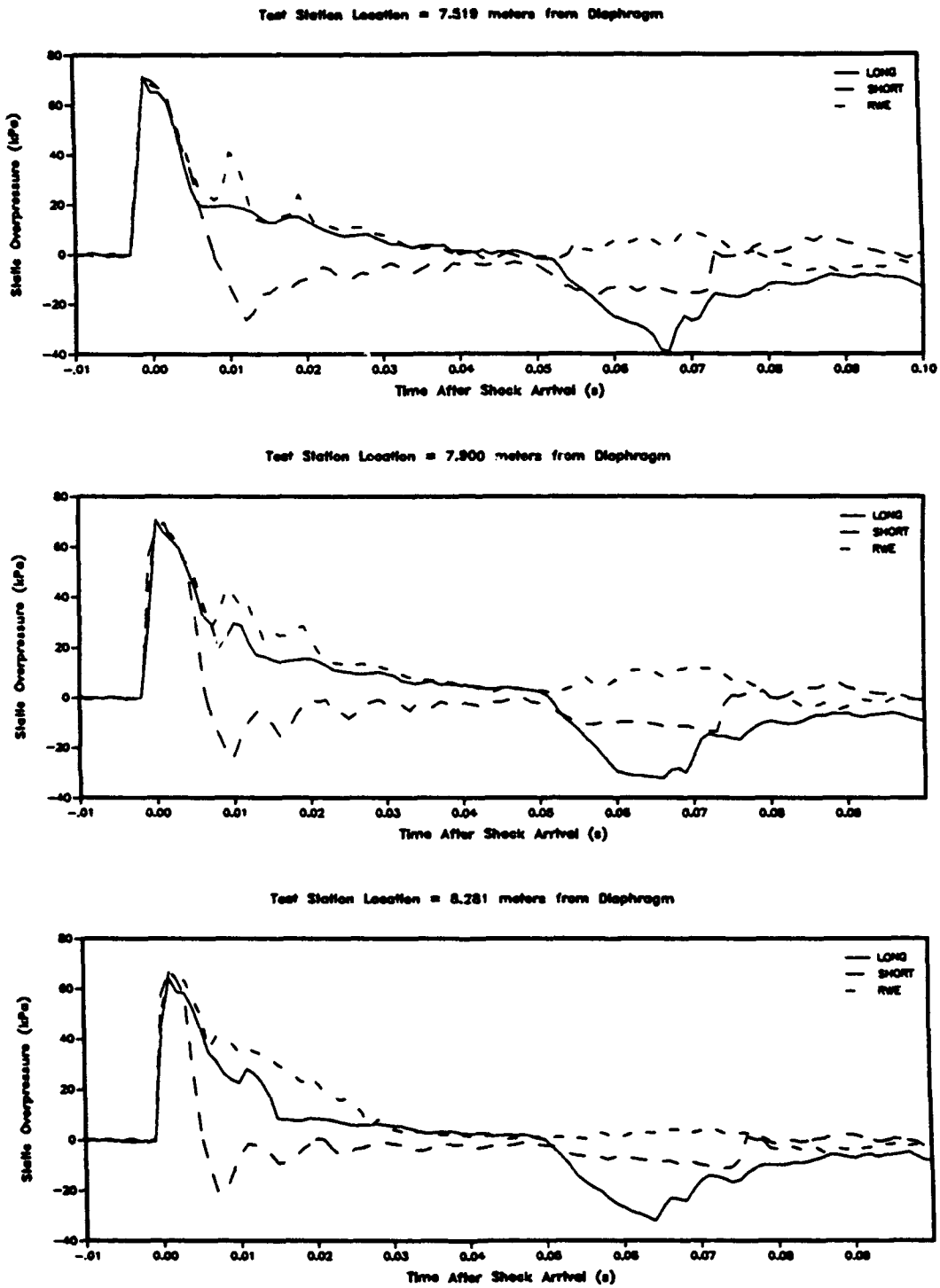

Figure B-2: Pressure Histories for 9018 cm^3 Driver; Pressure Level 2

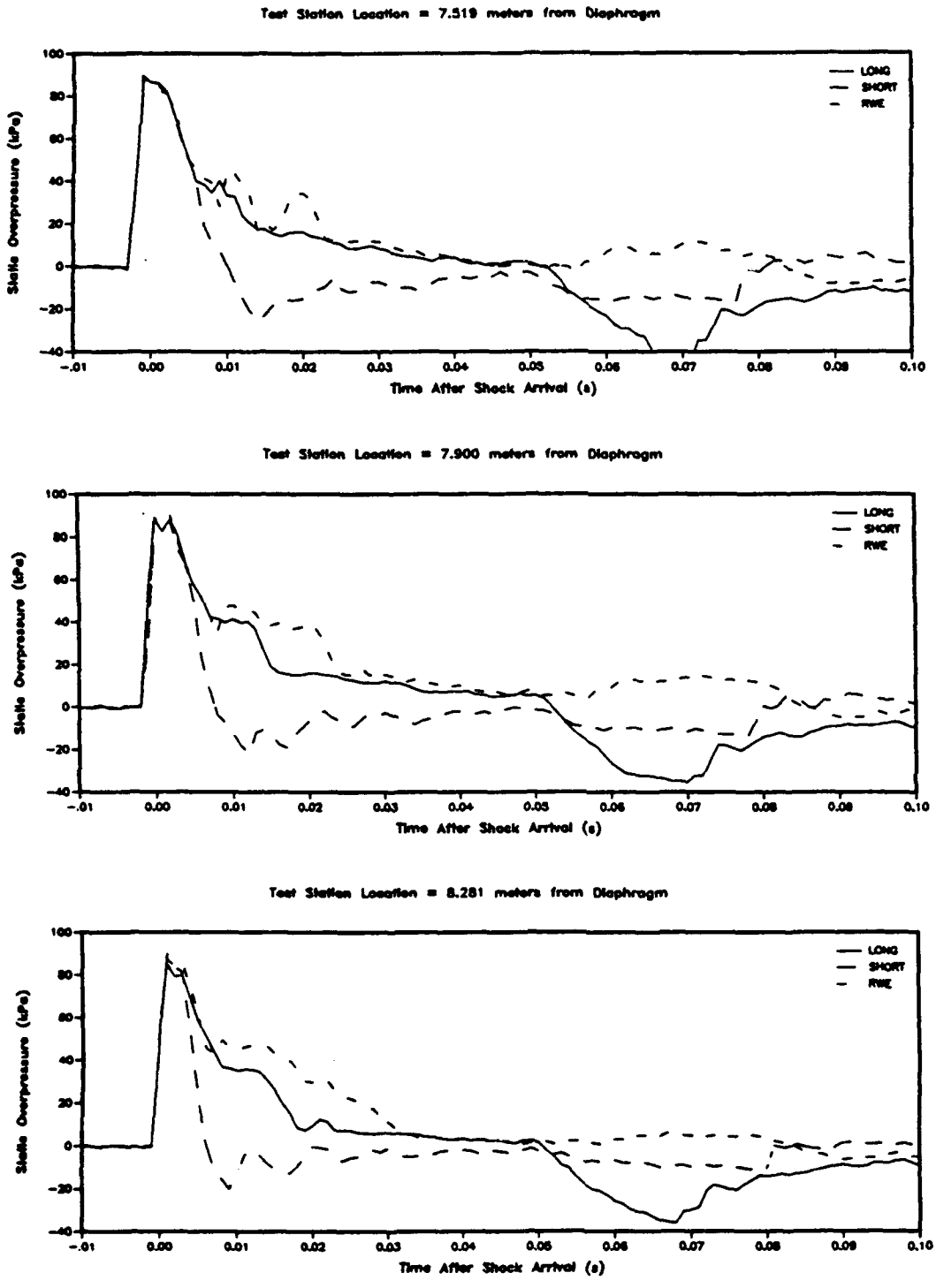

Figure B-3: Pressure Histories for 9018 cm^3 Driver; Pressure Level 3

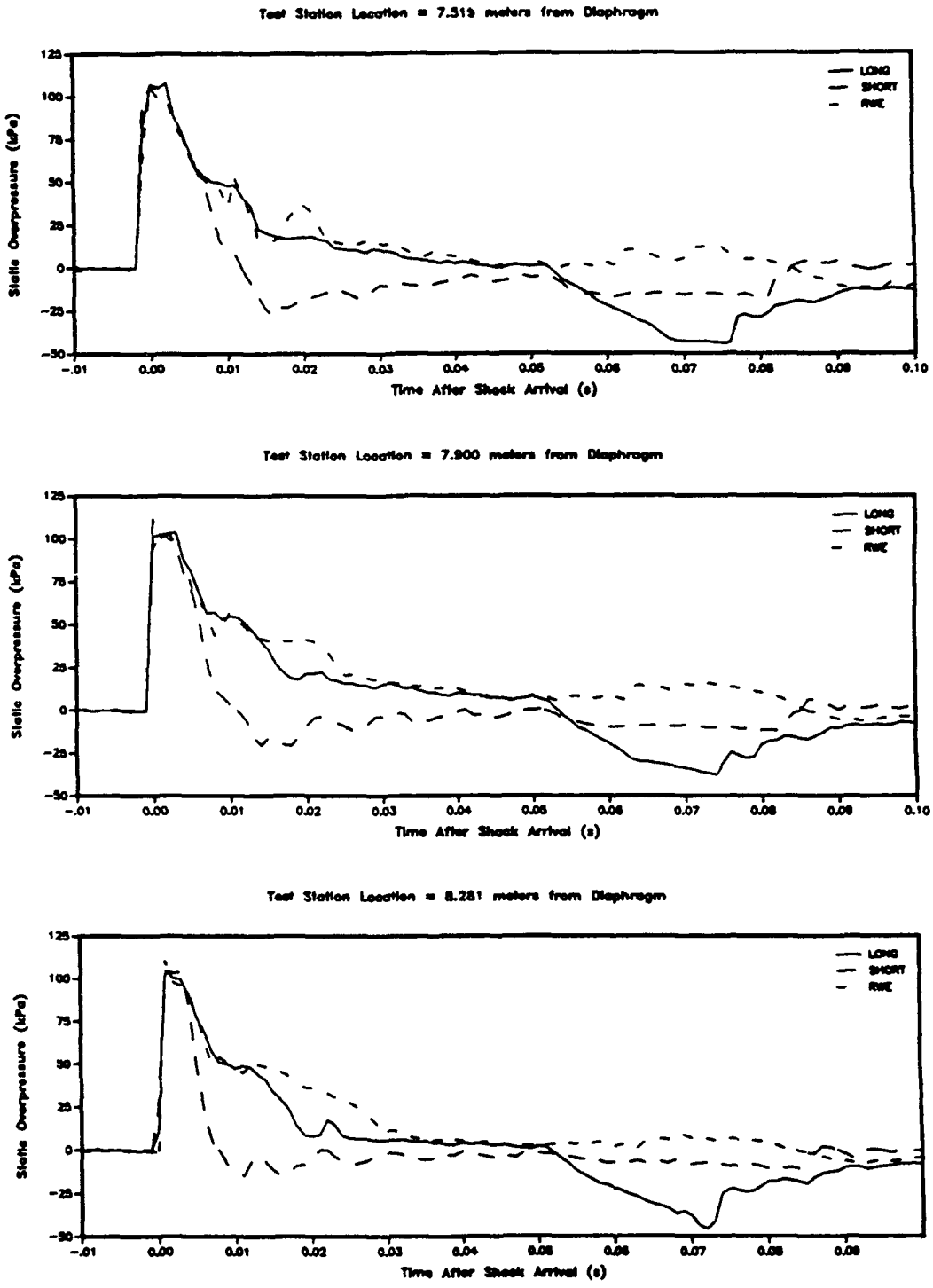

Figure B-4: Pressure Histories for 9018 cm^3 Driver; Pressure Level 4

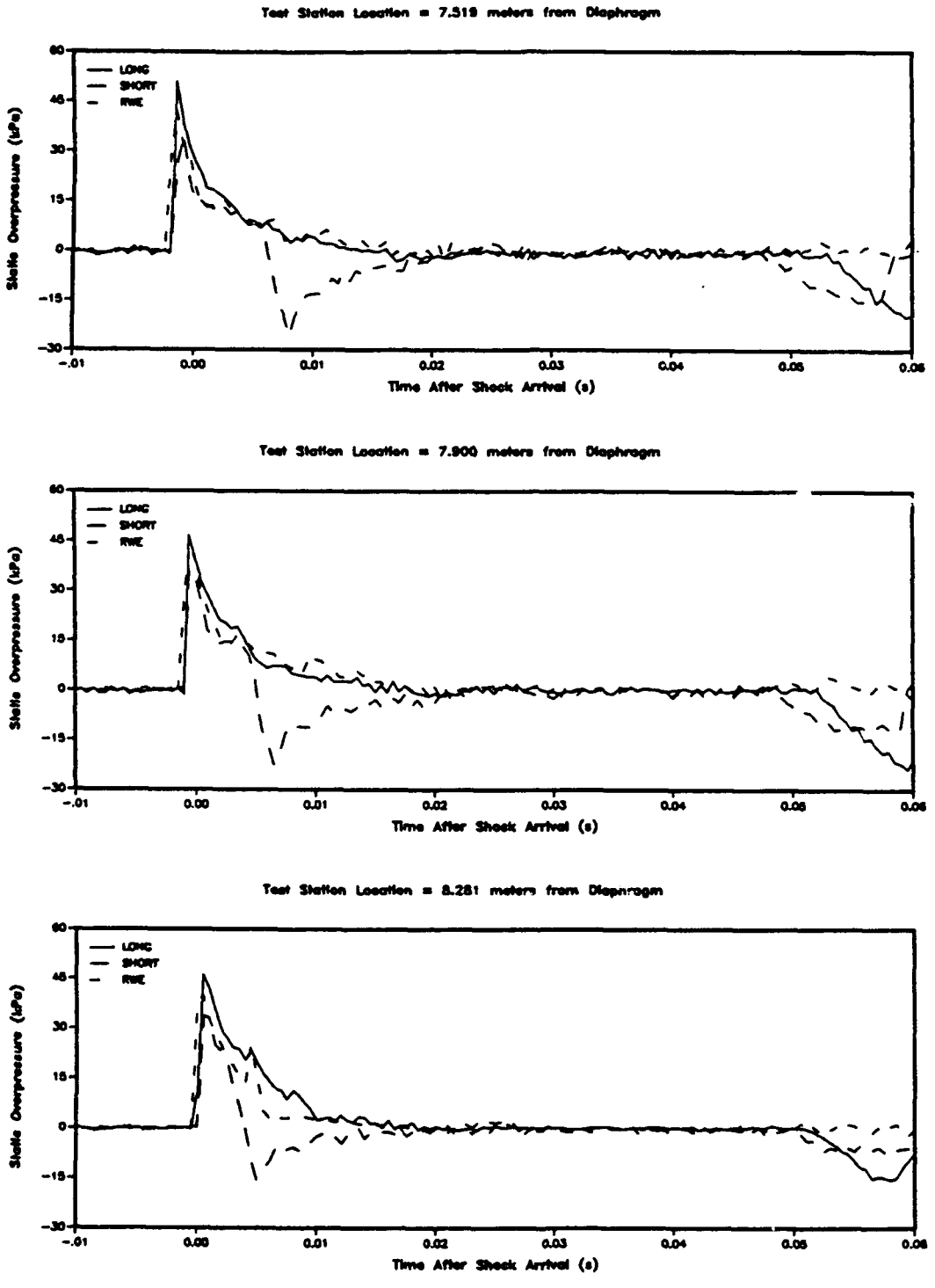

Figure B-5: Pressure Histories for 4988 cm^3 Driver; Pressure Level 1

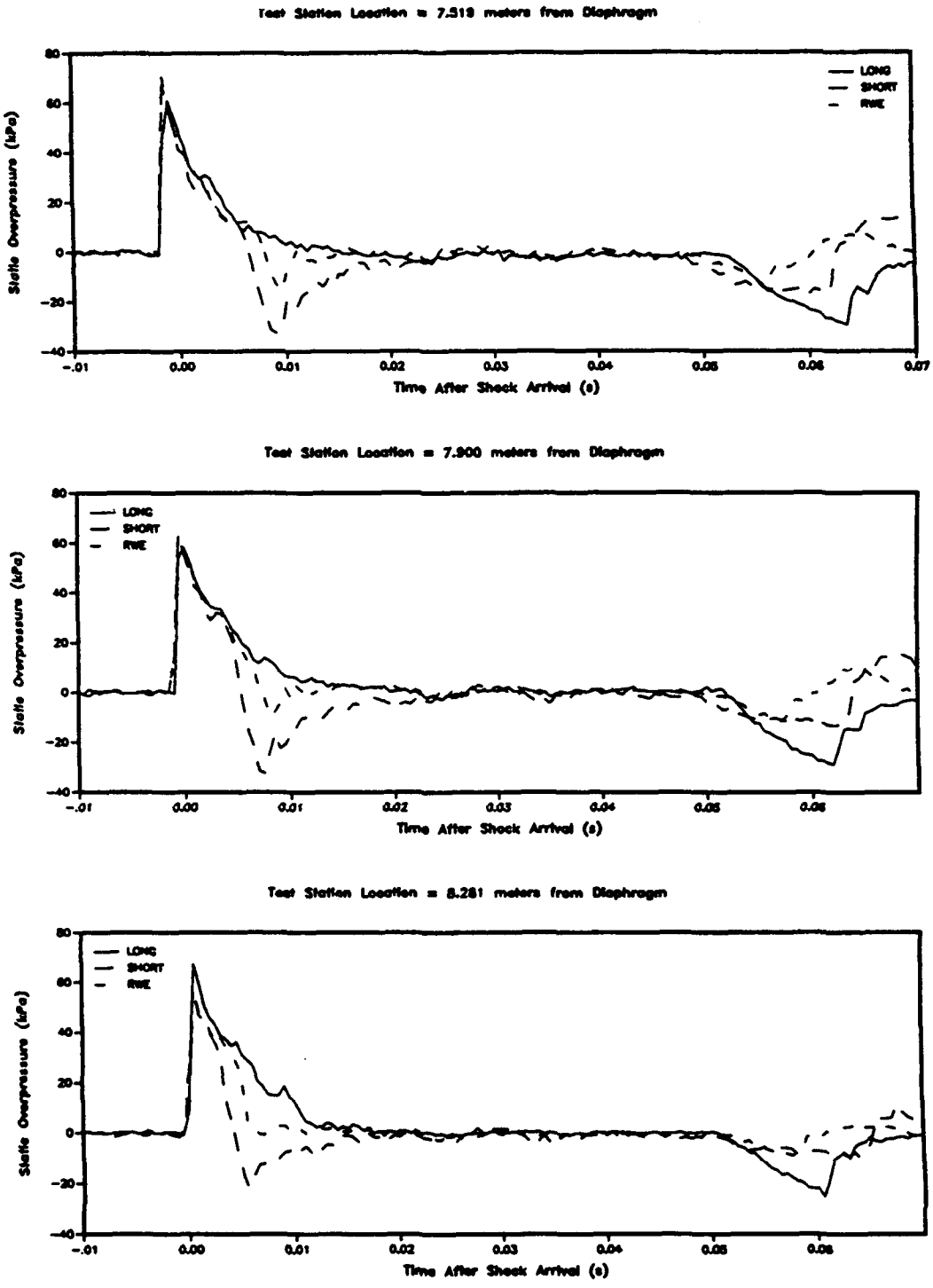

Figure B-6· Pressure Histories for 4988 cm^3 Driver; Pressure Level 2

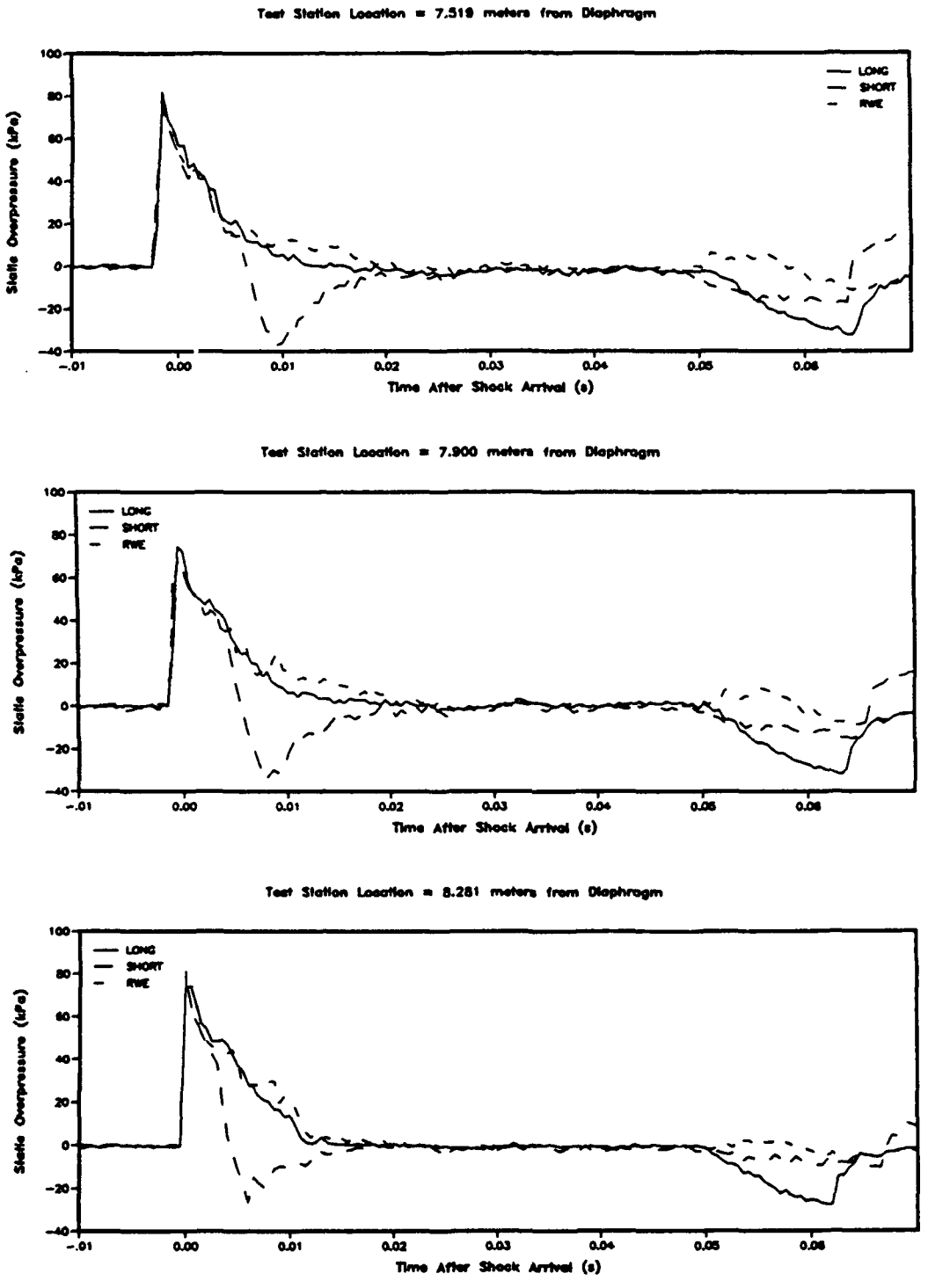

Figure B-7: Pressure Histories for 4988 cm^3 Driver; Pressure Level 3

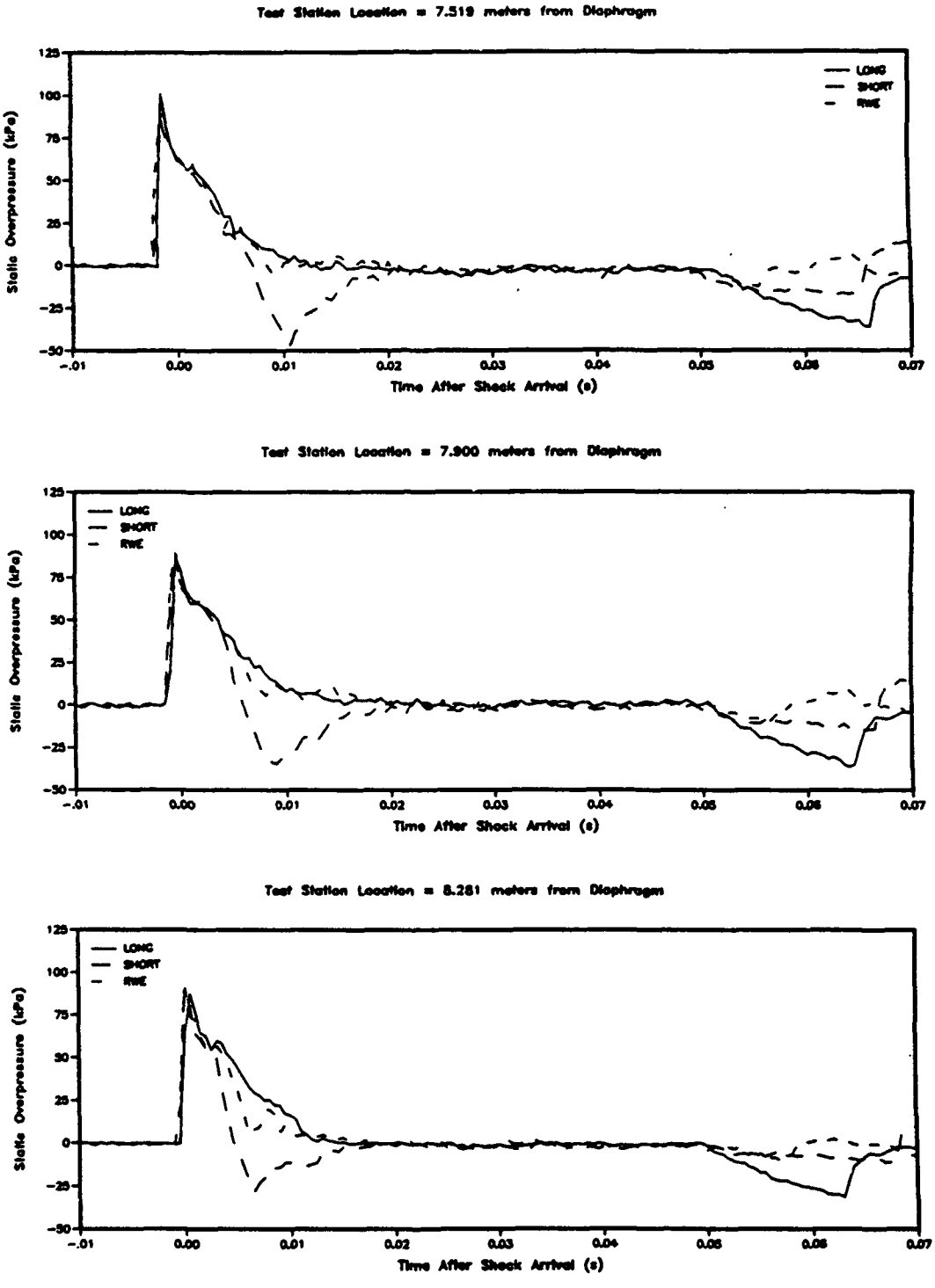

Figure B-8: Pressure Histories for 4988 cm^3 Driver; Pressure Level 4

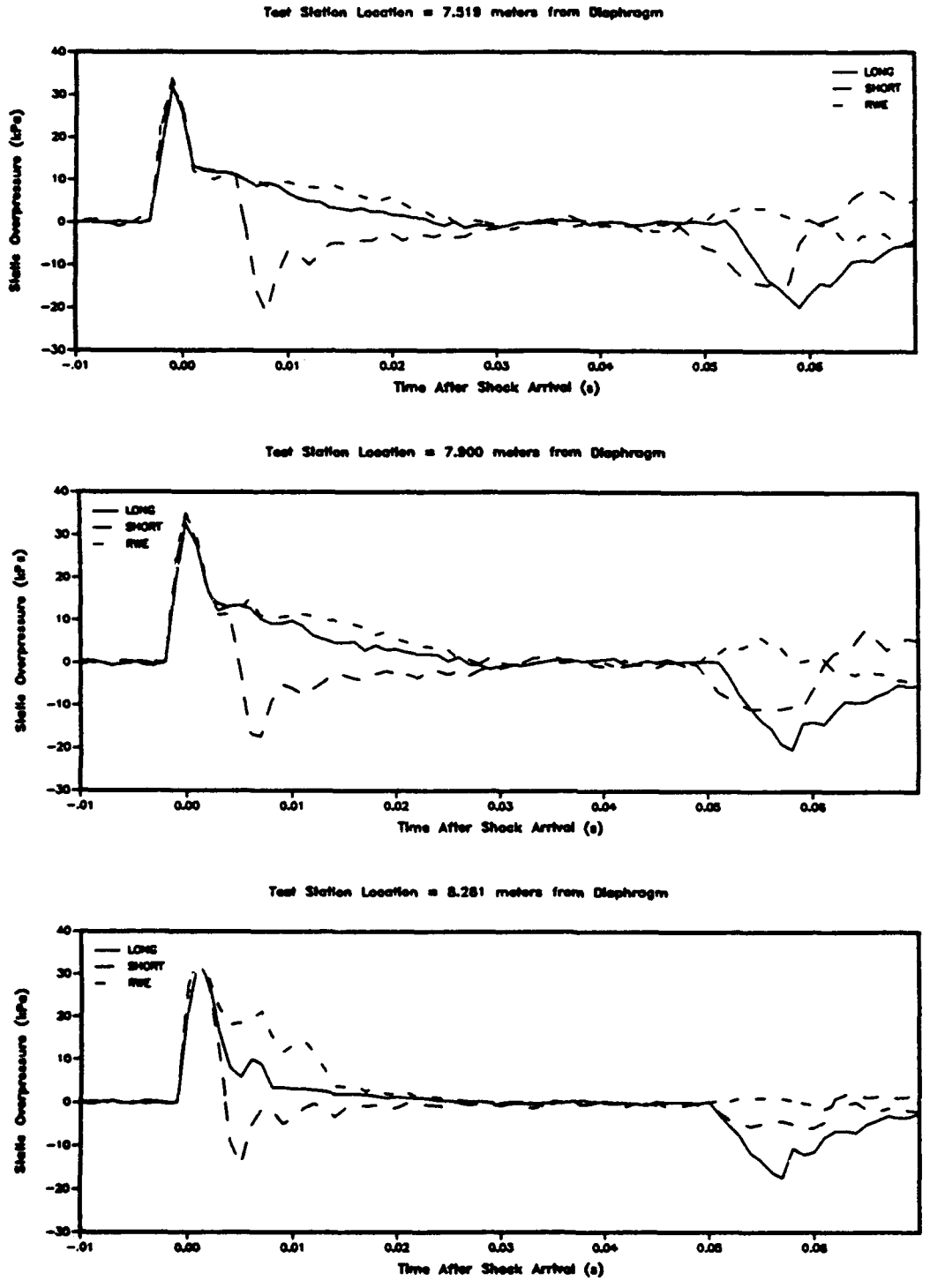

Figure B-9: Pressure Histories for 2840 cm^3 Driver; Pressure Level 1

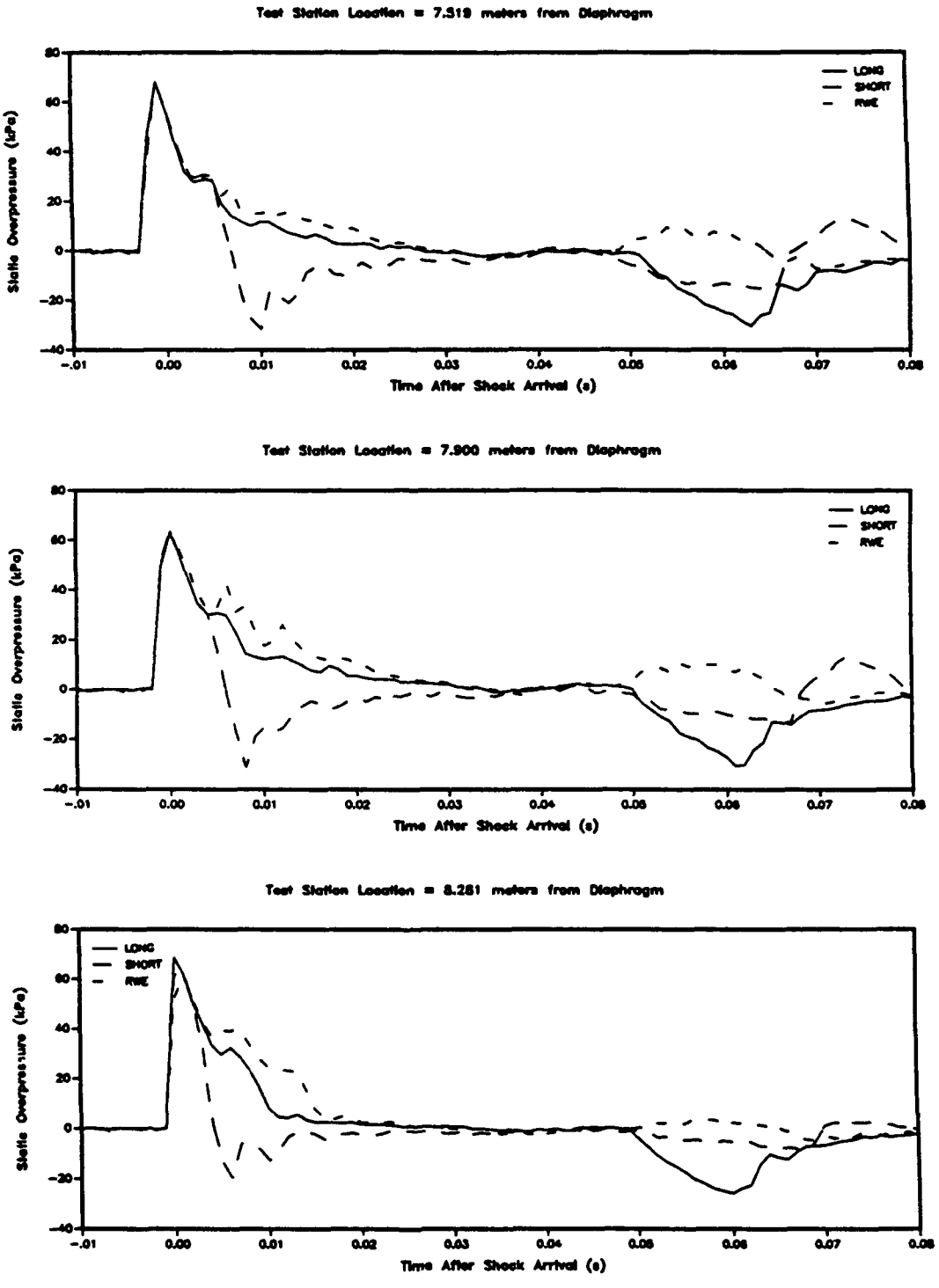

Figure B-10: Pressure Histories for 2840 cm^3 Driver; Pressure Level 2

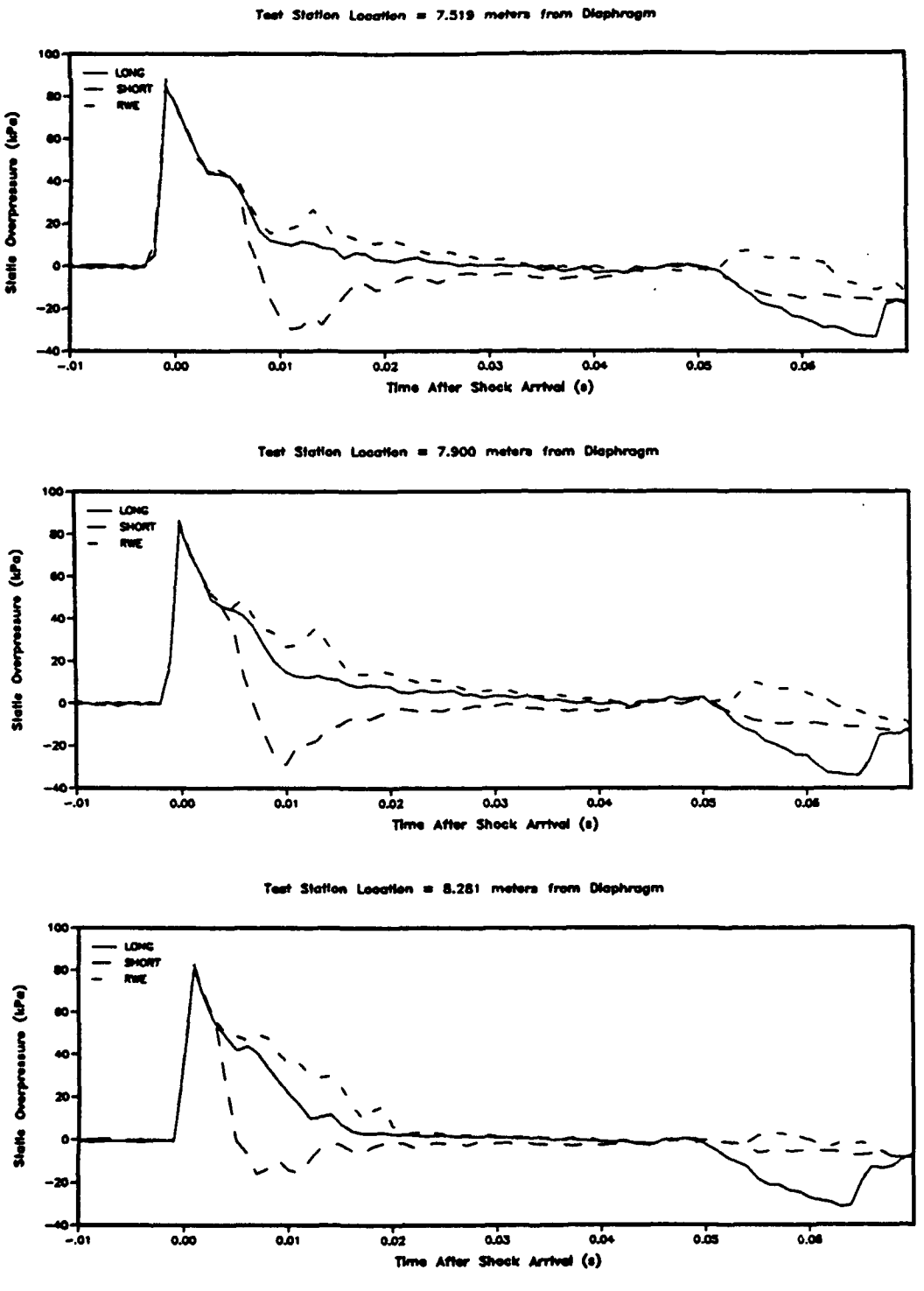

Figure B-11: Pressure Histories for 2840 cm^3 Driver; Pressure Level 3

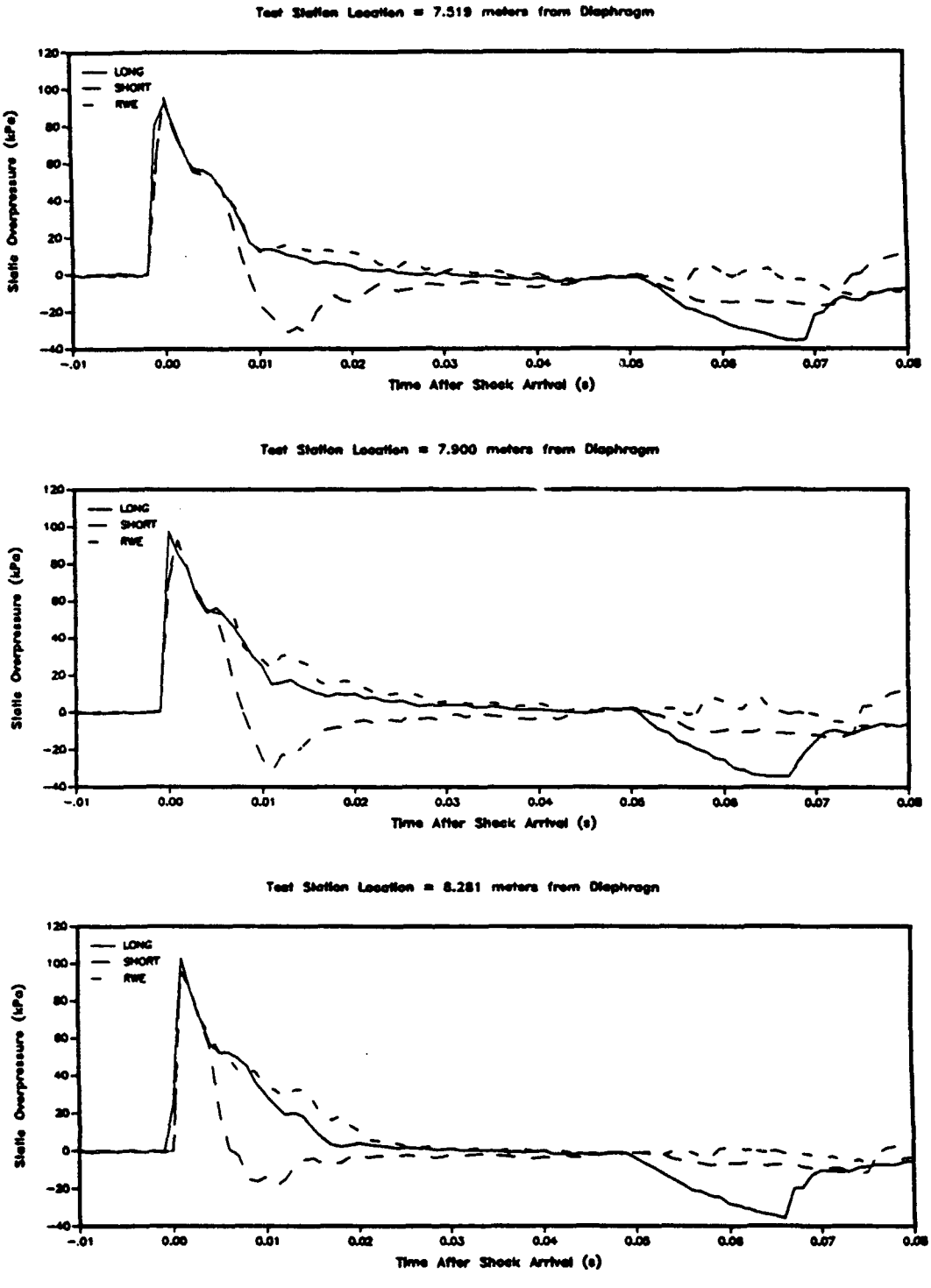

Figure B-12: Pressure Histories for 2840 cm^3 Driver; Pressure Level 4

INTENTIONALLY LEFT BLANK.

No of Copies	Organization
1	Office of the Secretary of Defense OUSD(A) Director, Live Fire Testing ATTN: James F. O'Bryon Washington, DC 20301-3110
2	Administrator Defense Technical Info Center ATTN: DTIC-DDA Cameron Station Alexandria, VA 22304-6145
1	HQDA (SARD-TR) WASH DC 20310-0001
1	Commander US Army Materiel Command ATTN: AMCDRA-ST 5001 Eisenhower Avenue Alexandria, VA 22333-0001
1	Commander US Army Laboratory Command ATTN: AMSLC-DL Adelphi, MD 20783-1145
2	Commander US Army, ARDEC ATTN: SMCAR-IMI-I Picatinny Arsenal, NJ 07806-5000
2	Commander US Army, ARDEC ATTN: SMCAR-TDC Picatinny Arsenal, NJ 07806-5000
1	Director Benet Weapons Laboratory US Army, ARDEC ATTN: SMCAR-CCB-TL Watervliet, NY 12189-4050
1	Commander US Army Armament, Munitions and Chemical Command ATTN: SMCAR-ESP-L Rock Island, IL 61299-5000
1	Commander US Army Aviation Systems Command ATTN: AMSAV-DACL 4300 Goodfellow Blvd. St. Louis, MO 63120-1798

No of Copies	Organization
1	Director US Army Aviation Research and Technology Activity ATTN: SAVRT-R (Library) M/S 219-3 Ames Research Center Moffett Field, CA 94035-1000
1	Commander US Army Missile Command ATTN: AMSMI-RD-CS-R (DOC) Redstone Arsenal, AL 35898-5010
1	Commander US Army Tank-Automotive Command ATTN: AMSTA-TSL (Technical Library) Warren, MI 48397-5000
1	Director US Army TRADOC Analysis Command ATTN: ATAA-SL White Sands Missile Range, NM 88002-5502
(Class. only) 1	Commandant US Army Infantry School ATTN: ATSH-CD (Security Mgr.) Fort Benning, GA 31905-5660
(Unclass. only) 1	Commandant US Army Infantry School ATTN: ATSH-CD-CSO-OR Fort Benning, GA 31905-5660
1	Air Force Armament Laboratory ATTN: AFATL/DLODL Eglin AFB, FL 32542-5000
	Aberdeen Proving Ground
2	Dir, USAMSAA ATTN: AMXSY-D AMXSY-MP, H. Cohen
1	Cdr, USATECOM ATTN: AMSTE-TD
3	Cdr, CRDEC, AMCCOM ATTN: SMCCR-RSP-A SMCCR-MU SMCCR-MSI
1	Dir, VLAMO ATTN: AMSLC-VL-D

No of Copies	Organization
1	Director of Defense Research & Engineering ATTN: DD/TWP Washington, DC 20301
1	Assistant Secretary of Defense (Atomic Energy) ATTN: Document Control Washington, DC 20301
1	Chairman Joint Chiefs of Staff ATTN: J-5 (R&D Div) Washington, DC 20301
2	Deputy Chief of Staff for Operations and Plans ATTN: Technical Library Director of Chemical and Nuclear Operations Department of the Army Washington, DC 20310
1	Director Defense Advanced Research Projects Agency ATTN: Tech Lib 1400 Wilson Boulevard Arlington, VA 22209
2	Director Federal Emergency Management Agency ATTN: Public Relations Office Technical Library Washington, DC 20472
1	Director Defense Intelligence Agency ATTN: DT-2/Wpns & Sys Div Washington, DC 20301
1	Director National Security Agency ATTN: R15 (E. F. Butala) Ft. George G. Meade, MD 20755
9	Director Defense Nuclear Agency ATTN: CSTI (Tech Lib) DDIR DFSP (Ullrich) NANS OPNA SPSD (Goering/Rohr) SPTD (Kennedy/Hrinishin) Washington, DC 20305
3	Commander Field Command, DNA ATTN: FCPR FCTMOF NMHE/CDR Lund Kirtland AFB, NM 87115
10	Central Intelligence Agency DIR/DB/Standard ATTN: GE-47 HQ Washington, DC 20505
2	Director Joint Strategic Target Planning Staff JCS ATTN: JLTW TPTP Offut AFB Omaha, NB 68113
1	Commandant Interservice Nuclear Weapons School ATTN: Technical Library Kirtland AFB, NM 87115

No of Copies	Organization
4	Director US Army Harry Diamond Labs ATTN: SLCHD-NW-RA, (L. Belliveau) SLCHD-NW-P, (Corrigan/Gwaltney) SLCHD-TA-L (Tech Lib) 2800 Powder Mill Road Adelphi, MD 20783-1197
1	Director US Army Laboratory Command USASMO ATTN: SLCSM-SE (J. Orsega) 2800 Powder Mill Road Adelphi, MD 20783-1197
2	Commander US Army CECOM ATTN: AMSEL-RD AMSEL-RO-TPPO-P Fort Monmouth, NJ 07703-5301
1	Commander, USACECOM R&D Technical Library ATTN: ASQNC-ELC-I-T, Myer Center Fort Monmouth, NJ 07703-5301
1	Director US Army Missile and Space Intelligence Center ATTN: AIAMS-YDL Redstone Arsenal, AL 35898-5500
1	Commander US Army Foreign Science and Technology Center ATTN: Research & Data Branch 220 7th Street, NE. Charlottesville, VA 22901
1	Director US Army TRAC - Ft. Lee ATTN: ATRC-L (R. Cameron) Fort Lee, VA 23801-6140
3	Commander US Army Materials Technology Laboratory ATTN: AMXMR-ATL SLCMT-MEC (W. Haskell) SLCMT-MRD-S, (K. Ofstedahl) Watertown, MA 02172-0001
1	Commander US Army Strategic Defense Command ATTN: CSSD-H-MPL (Tech Lib) CSSD-H-XM (Dr. Davies) P.O. Box 1500 Huntsville, AL 35807
2	Commander US Army Natick Research and Development Center ATTN: AMDNA-D (Dr. D. Sieling) STRNC-UE (J. Calligeros) Natick, MA 01762
1	Commander US Army Engineer Division ATTN: HNDED-FD P.O. Box 1500 Huntsville, AL 35807
3	Commander US Army Corps of Engineers Waterways Experiment Station ATTN: CAWES-SS-R (J. Watt) CAWES-SE-R (J. Ingram) CAWES-TL (Tech Lib) P.O. Box 631 Vicksburg, MS 39180-0631

No of Copies	Organization
1	Commander US Army Research Office ATTN: SLCRO-D P.O. Box 12211 Research Triangle Park, NC 27709-2211
3	Commander US Army Nuclear & Chemical Agency ATTN: ACTA-NAW MONA-WE Tech. Lib. 7500 Backlick Rd, Bldg. 2073 Springfield, VA 22150
1	Director HQ, TRADOC RPD ATTN: ATRC-RPR (Mr. Radda) Fort Monroe, VA 23651-5143
1	Director TRAC-WSMR ATTN: ATRC-WC (Mr. Kirby) White Sands Missile Range, NM 88002-5502
1	Director US Army TRADOC Center ATTN: ATRC Fort Leavenworth, KS 66027-5200
1	Commander US Army Test & Evaluation Command Nuclear Effects Laboratory ATTN: STEWS-TE-NO, (Dr. J.L. Meason) P.O. Box 477 White Sands Missile Range, NM 88002

No of Copies	Organization
2	Chief of Naval Operations ATTN: OP-03EG OP-985F Department of the Navy Washington, DC 20350
1	Chief of Naval Research ATTN: N. Perrone Department of the Navy Arlington, VA 22217
1	Director Strategic Systems Projects Office ATTN: NSP-43, Tech Library Department of the Navy Washington, DC 20360
1	Commander Naval Electronic Systems Command ATTN: PME 117-21A Washington, DC 20360
1	Commander Naval Facilities Engineering Command ATTN: Technical Library Washington, DC 20360
1	Commander Naval Sea Systems Command ATTN: Code SEA-62R Department of the Navy Washington, DC 20362-5101
1	Officer-in-Charge Naval Construction Battalion Center Civil Engineering Laboratory ATTN: Tech Lib Port Hueneme, CA 93041
1	Commanding Officer Naval Civil Engineering Laboratory ATTN: Code L51 (J. Tancreto) Port Hueneme, CA 93043-5003

No of Copies	Organization
1	Commander David Taylor Research Center ATTN: Code 522 (Tech Info Ctr) Bethesda, MD 20084-5000
1	Commander Naval Surface Warfare Center ATTN: Code DX-21 (Library) Dahlgren, VA 22448-5000
1	Officer in Charge White Oak Warfare Center Detachment ATTN: Code E232 (Tech Library) 10901 New Hampshire Ave Silver Spring, MD 20903-5000
1	Commanding Officer White Oak Warfare Center ATTN: Code WA501 (NNPO) Silver Spring, MD 20902-5000
1	Commander (Code 533) Naval Weapons Center Tech Library China Lake, CA 93555-6001
1	Commander Naval Weapons Evaluation Fac ATTN: Document Control Kirtland AFB, NM 87117
1	Commander Naval Research Laboratory ATTN: Code 2027, Tech Library Washington, DC 20375
1	Superintendent Naval Postgraduate School ATTN: Code 2124, Tech Library Monterey, CA 93940

No of Copies	Organization
2	Air Force Armament Laboratory ATTN: AFATL/DOIL AFATL/DLYV Eglin AFB, FL 32542-5000
1	AFESC/RDCS ATTN: Paul Rosengren Tyndall AFB, FL 32403
1	RADC (EMTLD/Docu Library) Griffiss AFB, NY 13441
3	Air Force Weapons Laboratory ATTN: NTE NTED NTES Kirtland AFB, NM 87117-6008
1	Commander-in-Chief Strategic Air Command ATTN: NRI-STINFO Lib Offutt AFB, NB 68113
1	AFIT ATTN: Tech Lib (Bldg 640/B) Wright-Patterson AFB, OH 45433
1	FTD/NIIS Wright-Patterson AFB, OH 45433
1	U.S. Department of Energy Idaho Operations Office ATTN: Spec Programs (J. Patton) 785 DOE Place Idaho Falls, ID 83402
2	Director Idaho National Engineering Laboratory EG&G Idaho Inc. ATTN: Mr. R. Guenzler, MS-3505 Mr. R. Holman, MS-3510 P.O. Box 1625 Idaho Falls, ID 83415

No of Copies	Organization
1	Director Lawrence Livermore Lab. ATTN: Tech Info Dept L-3 P.O. Box 808 Livermore, CA 94550
4	Director Los Alamos National Laboratory ATTN: Mr. Th. Dowler, MS-F602 Dr. J. Chapyak, MS-F664 Doc Control for Reports Library P.O. Box 1663 Los Alamos, NM 87545
3	Director Sandia Laboratories ATTN: Doc Control 3141 Mr. C. Cameron, Div 6215 Mr. A. Chabai, Div 7112 P.O. Box 5800 Albuquerque, NM 87185-5800
1	Director Sandia Laboratories Livermore Laboratory ATTN: Doc Control for Tech Library P.O. Box 969 Livermore, CA 94550
1	Director National Aeronautics and Space Administration ATTN: Scientific & Tech Info Fac P.O. Box 8757, BWI Airport Baltimore, MD 21240
1	Director NASA-Langley Research Center ATTN: Tech Lib Hampton, VA 23665
1	Director NASA-Ames Research Center Applied Computational Aerodynamics Branch ATTN: MS 202-14, Dr. T. Holtz Moffett Field, CA 94035
2	Applied Research Associates, Inc. ATTN: N.H. Ethridge J. Keefer P.O. Box 548 Aberdeen, MD 21001
1	Aerospace Corporation ATTN: Tech Info Services P.O. Box 92957 Los Angeles, CA 90009
1	Agbabian Associates ATTN: M. Agbabian 250 North Nash Street El Segundo, CA 90245
1	Applied Research Associates, Inc. ATTN: R. L. Guice 7114 West Jefferson Ave., Suite 305 Lakewood, CO 80235
1	Black & Veatch Engineers-Architects ATTN: H. D. Laverentz 1500 Meadow Lake Parkway Kansas City, MO 64114
1	The Boeing Company ATTN: Aerospace Library P.O. Box 3707 Seattle, WA 98124
1	California Research & Technology, Inc. ATTN: M. Rosenblatt 20943 Devonshire Street Chatsworth, CA 91311

No of Copies	Organization
1	Carpenter Research Corporation ATTN: H. Jerry Carpenter 27520 Hawthorne Blvd., Suite 263 P.O. Box 2490 Rolling Hills Estates, CA 90274
1	Dynamics Technology, Inc. ATTN: D. T. Hove Suite 300 21311 Hawthorne Blvd. Torrance, CA 90503
1	EATON Corporation Defense Valve & Actuator Div. ATTN: Mr. J. Wada 2338 Alaska Ave. El Segundo, CA 90245-4896
2	FMC Corporation Advanced Systems Center ATTN: Mr. J. Drotleff Ms. C. Krebs, MDP95 2890 De La Cruz Boulevard Box 58123 Santa Clara, CA 95052
1	Goodyear Aerospace Corporation ATTN: R. M. Brown, Bldg 1 Shelter Engineering Litchfield Park, AZ 85340
4	Kaman AviDyne ATTN: Dr. R. Ruetenik (2 cys) Mr. S. Criscione Mr. R. Milligan 83 Second Avenue Northwest Industrial Park Burlington, MA 01830
3	Kaman Sciences Corporation ATTN: Library P. A. Ellis F. H. Shelton 1500 Garden of the Gods Road Colorado Springs, CO 80907
1	Kaman Sciences Corporation ATTN: Mr. F. W. Balicki 6400 Uptown Boulevard N.E. Suite 300 Albuquerque, NM 87110
2	Kaman-TEMPO ATTN: DASIAC Don Sachs P.O. Drawer QQ 816 State Street Santa Barbara, CA 93102
1	Ktech Corporation ATTN: Dr. E. Gaffney 901 Pennsylvania Avenue, N.E. Albuquerque, NM 87111
1	Lockheed Missiles & Space Co. ATTN: J. J. Murphy, Dept. 81-11, Bldg. 154 P.O. Box 504 Sunnyvale, CA 94086
2	McDonnell Douglas Astronautics Corporation ATTN: Robert W. Halprin K.A. Heinly 5301 Bolsa Avenue Huntington Beach, CA 92647
1	Orlando Technology, Inc. ATTN: Mr. D. Matuska P.O. Box 855 Shalimar, FL 32579

No of Copies	Organization
2	Physics International Corporation 2700 Merced Street San Leandro, CA 94577
2	R&D Associates ATTN: Technical Library Dr. Allan Kuhl P.O. Box 9695 Marina Del Rey, CA 90291
1	R&D Associates ATTN: G.P. Ganong P.O. Box 9377 Albuquerque, NM 87119
2	Science Applications, Inc. ATTN: W. Layson John Cockayne P.O. Box 1303 1710 Goodridge Drive McLean, VA 22102
1	Science Applications International Corp. ATTN: Mr. J. Guest 2109 Air Park Rd, SE Albuquerque, NM 87106
1	Sparta, Inc. Los Angeles Operations ATTN: I. B. Osofsky 3440 Carson Street Torrance, CA 90503
1	Sunburst Recovery, Inc. ATTN: Dr. C. Young P.O. Box 2129 Steamboat Springs, CO 80477
1	Sverdrup Technology, Inc. ATTN: R. F. Starr P.O. Box 884 Tullahoma, TN 37388
3	SRI International ATTN: Dr. G. R. Abrahamson Dr. J. Gran Dr. B. Holmes 333 Ravenswood Avenue Menlo Park, CA 94025
2	S-CUBED A Division of Maxwell Laboratories, Inc. ATTN: C. E. Needham Dr. Lynn Kennedy 2501 Yale Blvd., SE Albuquerque, NM 87106
3	S-CUBED A Division of Maxwell Laboratories, Inc. ATTN: Technical Library R. Duff K. Pyatt PO Box 1620 La Jolla, CA 92037-1620
1	Texas Engineering Experiment Station ATTN: Dr. D. Anderson 301 Engineering Research Center College Station, TX 77843
1	Thermal Science, Inc. ATTN: R. Feldman 2200 Cassens Dr. St. Louis, MO 63026
1	TRW Ballistic Missile Division ATTN: H. Korman, Mail Station 526/614 P.O. Box 1310 San Bernadino, CA 92402

No of Copies	Organization
1	Battelle Memorial Institute ATTN: Technical Library 505 King Avenue Columbus, OH 43201
1	California Institute of Technology ATTN: T. J. Ahrens 1201 E. California Blvd. Pasadena, CA 91109
2	Denver Research Institute ATTN: Mr. J. Wisotski Technical Library P.O. Box 10758 Denver, CO 80210
1	Massachusetts Institute of Technology Aeroelastic and Structures Research Laboratory ATTN: Dr. E. A. Witmer Cambridge, MA 02139
1	Massachusetts Institute of Technology ATTN: Technical Library Cambridge, MA 02139
2	New Mexico Engineering Research Institute (CERF) University of New Mexico ATTN: Dr. J. Leigh Dr. R. Newell P.O. Box 25 Albuquerque, NM 87131
1	Northrop University ATTN: Dr. F. B. Safford 5800 W. Arbor Vitae St. Los Angeles, CA 90045
4	Southwest Research Institute ATTN: Dr. W. E. Baker A. B. Wenzel Dr. C. Anderson S. Mullin 6220 Culebra Road San Antonio, TX 78284
1	Stanford University ATTN: Dr. D. Bershader Durand Laboratory Stanford, CA 94305
3	University of Maryland Department of Mechanical Engineering ATTN: Dr. W. Fourney Dr. R. Dick Dr. J. Williams College Park, MD 20742

Aberdeen Proving Ground

1	Cdr, USATECOM ATTN: AMSTE-TE-F (L. Teletski)
1	Cdr, USATHMA ATTN: AMXTH-TE

INTENTIONALLY LEFT BLANK.

USER EVALUATION SHEET/CHANGE OF ADDRESS

This Laboratory undertakes a continuing effort to improve the quality of the reports it publishes. Your comments/answers to the items/questions below will aid us in our efforts.

1. BRL Report Number BRL-TR-3149 Date of Report SEPTEMBER 1990

2. Date Report Received _____

3. Does this report satisfy a need? (Comment on purpose, related project, or other area of interest for which the report will be used.) _____

4. Specifically, how is the report being used? (Information source, design data, procedure, source of ideas, etc.) _____

5. Has the information in this report led to any quantitative savings as far as man-hours or dollars saved, operating costs avoided, or efficiencies achieved, etc? If so, please elaborate. _____

6. General Comments. What do you think should be changed to improve future reports? (Indicate changes to organization, technical content, format, etc.) _____

CURRENT ADDRESS

Name

Organization

Address

City, State, Zip Code

7. If indicating a Change of Address or Address Correction, please provide the New or Correct Address in Block 6 above and the Old or Incorrect address below.

OLD ADDRESS

Name

Organization

Address

City, State, Zip Code

(Remove this sheet, fold as indicated, staple or tape closed, and mail.)

---FOLD HERE---

DEPARTMENT OF THE ARMY
Director
U.S. Army Ballistic Research Laboratory
ATTN: SLCBR-DD-T
Aberdeen Proving Ground, MD 21005-5066
OFFICIAL BUSINESS

NO POSTAGE NECESSARY IF MAILED IN THE UNITED STATES

BUSINESS REPLY MAIL
FIRST CLASS PERMIT No 0001, APG, MD

POSTAGE WILL BE PAID BY ADDRESSEE

Director
U.S. Army Ballistic Research Laboratory
ATTN: SLCBR-DD-T
Aberdeen Proving Ground, MD 21005-9989

---FOLD HERE---